FACULTY OF ENGINEERING AND ARCHITECTURE

Impact of the spatial distribution of active material on the performance of n-hexane hydrocracking with a bifunctional catalyst

Seniz Rodoplu
Student number: 01801037

Supervisors: Prof. dr. Vladimir Galvita, Juan Mirena Seguias
Counsellor: Prof. dr. ir. Joris Thybaut

Master's dissertation submitted in order to obtain the academic degree of
Master of Science in Chemical Engineering

Academic year 2019-2020

GHENT UNIVERSITY

FACULTY OF ENGINEERING AND ARCHITECTURE

Impact of the spatial distribution of active material on the performance of n-hexane hydrocracking with a bifunctional catalyst

Seniz Rodoplu
Student number: 01801037

Supervisors: Prof. dr. Vladimir Galvita, Juan Mirena Seguias
Counsellor: Prof. dr. ir. Joris Thybaut

Master's dissertation submitted in order to obtain the academic degree of
Master of Science in Chemical Engineering

Academic year 2019-2020

GHENT UNIVERSITY

Acknowledgments

I would like to express my deepest gratitude and appreciation to my supervisor, Prof. dr. Vladimir Galvita, for providing me the opportunity to work for this interesting thesis topic and his valuable guidance.

I also would like to extend my deepest gratitude to my supervisor, Juan Mirena, for providing guidance and helpful feedback throughout this project. I have learned many things from him about how to write a paper, search literature, and collect data. His practical suggestions and expert advice have been invaluable throughout all stages of this work.

I would like to extend my sincere thanks to Prof. dr. ir. Joris Thybaut and dr. Pedro Mendes for their constructive advices about the experimentation and simulation before the pandemic.

Special thanks are given to all professionals within the Laboratory for Chemical Technology. During my 2-year chemical engineering master program, I gain many fundamental knowledge and concepts that improved my engineering aspect and provided me substantial skills for my future work life. Also, thanks to the scholarship provided by Ghent University, I realized my dreams and completed my study abroad. I would like to thank everyone who contributed in this respect.

Finally, I express my very profound gratitude to my precious parents, Filiz Rodoplu and Şenol Rodoplu, my beloved little sister, Şevval Rodoplu, my valuable friend, Cenk Öztürk, and all of my friends who were with me in this master education for providing me unfailing support and continuous encouragement throughout my years of study and through the process of researching and writing this thesis. This accomplishment would not have been possible without them.

Preamble

The original scope of this study included an experimental examination of the impact of different metal and acid site distances on the performance of a bifunctional catalyst for n-hexane (n-C_6) conversion. Due to the unexpected COVID-19 pandemic, the planned experiments could not be executed. Therefore, the focus of this project had to be converted to a literature review of the current research trends about the consequences of varying the balance and distance between metal and acid sites on the performance of bifunctional catalysts.

Before the pandemic, a bifunctional catalyst consisting of erionite/alumina particles with different distributions of platinum (Pt) nanoparticles was to be supplied by KU Leuven for experimental testing at the Laboratory for Chemical Technology (LCT). In general, two types of catalysts were planned to be produced with the Pt nanoparticles either inside the zeolite or on the alumina binder. n-C_6 was supposed to be used as the model hydrocarbon for reaction in the High-throughput reactor system (HTK) in order to obtain steady-state information about the effect of the active site distribution on catalyst activity and performance. Catalyst samples were to be diluted with inert material in several different ways, under different flow, temperature, and pressure conditions, in order to test various active site spatial distributions. The obtained experimental data was intended to be employed as input for a microkinetic model with the aim of evaluating the effect of site dispersion on the obtained kinetic parameters. Furthermore, these experimental results were to be compared to transient experiments conducted in the Temporal Analysis of Products (TAP) reactor under similar dispersion and dilution conditions. Transient experimental data was to be analyzed in order to obtain information on the possible reaction steps that are affected by a change in the metal and acid distance. Both sets of experiments could have also provided information about specific reaction steps in the mechanism for modeling purposes, ultimately serving as a basis for incorporating the distribution of active material as a design factor in catalyst optimization. The effect of the distance between the metal and the acid sites was planned to be added to the microkinetic model by using the Fortran code from the studies conducted by Vandegehuchte et al. [1] [2].

LABORATORY FOR CHEMICAL TECHNOLOGY
Technologiepark 125, 9052 Gent, Belgium

Declaration concerning the accessibility of the master thesis

Undersigned,

Şeniz Rodoplu

Graduated from Ghent University, academic year 2019-2020 and is author of the master thesis with title:

Impact of the spatial distribution of active material on the performance of n-hexane hydrocracking with a bifunctional catalyst

The author(s) gives (give) permission to make this master dissertation available for consultation and to copy parts of this master dissertation for personal use.
In the case of any other use, the copyright terms have to be respected, in particular with regard to the obligation to state expressly the source when quoting results from this master dissertation.

May 31, 2020

Şeniz Rodoplu

GHENT UNIVERSITY

LCT
DRIVING CHEMICAL TECHNOLOGY

Impact of the spatial distribution of active material on the performance of n-hexane hydrocracking with a bifunctional catalyst

Şeniz Rodoplu
Student number: 01801037

Supervisors: Prof. dr. Vladimir Galvita, Ir. Juan I. Mirena
Counsellor: Prof. dr. ir. Joris Thybaut

Master's dissertation submitted in order to obtain the academic degree of
Master of Science in Chemical Engineering

Academic year 2019-2020

Faculty of Engineering and Architecture

Abstract

The isomerization of n-alkanes over bifunctional catalysts has a significant role in the petrochemical industry since it provides high-quality fuels. Bifunctional catalysts usually consist of noble metals deposited over an acidic zeolite. Catalyst performance is mainly governed by two properties: the balance between metal and acid functions and the distance between both sites. Optimal catalytic performance is typically defined by a high degree of Hydrogenation/Dehydrogenation (HD/DHD) reactions and reduced cracking, in which the acid catalyzed steps are rate-limiting. Different studies have found that this behavior can be achieved if Pt metal particles are placed close to the micropore mouth of the zeolite, within a nanometer scale proximity with the acid sites. Furthermore, if zeolite crystals have around 400-500 nm particle size, greater bifunctionality and an optimal production of high-quality diesel can be obtained. Metal sites close to the micropore mount and smaller zeolite particle sizes provide a reduced diffusion distance between both sites and reduce the possibility of unwanted secondary reactions, such as multiple branching and cracking. This study aims to review the most prominent research directions and results on the study of the influence of metal and acid site balance and dispersion on hydrocarbon hydroisomerization over bifunctional catalysts.

Keywords

hydroisomerization, ideal bifunctional catalyst, metal/acid balance, metal/acid intimacy, platinum, alkene intermediate

Impact of the spatial distribution of active material on the performance of n-hexane hydrocracking with a bifunctional catalyst

Şeniz Rodoplu

Counsellor: Prof. Dr. Ir. Joris Thybaut

Supervisors: Prof. Dr. Vladimir Galvita, Ir. Juan I. Mirena

***Abstract*: The isomerization of n-alkanes over bifunctional catalysts has a significant role in the petrochemical industry since it provides high-quality fuels. Bifunctional catalysts usually consist of noble metals deposited over an acidic zeolite. Catalyst performance is mainly governed by two properties: the balance between metal and acid functions and the distance between both sites. Optimal catalytic performance is typically defined by a high degree of Hydrogenation/Dehydrogenation (HD/DHD) reactions and reduced cracking, in which the acid catalyzed steps are rate-limiting. Different studies have found that this behavior can be achieved if Pt metal particles are placed close to the micropore mouth of the zeolite, within a nanometer scale proximity with the acid sites. Furthermore, if zeolite crystals have around 400-500 nm particle size, greater bifunctionality and an optimal production of high-quality diesel can be obtained. Metal sites close to the micropore mount and smaller zeolite particle sizes provide a reduced diffusion distance between both sites and reduce the possibility of unwanted secondary reactions, such as multiple branching and cracking. This study aims to review the most prominent research directions and results on the study of the influence of metal and acid site balance and dispersion on hydrocarbon hydroisomerization over bifunctional catalysts.**

***Keywords*: hydroisomerization, ideal bifunctional catalyst, metal/acid balance, metal/acid intimacy, platinum, alkene intermediate**

I. Introduction

More stringent environmental restrictions and fuel regulations, the decreased quality of crude oil reserves, and an increasing energy demand and oil prices have driven the development of processes for upgrading heavy feedstocks such as heavy oil and bitumen [1,2,3]. These oil resources require a greater deal of treatment and refining for producing high-quality middle distillate fuels such as jet fuel, diesel, and gasoline with smaller quantities of aromatics, olefins and oxygen-containing compounds [4,5]. Even though aromatics and olefins provide high octane numbers, their usage is restricted due to recent environmental regulations and the risk of enhanced pollution. As an alternative, fuel quality can be compensated by blending gasoline with branched alkane isomers, which have a higher-octane number than linear n-alkane forms [5].

The hydrocracking process is one of the most effective and flexible upgrading processes for converting heavy hydrocarbons into high-quality oil products. including mainly the hydroisomerization and hydrocracking reaction steps [6]. The hydroisomerization of n-alkanes has become the key interest since it improves the fuel quality and cold flow properties of fuels, such as viscosity, pour point, and freezing point and provides gasoline/diesel with a high octane/cetane number [7]. Hydroisomerization and hydrocracking reactions are executed under a hydrogen atmosphere over a bifunctional catalyst including metal sites for HD/DHD reactions and acid sites for skeletal isomerization or cracking reactions [8]. These catalysts are used in many industrial chemical processes, instead of their monofunctional alternatives, since they require milder operation conditions, broader product distributions, and higher selectivity toward desired products [9]. Moreover, the production of petroleum products such as diesel, jet fuels, the isomerization of ethylbenzene and the synthesis of fine chemicals such as the production of methylisobutylketone from acetone can be conducted in one apparent step over the bifunctional catalyst, resulting in a reduction in energy consumption and waste generation [10]. The HD/DHD function is usually a noble metal such as Pt or Pd due to their excellent hydrogenation activity and good resistance to coke formation [1]. Typical acidic supports for bifunctional catalysts are zeolites, silicoaluminophosphates, mesoporous materials, and amorphous oxides or mixtures of oxides. Among them, zeolites are one of the most promising supports due to their higher acid strength, low coke-forming tendency, high resistance to contaminants, and molecular shape selectivity [9].

The general mechanism of alkane hydroisomerization over a bifunctional metal/acid zeolite catalyst is shown in Figure 1 [10]. Firstly, the n-alkanes diffuse toward the metal site and dehydrogenation reaction occurs. Then, intermediates diffuse toward acid sites through the microporous channels of acid supports, where the isomerization and/or cracking reactions occur. After that, the i-alkenes diffuse back to the metal site and hydrogenated [10]. However, there is a possibility for alkene intermediates to undergo further undesired secondary reactions on other acid sites before reaching the metal site, resulting in the production of the multi-branched isomers or cracked products. Also, since multi-branched alkenes are more sensitive to cracking than mono-branched alkenes, the production of multi-branched alkenes should be limited to reduce the further cracking reactions [1].

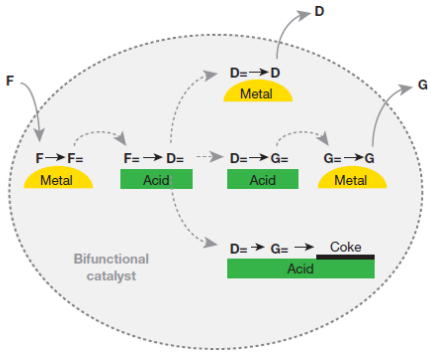

Figure 1: Scheme of alkane hydroisomerization over bifunctional catalysts [11]

There are plenty of studies with the goal of limiting the secondary cracking reactions of the isomerization products in order to achieve high isomerization yields [11,12,13]. Catalyst performance is mainly governed by the balance between the metal and acid activity and the distance between both sites [14]. The metal and acid activity can be quantified by the ratio of the concentration of metal and acid sites (nMe/nA) [8]. When the nMe/nA ratio is gradually increased, the activity of the catalyst initially increases and then reaches a plateau where the rate limiting step is changed from the HD/DHD reactions on the Pt sites to the skeletal isomerization and cracking reactions on acid sites [8]. In this case, both the activity and selectivity of the catalyst depend solely on the acid function [15]. Since the reaction mechanism includes the diffusion of alkene intermediates between Pt and acid sites alongside the reactions on both types of sites, the diffusion distance between sites has an influence on the bifunctional performance of the catalyst [8,13]. Therefore, the distance between Pt and acid sites is another major feature that can be tuned to improve the bifunctional performance of the catalyst [8]. Whereas most research has indicated that the maximal proximity between metal and acid sites improves the yield of isomerized products, recent studies suggest different approaches.

In this review, the main objective of this project is to explore the possibilities of increasing the yield of isomer products by optimizing hydroisomerization and cracking reactions. To fulfill this objective, bifunctional catalysts typically used for hydrocarbon hydroisomerization will be investigated to obtain information about the most ideal catalyst design, including an examination of various catalyst samples prepared by different methodologies and their reaction mechanisms. An ideal catalyst design can be achieved with an optimal balance and distance between metal and acid sites to maximize isomer products from n-alkane conversion. This study includes a review of the most relevant articles, explanation of the conducted work, and a comparison of the results with the focus on finding the optimal distance between bifunctional active sites.

II. The Effects of Metal/Acid Balance on Catalytic Performances for N-Alkane Hydroisomerization over Bifunctional Catalysts

A. The Effects of Metal/Acid Balance on the Mechanism and Performance of Bifunctional Catalysts

The effects of metal/acid balance can be experimentally investigated by modifying the ratio between metal and acid sites, nMe/nA. The fundamental requirement for ideal catalytic performance is that the nMe/nA ratio should be sufficiently high to set the acid-catalyzed skeletal isomerization and cracking reactions as the rate-limiting steps [15]. Numerous studies have specifically investigated the effect of different nMe/nA values.

The n-hexadecane (n-C_{16}) hydroisomerization over Pd/SAPO-41 catalysts with nMe/nA was tested by Wang et al. [15]. They found that Pd/SAPO-41 catalysts with nMe/nA values between 0.18 and 0.78 show adequate catalytic performance, i.e. higher activity and selectivity towards iso-alkanes products. On the other hand, for catalysts with nMe/nA smaller than 0.18, the cracking of isomer products was increased by the favored acid function. Furthermore, for catalysts with nMe/nA larger than 0.78, the excess amount of Pd particles blocked the micropores of SAPO-41, seriously restraining the diffusion of hydrocarbon chains inside the catalyst [15].

Zhang et al. [16] investigated the effect of bimetallic sites on the metal/acid balance by preparing the Pd–Ni_2P/SAPO-31 catalyst. The highest isomerization yield achieved by the addition of bimetallic sites was 72 %. On the other hand, the isomerization yield obtained by only Pd or Ni_2P loadings were 1.74 and 1.10 times lower, respectively. This significant improvement induced by the bimetallic sites is mainly caused by the enhanced metal/acid balance [16].

Alvarez et al. [17] also studied the effect of different nMe/nA values, increasing from 0.002 to 0.48, for the hydroisomerization of n-decane (n-C_{10}) over a series of Pt/HY bifunctional catalysts. They aimed to understand the effect of the nMe/nA ratio on the hydroisomerization mechanism. In Figures 2a, 2b, and 2c, representative schemes for n-C_{10} hydroconversion at low, intermediate, and high values of nMe/nA are shown. For catalysts with relatively low nMe/nA values (nMe/nA<0.03), all i-decanes (i-C_{10}) and cracking products were directly derived from n-C_{10} molecules as shown in Figure 2a. Since there is insufficient Pt on the catalyst, the number of acid sites that alkene intermediates encounter during the diffusion through the Pt site is quite high, resulting in a high possibility of consecutive conversions of alkene intermediates. For catalysts with intermediate nMe/nA values (0.03>nMe/nA>0.17), there is still a great distance between two Pt sites for some of the n-alkene molecules, resulting in several consecutive transformations of n-C_{10} into the mono-branched or multi-branched isomers as shown in Figure 2b. Lastly, for catalysts with relatively high nMe/nA ratio (nMe/nA>0.17), no deactivation due to coking was detected and n-C_{10} molecules were converted sequentially into mono-branched i-C_{10}, then multi-branched i-C_{10} and finally into cracking products as shown in Figure 2c. For these catalysts, n-C_{10} undergoes only one isomerization/cracking step prior to hydrogenation due to the lower number of encountered acid sites. Since it provides the higher isomer/cracking and mono-branched/multi-branched isomer ratios, this reaction mechanism can be considered as ideal for higher isomer production [17].

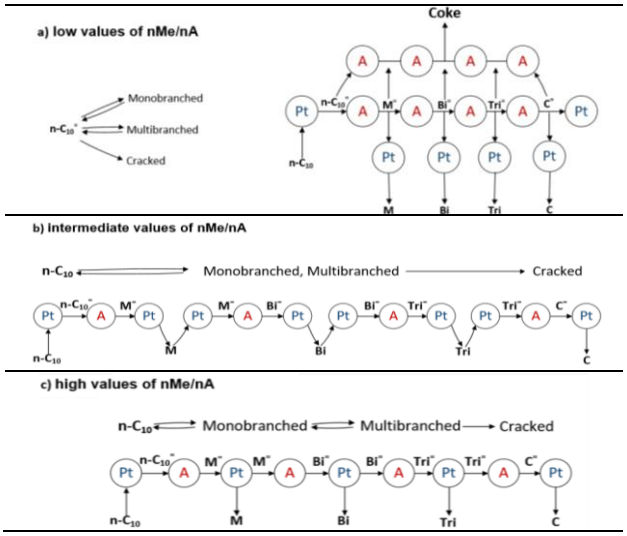

Figure 2: n-C_{10} transformations over bifunctional catalysts at: (a) low values of nMe/nA, (b) intermediate values of nMe/nA, and (c) high values of nMe/nA

Batalha et al. [18] conducted a study over bifunctional catalysts with Pt and HBEA as metal and acid functions to investigate the influences of the metal/acid balance on n-C_{16} hydroisomerization. In the first series (S1), metal functions were located on the outer surface of the HBEA zeolite crystals of 12.5 µm with Pt contents from 0.2 to 1.5 wt.%. The second (S2) and third (S3) series were obtained from an intimate mixture of Pt-Al_2O_3 and HBEA particles of 70 µm and a physical mixture of Pt-Al_2O_3 and HBEA particles of 300 µm, respectively. For all catalyst series, TOF increases with nMe/nA until it approaches a nearly constant behavior, where the acid functions become rate limiting. For the same nMe/nA values, the S1 series of catalysts exhibit the highest TOF, followed by S2 and S3, suggesting higher activity with an increased degree of proximity between metal and acid functions. These findings also suggest that bifunctional catalyst performance is affected not only by the nMe/nA but also by the separation of metal and acid sites. The degree of proximity was quantified by the number of acid sites encountered by intermediates throughout their diffusion between two Pt sites, n_{as}. This value should be close to 1 to catalyze only one skeletal rearrangement or cracking reaction of the olefinic intermediates diffusing between two Pt sites. When the distance between two active sites increases from 0.01 µm to 300 µm, all the n_{as} values change from 1 to 3.05 and the yield of i-hexadecane (i-C_{16}) decreases from 80 % to 20 % [18].

As a general conclusion of the aforementioned studies, the average number of acid sites in contact with an n-alkane molecule during hydroisomerization should be close to one in order to obtain a single reaction on the acid sites during their diffusion from the Pt sites. For this condition to occur, nMe/nA values would need to be high enough. However, an excessive amount of metal sites would block the pore openings and, consequently, limit n-alkane conversion and increase the cost of preparation. Thus, the possibility of an optimal range of nMe/nA values for achieving catalytic performances over bifunctional catalysts should be investigated [15]. Lastly, the nMe/nA value is not the only parameter affecting the catalytic properties, but the proximity between metal and acid sites also has a strong effect on the catalytic performance of the bifunctional catalyst.

B. The Effects of the Distance Between Metal and Acid Sites on the Bifunctional Catalyst Performance

The distance between the metal and acid sites has also been presented as a strong influence in the catalytic performance of bifunctional catalysts. A well-balanced catalyst is described as an ideal bifunctional catalyst if it satisfies the metal acid balance and proximity criteria [14]. The distance between metal and acid sites is mainly dependent on the noble metal site deposition location and the zeolite crystal particle size and thickness.

1) The effects of different metal site depositions on the diffusion distance and bifunctional catalyst performance

A criterion for optimal site proximity was initially proposed by Weisz et al. [19], who stated that the closest distance between the metal and acid sites is necessary for optimal activity and selectivity. Pt/C or Pt/SiO_2 metal site particles and silica-alumina acid site particles in millimeter and micrometer scales were prepared and then mixed together. Due to the limitation of techniques at that time, the distance between metal and acid sites was tuned by varying the size of the mentioned particles for n-heptane (n-C_7) hydroisomerization. It was found that the yields of i-heptane (i-C_7) over catalysts with smaller component particle size, such as 5 or 70 µm, were higher than those of catalysts with 1000 µm particle size. The reason can be explained by the diffusivity of n-alkane intermediates. If there is a large distance between sites, reactions become controlled by the slower diffusion processes, resulting in a diminishment of catalytic activity. As a result, i-alkenes are more likely to undergo secondary reactions, leading to a rise in the production of both gas and coke [19].

Since the abovementioned research examined the effects of metal sites acid sites distance on the millimeter and micrometer scales, further research of the effects of intersite distances in the nanometer and atomic scales distance between two active sites needed to be conducted. In recent years, several researchers have looked into these scales by employing enhanced deposition methods.

Samad et al. [12] studied the proximity criterion using several bifunctional catalysts with different Pt distribution over an acidic silica-aluminum support for n-C_7 isomerization. Different degrees of proximity between metal and acid sites were explored, including atomic, nanometer, micrometer, and millimeter scales, as shown in Figure 3. The Pt sites were electrostatically deposited onto silica by utilizing cationic tetraamine ($Pt(NH_3)_4^{2+}$) precursors (PTA-11) at high pH values (atomic scale proximity), onto alumina by employing anionic hexachloride ($PtCl_6^{2-}$) Pt precursors (CPA-4) at low pH values (nanometer scale proximity). The micrometer and millimeter scale proximities between metal and acid sites were obtained by physical mixtures (PM) of metal and acid functions and addition of inert layers (L-1) made of quartz wool to further separate the metal and acid functions, respectively.

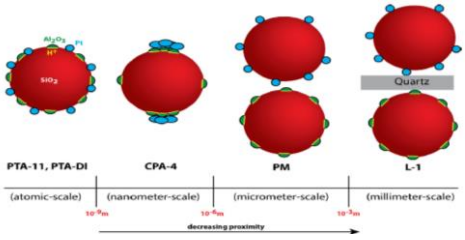

Figure 3: Schematics of catalyst configurations with varying degrees of intimacy between active sites [12]

Results of this study showed that if the distance between two active sites increases to the millimeter scale, catalysts will approximately behave as monofunctional catalysts and their performance will decline quickly due to the fact that alkene intermediates cannot diffuse very far between two active sites. Thus, a large distance between sites prevents the isomerization reaction from taking place. Moreover, a higher selectivity toward isomer products is achieved by nanometer and micrometer scale proximities between metal and acid instead of an atomic scale separation [12].

Gutierrez-Acebo et al. [14] explored the performance of Pt/EU-1 zeolite catalysts for ethylcyclohexane (ECH) hydroconversion with a metal/acid proximity in the nanometer and micrometer scales. The distance between sites was adjusted by depositing Pt particles either on the zeolite (Pt-HEU-1/Al_2O_3) or the alumina support (Pt-Al_2O_3/HEU-1). The results show that similar activities and selectivities are achieved for both types of catalysts at the same nMe/nA values. It indicates that the proximity of Pt and acid sites provides enhanced results toward isomerized products in both the micrometer and nanometer scale distances [14]. These results are in line with those found by Samad et al. [12].

Zecevic et al. [11] also performed a study to investigate the nanometer and atomic scale proximity between the active sites over bifunctional Pt/Y catalysts. The Pt metal precursors were deposited on the Al-binder by an electrostatic adsorption method (Pt-A/Y) and in the zeolite by an ion-exchange method (Pt-Y/A). In Figure 4a, Pt particles are located inside the zeolite pores with the closest proximity to the acid sites, whereas in Figure 4b, Pt is deposited on the binder within a nanometer scale distance from the metal sites.

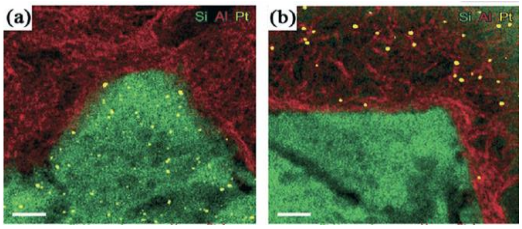

Figure 4: EDX map of (a) Pt- Y/A and (b) Pt- A/Y catalyst [11]

According to the isomerization results shown in Figure 5, the conversion activity of n-C_{10} and n-nonadecane (n-C_{19}) feedstocks over both catalysts are almost identical. The product selectivities for both feedstocks show that the Pt-A/Y catalyst yields more isomer products than the Pt-Y/A catalyst. For the Pt-Y/A catalyst, the alkane feedstock diffuses through the micropores of the zeolite to undergo an HD/DHD reaction at the metal site. It is suggested that the intermediate molecules generated on the metal sites are retained in the zeolite micropore network due to the strong adsorption on acid sites. Consequently, it results in an increment in their residence time in the acidic environment, which leads to an increase in their cracking possibility and a decreased selectivity towards the desired products. On the other hand, for the Pt-A/Y catalyst, the acid sites are more reachable for the alkene intermediates formed on the metal sites. The alkene intermediates generated on the metal site diffuse from the wider pores of the alumina binder to the Y-zeolite, where they undergo isomerization on the outside and then diffuse immediately back to a metal site on the alumina binder. Consequently, the cracking of alkene intermediates is reduced and the isomer product yield is increased. In this study, it was found that closer distances between both functions are detrimental for the isomerization selectivity [11].

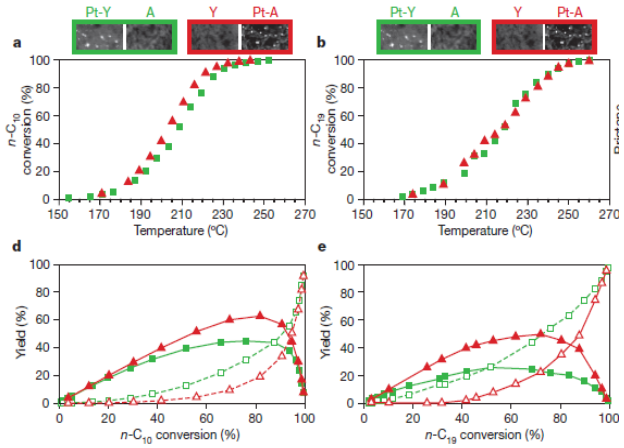

Figure 5: The conversion of the (a) n-C_{10}, and (b) n-C_{19} versus the reaction temperature for Pt-Y/A (green squares) or Pt-A/Y (red triangles) catalysts. Product yields from (d) n-C_{10} and (e) n-C_{19} feedstock. (Solid lines and filled symbols: isomerized products; dashed lines and open symbols: cracked products) [11]

In the study conducted by Lv et al. [8], a series of Pt/SAPO-11 catalysts were prepared by using IWI, CI, and a combination of CI and IWI (CI-IWI) methods with different Pt loadings (wt.%). Catalytic performance of the bifunctional catalyst, including conversion and selectivity, was assessed using n-C_{19} as a model feedstock. The characterization results indicate that Pt sites on CI-prepared catalysts were primarily located on the external surface through electrostatic interactions, whereas the Pt sites on IWI-prepared catalysts were mostly distributed near the micropore mouth of SAPO-11 and a small amount of them on the external surface. In Figures 6a and 6b, the IWI0.25 and CI0.5-IWI0.25 catalysts show higher activity and isomerization selectivity than the catalyst prepared by the CI method. Moreover, when only the catalysts prepared by the CI method are evaluated, it is found that performance increases up to the catalyst with 0.5 % Pt loading. Activity and selectivity for higher Pt loading remain largely the same. However, it can be seen in Figure 6 that increasing the Pt sites near to the micropores mounts (IWI-prepared catalyst) provides a higher activity than increasing the amount of the Pt particle in the CI-prepared catalysts. It was proposed that isomerization selectivity can be enhanced by raising the concentration of the Pt sites close to the micropore mouth. Therefore, n-alkenes can diffuse more easily to the acid sites for their subsequent transformation into i-alkene intermediates, achieving higher isomerization selectivity.

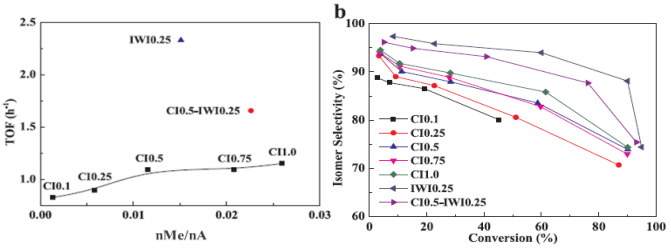

Figure 6: (a) TOF versus nMe/nA value and (b) isomerization selectivity as a function of conversion of n-C_{19} [8]

As a conclusion, the placement of the Pt sites, and their separation with acid sites, can have a significant impact on product selectivity. It would be preferable to deposit the Pt sites close to the micropore mouth aiming for a nanometer scale proximity with acid sites [8].

2) The effects of zeolite crystal particle size and thickness on the diffusion distance and catalyst performance

In addition to the Pt loading method, the particle size and thickness of zeolite crystals also affects the distance between metal and acid functions within the microporous or mesoporous structure on the catalyst.

Li et al. [1] studied the hydroisomerization of n-C_{10} over two different bifunctional catalysts with an original zeolite (Pt/AY-ori) and an alkali-treated zeolite (Pt/AY-alk). The average size of zeolite crystals for Pt/AY-ori and Pt/AY-alk catalysts were found by XRD analysis to be 687 nm and 501 nm, respectively. It is clear that the particle size of the original zeolite crystals is reduced by the alkali treatment. It was found that the Pt/AY-alk catalyst displays slightly higher activity than the Pt/AY-ori catalysts. Since the Pt/AY-alk catalyst has particle sizes, it possesses the improved dispersion of the protonic sites than in Pt/AY-ori [7]. Therefore, the alkene intermediates are less likely to only diffuse through the non-acidic alumina route between two Pt sites in Pt/AY-alk. Also, the Pt/AY-alk catalyst provides more isomerized products with a high mono-branched to multi-branched ratio than the Pt/AY-ori catalyst. It is claimed that the shorter transport distance of an intermediate molecule within the micropores can be achieved with a smaller zeolite crystal size. It results in a lower number of acid sites that intermediate molecules can encounter during their movement inside the zeolite microporous structure and a decreased possibility of undesired secondary reactions [1].

Zhang et al. [13] studied the performance of the micro/mesoporous Pt metal loaded Y/MCM-41 bi-porous composite bifunctional catalysts, Pt/MY-0, Pt/MY-2, and Pt/MY-5, for the hydroisomerization of the n-dodecane (n-C_{12}). The Y/MCM-41 materials include the original Y zeolite and alkali-treated Y zeolites for 2 and 5 hours, which are respectively represented as MY-0, MY-2, and MY-5. As shown in Figure 7, the particle sizes of the Y zeolite crystals become diminished with the alkali-treatment and particle size reduction is determined by the treatment time. The mean particle size for MY-0, MY-2, and MY-5 were found to be 653 nm, 548 nm, and 421 nm, respectively. Also, the original sample has a cleaner and smoother outer surface, whereas the alkali-treated particles have irregular shapes, rough boundaries, and large openings on the zeolite other layers. Deposited Pt particles were located on the mesoporous MCM-41 materials and the external surfaces of the Y zeolite crystals since the average diameters of Pt crystal particles (4.0 nm) were larger than the zeolite micropores (1.0 nm).

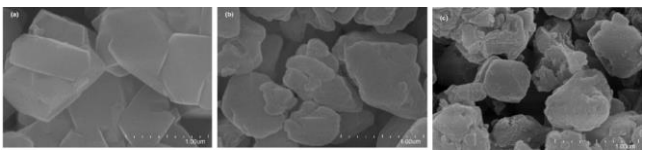

Figure 7: SEM images of Y zeolite crystals: (a) Y-0, (b) Y-2 and (c) Y-5 [13]

The Pt metal-loaded micro/mesoporous composite catalyst is developed by combining the most favorable features of both microporous crystalline zeolites and mesoporous materials. The microporous zeolite provides high acidity, whereas the mesoscale pores ensure reduced diffusion limitations and lower molecular residence time [13]. The composite catalyst is formed as a result of coating the external surface of Y-zeolite crystals with the mesoporous MCM-41 layer. Additionally, there is another independent MCM-41 mesoporous phase around the composite particles. Both MCM-41 phases, the layer covering the Y-zeolite surface and the independent layer, work harmoniously to prevent the closer proximity of the Y-zeolite crystals, providing better dispersion of the Y crystals in the bi-porous catalytic system. With better dispersion, the possibility of an extended diffusion distance due to the close proximity of zeolite crystals is minimized [13].

The conversion activity and the product selectivity results are in the same approach as Li et al. [1]'s study. The Pt/MY-5 and Pt/MY-2 alkali-treated catalysts have superior conversion than the Pt/MY-0 catalyst. Also, the alkali-treated catalysts, with a smaller particle size of the zeolite component, provide more isomerized products and less cracked products than Pt/MY-0 catalyst, yielding mostly mono-branched isomers. Diffusion distances of the alkene intermediates in alkali-treated Pt/MY-2 and Pt/MY-5 catalysts are shorter than in the Pt/MY-0 catalyst due to smaller particle size. There is a lower possibility for alkene intermediates to encounter multiple acid sites throughout their movement within the zeolite crystal of the Pt/MY-0 catalyst, which leads to less skeletal transformations of alkene intermediates and more unwanted secondary reactions such as multiple branching and cracking reactions [13].

Kim et al. [20] prepared a bifunctional catalyst with Pt nanoparticles (NPs) loaded on MFI-type (ZSM-5) zeolites and different crystal thicknesses ranging from 2 to 300 nm to explore the effect of zeolite crystal thickness and Pt location on the hydroisomerization of n-C_7. In this study, 2 nm thick MFI zeolite nanosheets, a nanocrystalline MFI zeolite of 10 nm thick, a bulk zeolite with approx. 300 nm crystal thickness and a commercial MFI zeolite of 40 nm crystal thickness were produced and identified as NS-2, NC-10, B-300, and C-40, respectively. It was suggested that reducing the length of the diffusional paths by creating nanocrystalline zeolites or mesopores within the zeolite crystal facilitates diffusion in the zeolite, resulting in increased isomer selectivity.

The location and size of Pt particles on the conventional ZSM-5 and 2 nm thick MFI nanosheets prepared by IE and CI are displayed in Figure 8 [20]. For the catalysts prepared by the IE method, the Pt NPs are near the acid sites, whereas for the catalysts prepared by the CI method, the Pt NPs are deposited only on the external surfaces. Moreover, it can be seen that for the 2 nm nanosheets the distance between metal and acid sites is almost the same, independent of the preparation method, whereas, for larger nanosheets, there is a big difference in the distance between metal and acid sites for both methods.

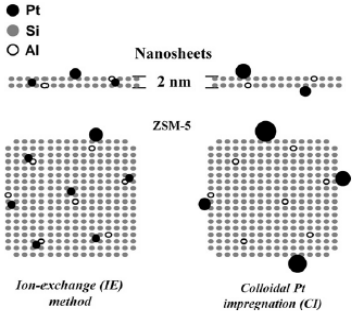

Figure 8: Schematic representation of Pt locations in conventional ZSM-5 and 2-nm thick MFI nanosheets prepared by the IE and CI methods [20]

In this study, it was found that the i-C_7 yield increases with decreasing crystal thickness for both catalyst preparation methods, as shown in Figure 9. The maximum selectivity towards i-C_7 was 48 % and 49 % for Pt(IE)/NS-2 and Pt(CI)/NS-2, respectively. When comparing both methods, all catalysts show a very similar maximum i-C_7 selectivity except the Pt(IE)/B-300 and Pt(CI)/B-300 catalysts. Nevertheless, the effect of the zeolite crystal thickness is more impactful than the location of the Pt NPs on bifunctional performance. For example, the selectivity difference between Pt(IE)/NS-2 and Pt(IE)/B-300 is much larger than the difference between Pt(IE)/B-300 and Pt(CI)/B-300. This increase in isomer selectivity for the thin zeolite crystals can be linked to shorter diffusion distances of branched isomers inside the zeolite, resulting in a lower probability of cracking reactions [20].

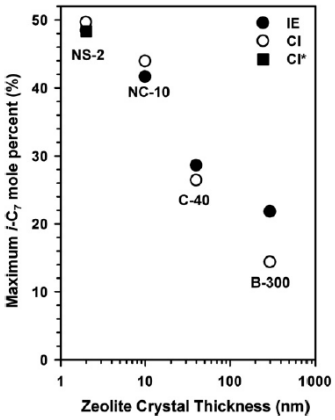

Figure 9: Summary of maximum isomer yield

III. Conclusions and Recommendations

As a result of this literature review, it was found that a relatively high nMe/nA value is required for an ideal catalytic performance over a bifunctional catalyst. Moreover, it is suggested that if Pt metal particles are placed within a nanometer scale proximity to the micropore mouth of the zeolite and if the zeolite crystals have a comparably smaller size, greater bifunctionality and optimal high-quality diesel production can be achieved. Under these conditions, alkene intermediates created at metal sites have a diminished residence in the zeolite micropores. This could potentially decrease the likelihood of secondary unwanted reactions, such as multi-branching and cracking, and increases the fuel quality by enhancing the selectivity toward the isomerized products.

The original scope of this study included an experimental examination of the impact of different metal and acid site dispersions on the performance of a bifunctional catalyst for n-hexane (n-C_6) conversion. Then, the distance between the metal and acid sites was planned to be included in a microkinetic model using the obtained experimental results. Due to the unexpected COVID-19 pandemic, the planned experiments could not be executed. As a future study, experimental data could be used to develop a kinetic model that directly considers the influence of the distance between metal and acid sites. A rate equation that takes the degree of intimacy as an additional parameter could be employed as a reference for improving or optimizing the design of bifunctional catalysts.

Acknowledgments

The author would like to thank J.I. Mirena, V. Galvita, J. Thybaut, and P. Mendes for their guidance and supports, and Ghent University for its financial support.

References

[1] M. Li, Y. Zhang, H. Wang, S. Yu, D. Liu and Y. Wang, "Influence of zeolite crystal size on selective conversion of n-alkane: Controlling intermediates' diffusion distances inside the micropores," Fuel, vol. 254, p. 115709, 2019.

[2] S. Dehkissia, F. Larachi and E. Chornet, "Catalytic (Mo) upgrading of Athabasca bitumen vacuum bottoms via two-step hydrocracking and enhancement of Mo–heavy oil interaction," Fuel, vol. 83, no. 10, pp. 1323-1331, 2004.

[3] "International Energy Outlook," U.S. Energy Information Administration, Washington, DC, 2019.

[4] L. C. Castañeda, J. A. D. Muñoz and J. Ancheyta, "Combined process schemes for upgrading of heavy petroleum," Fuel, vol. 100, pp. 110-127, 2012.

[5] L. L. Cam, T. Nguyen, T. D. T. Kim, N. A. Gaidai, Y. A. Agafonov, A. H. Cam, H. T. Cuong and A. L. Lapidus, "Kinetics of n-hexane isomerization over supported palladium catalysts," Kinetics and Catalysis, vol. 58, no. 3, pp. 311-320, 2017.

[6] S. C. Korre, M. T. Klein and R. J. Quann, "Hydrocracking of polynuclear aromatic hydrocarbons. Development of rate laws through inhibition studies," Industrial & engineering chemistry research, vol. 36, no. 6, pp. 2041-2050, 1997.

[7] P. M. Lima, T. Garetto, C. L. Cavalcante Jr and D. Cardoso, "Isomerization of n-hexane on Pt–Ni catalysts supported on nanocrystalline H-BEA zeolite," Catalysis Today, vol. 172, no. 1, pp. 195-202, 2011.

[8] G. Lv, C. Wang, K. Chi, H. Liu, P. Wang, H. Ma, Q. Wei and Z. Tian, "Effects of Pt site distributions on the catalytic performance of Pt/SAPO-11 for n-dodecane hydroisomerization," Catalysis Today, vol. 316, pp. 43-50, 2018.

[9] P. S. Mendes, J. M. Silva, M. F. Ribeiro, A. Daudin and C. Bouchy, "Synergies, cooperation and other effects: a review for hydroconversion catalysts," Catalysis Today, 2019.

[10] M. Guisnet, ""Ideal" bifunctional catalysis over Pt-acid zeolites," Catalysis today, vol. 218, pp. 123-134, 2013.

[11] J. Zecevic, G. Vanbutsele, K. P. de Jong and J. A. Martens, "Nanoscale intimacy in bifunctional catalysts for selective conversion of hydrocarbons," Nature, vol. 528, no. 7581, p. 245, 2015.

[12] J. E. Samad, J. Blanchard, C. Sayag, C. Louis and J. R. Regalbuto, "The controlled synthesis of metal-acid bifunctional catalysts: The effect of metal: acid ratio and metal-acid proximity in Pt silica-alumina catalysts for n-heptane isomerization," Journal of catalysis, vol. 342, pp. 203-212, 2016.

[13] Y. Zhang, D. Liu, Z. Men, K. Huang, Y. Lv, M. Li and B. Lou, "Hydroisomerization of n-dodecane over bi-porous Pt-containing bifunctional catalysts: Effects of alkene intermediates' journey distances within the zeolite micropores," Fuel, no. 236, pp. 428-436, 2019.

[14] E. Gutierrez-Acebo, C. Leroux, C. Chizallet, Y. Schuurman and C. Bouchy, "Metal/acid bifunctional catalysis and intimacy criterion for ethylcyclohexane hydroconversion: when proximity does not matter," ACS Catalysis, vol. 8, no. 7, pp. 6035-6046, 2018.

[15] W. Wang, C. J. Liu and W. Wu, "Bifunctional catalysts for the hydroisomerization of n-alkanes: the effects of metal-acid balance and textural structure," Catalysis Science & Technology, 2019.

[16] Y. Zhang, W. Wang, X. Jiang, X. Su, O. Kikhtyanin and W. Wu, "Hydroisomerization of n-hexadecane over a Pd–Ni2P/SAPO-31 bifunctional catalyst: synergistic effects of bimetallic active sites," Catalysis Science & Technology, pp. 1-10, 2017.

[17] F. Alvarez, F. R. Ribeiro, G. Perot, Y. C. Thomazeau and M. Guisnet, "Hydroisomerization and Hydrocracking of Alkanes: 7. Influence of the Balance between Acid and Hydrogenating Functions on the Transformation ofn-Decane on PtHY Catalysts," Journal of Catalysis, vol. 162, no. 2, pp. 179-189, 1996.

[18] N. Batalha, L. Pinard, Y. Pouilloux and M. Guisnet, "Bifunctional hydrogenating/acid catalysis: quantification of the intimacy criterion," Catalysis letters, vol. 143, no. 6, pp. 587-591, 2013.

[19] P. B. Weisz, "Polyfunctional heterogeneous catalysis," Advances in Catalysis, vol. 13, pp. 137-193, 1962.

[20] J. Kim, W. Kim, Y. Seo, J. C. Kim and R. Ryoo, "n-Heptane hydroisomerization over Pt/MFI zeolite nanosheets: Effects of zeolite crystal thickness and platinum location," Journal of catalysis, vol. 301, pp. 187-197, 2013.

Table of contents

List of figures

List of tables

List of symbols

C_{Pt}^{mouth}	Pt site concentration near the micropore mouth
C_{Pt}^{surf}	Pt site concentration on the external surface
C_{Pt}^{total}	Pt site concentration on Pt/SAPO-11
k_i	Forward rate constant in of the i-th step
k_{-i}	Reverse reaction rate constant of the i-th step
$P_{alkenes}$	Partial pressure of alkenes
P_{H2}	Partial pressure of hydrogen
P_{i-P}	Partial pressure of the isomerized product
$P_{isohexanes}$	Partial pressures of isohexanes
$P_{n-hexane}$	Partial pressures of n-hexane
P_{n-P}	Partial pressure of alkane
r_i	Reaction rate of the i-th step
$\theta_{0,a}$	Empty fraction of zeolite micropore sites
$\theta_{0,H+}$	Empty fraction of acid sites
$\theta_{0,Pt}$	Empty fraction of platinum sites
$\theta_{i-carb,H+}$	Coverage of acid sites by isocarbenium ion
$\theta_{i-O,Pt}$	Coverage of platinum sites by isoolefin
$\theta_{i-P,Pt}$	Coverage of platinum sites by isoalkane
$\theta_{i-P,a}$	Coverage of zeolite micropore sites by isoalkane
$\theta_{n,carb,H+}$	Coverage of acid sites by n-carbenium ion
$\theta_{n-O,Pt}$	Coverage of platinum sites by n-olefin
$\theta_{n-P,a}$	Coverage fraction of zeolite micropore sites by n-alkane
$\theta_{n-P,Pt}$	Coverage fraction of platinum sites by n-alkane

List of abbreviations

BAS	Bronsted Acid Sites
Bi/M	Di-branched/Mono-branched isomers yield weight ratio
BTU	British Thermal Units
C/I	Cracking/Isomers yield weight ratio
CI	Colloidal Impregnation
CPA	Anionic hexachloride precursors
DI	Dry Impregnation
EDX	Energy Dispersive X-ray
H/C	Hydrogen/Carbon ratio
HAADF-STEM	High-Angle Annular Dark-Field Scanning Transmission Electron Microscopy
HD/DHD	Hydrogenation/Dehydrogenation
HDM	Hydrodemetallation
HDN	Hydrodenitrogenation
HDO	Hydrodeoxygenation
HDS	Hydrodesulfurization
HTK	High-Throughput Reactor System
IE	Ion-Exchange technique
IWI	Incipient Wetness Impregnation
LHSV	Liquid Hourly Space Velocity
LPG	Liquefied Petroleum Gas
MCM	Mobil Composition of Matter
MD	Middle Distillate
MuB/MB	Multi-branched/Mono-branched isomers yield weight ratio
nMe/nA	Ratio between the total amount of exposed metal sites and the total amount of acid sites
NPs	Nanoparticles
PM	Physical Mixtures
PTA	Cationic tetraamine precursors
SAPO	Silicoaluminophosphate
SIRAL	Silica-alumina hydrates
TAP	Temporal Analysis of Products
TOF	Turnover Frequency
TOS	Time on Stream
Tri	Tri-branched isomer
USY	Ultrastable Y Zeolites
WHSV	Weight Hourly Space Velocity
XRD	X-Ray Diffraction
Y	Zeolite Y
ZSM	Zeolite Socony Mobil

1 Introduction

This study aims to review the most prominent research directions and results on the study of the influence of metal and acid site balance and dispersion on hydrocarbon hydrocracking over bifunctional catalysts. In the first part of the project, the current consumption of the refined petroleum products, the present status of the crude oil reserves, new environmental restrictions, and future projections of oil prices will be examined. Then, the types and features of the various heavy feedstock upgrading processes used in the production of the lighter high-quality petroleum products will be investigated. Hydrocracking processes, which are some of the most essential heavy feedstock upgrade processes in the petrochemical industry, will be examined in more detail, including process operation conditions, raw materials, and product types, process conditions, chemical reactions, and types of catalyst used in the reactor. The main objective of this project is to explore the possibilities of increasing the yield of the isomer products from the hydrocracking process by optimizing hydroisomerization and controlling cracking reactions. To fulfill this objective, bifunctional catalysts typically used for hydrocarbon hydroisomerization will be investigated to obtain information about the most ideal catalyst design, including an examination of various catalyst samples prepared by different methodologies and their reaction mechanisms. The ideal catalyst design can be achieved with an optimal balance and distance between metal and acid sites to maximize isomer products from n-alkane conversion. This study includes a review of the most relevant articles, explanation of the conducted work, and a comparison of the results with the focus on finding the optimal distance between two active sites.

1.1 World energy outlook

World energy consumption is estimated to increase around 50 % between 2019 and 2050 as seen in Figure 1, due to rapid population growth, strong economic development, and enhanced access to energy on the market [3]. Therefore, it is highly necessary to find alternative energy sources or to use current resources in the most effective way considering future energy demands.

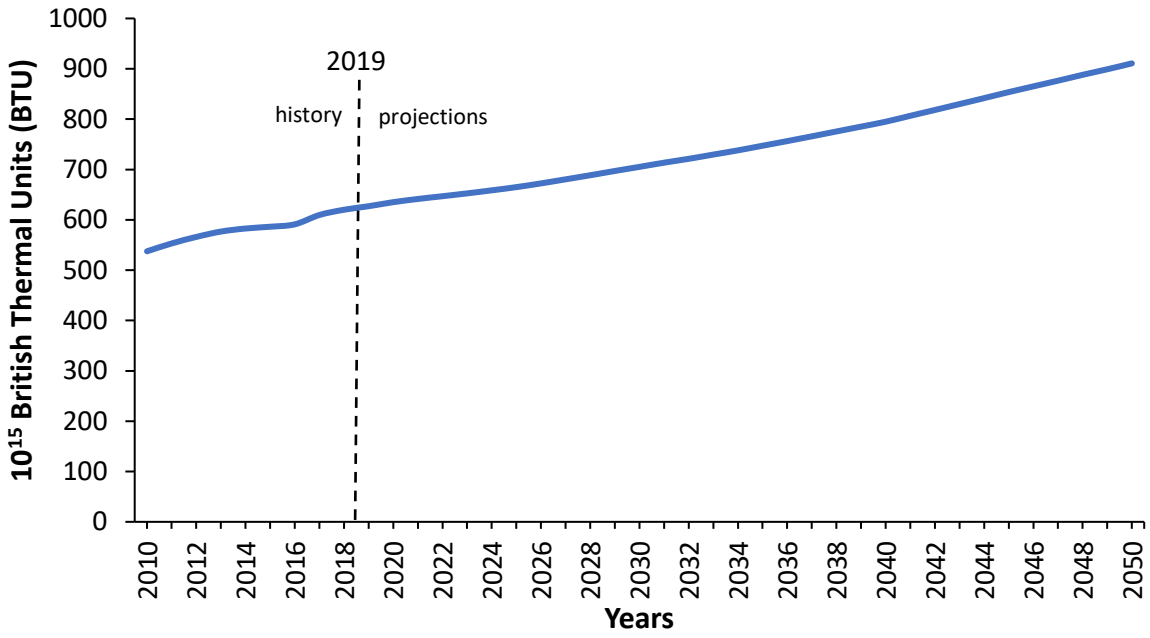

Figure 1. World energy consumption outlook [3]

The world total energy consumption per energy source is presented in Figure 2. It can be seen that the energy consumption is projected to increase for all sources other than coal. Although renewable energy is the world's fastest-growing energy form, fossil fuels will continue to meet much of the world's energy demand. Global consumption of liquid fuels is estimated to rise by more than 20 % between 2019 and 2050, approaching 250 10^{15} BTU in 2050 [3].

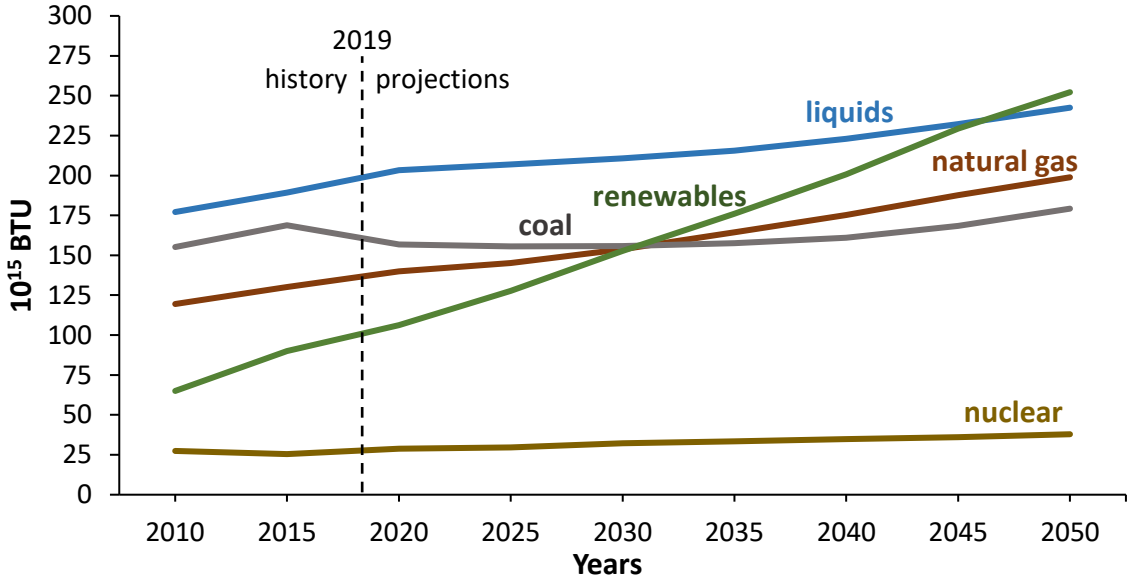

Figure 2. World primary energy consumption per energy source [3]

It can be seen in Figure 3 that, although the overall consumption of refined petroleum and other liquids is expected to increase in the next decades, the consumption share per end-use

sector is estimated to be relatively stagnant. The transportation sector is expected to remain as the largest consumer of liquid fuels such as gasoline, diesel, and jet fuel between 2020 and 2050. The use of petroleum and other liquids in the industry as chemical feedstocks or energy sources is expected to have a slower increase until 2050. The use of liquid fuels in residences, primarily liquefied petroleum gas (LPG) providing heat, is expected to remain constant [3].

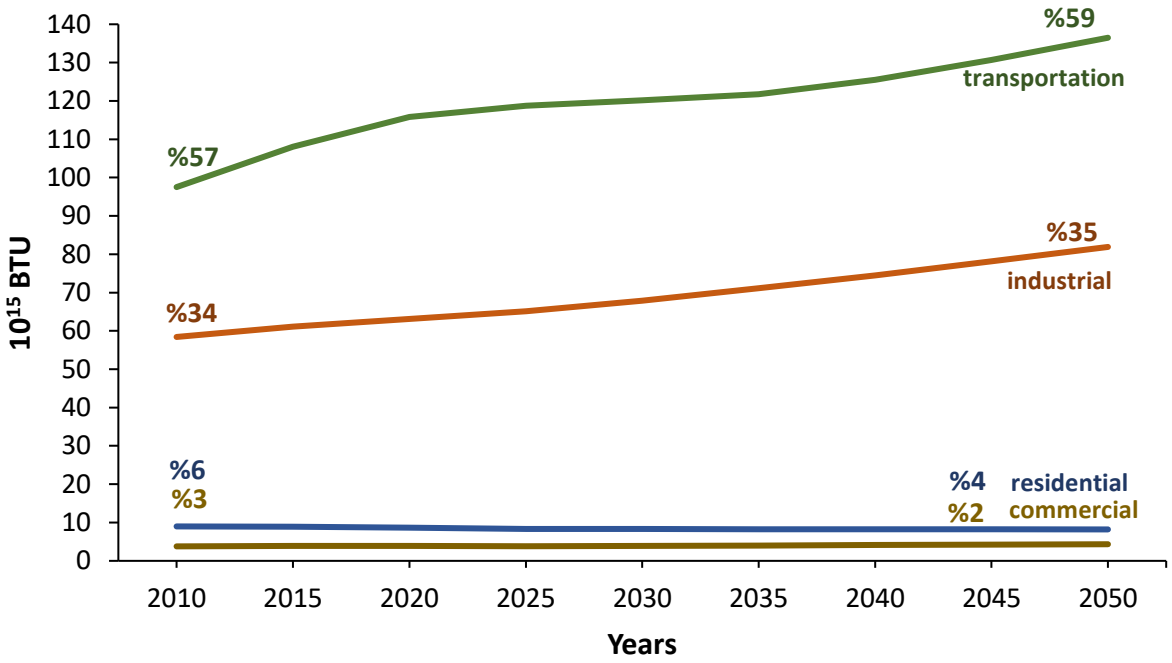

Figure 3. Consumption of refined petroleum and other liquids by end-use sector [3]

Transportation, which constitutes the sector with the largest liquid fuel consumption, has been examined in detail in Figure 4. The estimated consumption of jet fuel, diesel, and gasoline increases between 2018 and 2050. Jet fuel is one of the fastest growing fuels, averaging an increase of 1.76 % per year between 2018 and 2050 due to the expected growth in the air travel sector. Also, diesel presents the second-highest demand, accounting for almost 35 % of all consumption in the transportation sector in 2018. In the long-term, the energy consumption for diesel is anticipated to rise by 6.5 % to attain 46.2 10^{15} BTU in 2050. The consumption of residual fuel oil is expected to decrease by 28 % to reach 5.8 BTU in 2050 because of more strict regulations that would possibly incite a migration from residual fuel oil to diesel [3].

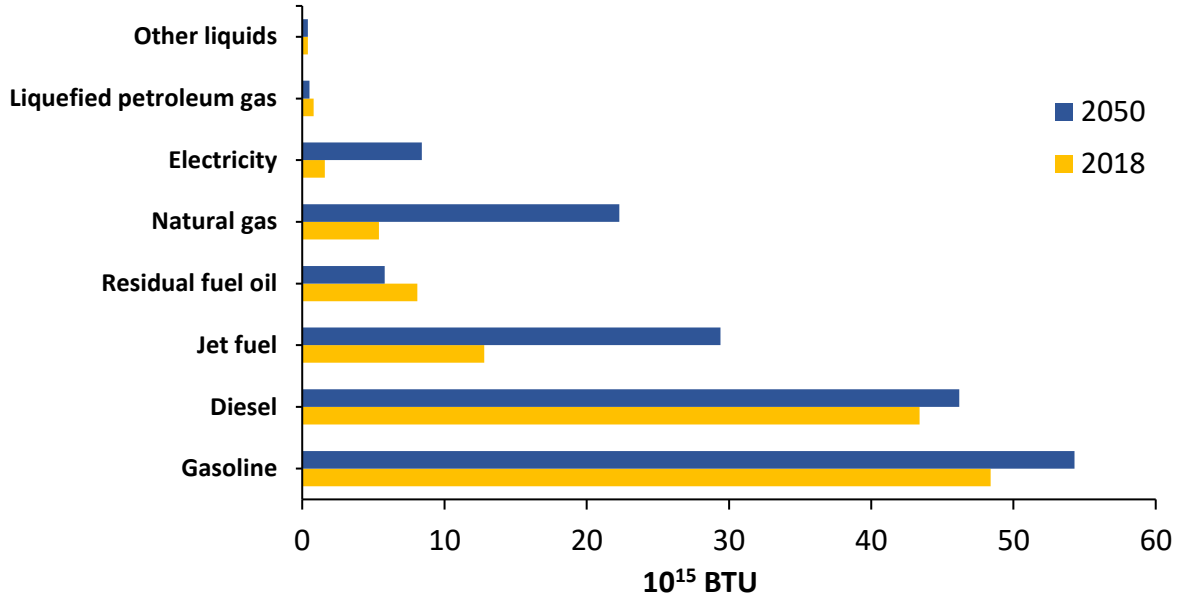

Figure 4. Transportation fuel consumption [3]

Fossil fuels, including gasoline, diesel, and kerosene, still are and will be the primary energy sources for the industrial and transportation sectors. Since most of the crude oil reserves are of heavy or extra-heavy crude oil, the oil industry has been moving in recent years towards refining lower quality, unconventional oil resources such as extra heavy oil, oil sand, and bitumen, to meet the demand for oil derived products [4] [5] [6]. These oil resources require a greater deal of treatment and refining for producing high-quality fuels [7]. Such processes eventually result in the production of significant amounts of petroleum residues such as vacuum residues, atmospheric residues, and de-oiled asphalt, which include contaminants like copper, vanadium, iron, calcium, and silica, phosphorus, oxygen, and sulfur [8]. In order to satisfy future energy demands while minimizing environmental impact, it is crucial to produce high quality fossil fuels with high combustion efficiency and lower emissions of pollutants such as sulfur dioxide (SO_2), nitrogen oxide (NO_x), carbon dioxide (CO_2), carbon monoxide (CO), methane (CH_4), dioxins, hydrogen fluoride (HF), and others [6] [9].

The conversion of residues and heavy crude oils becomes desirable in order to recover lighter, high-value products due to the increasing trend of the price of crude oil, shown in Figure 5 [3]. In a refinery without additional residue upgrading processes, heavy crudes cannot be processed because of the high proportions of impurities and the possibility of coke formation. Therefore, the declining reserves of lighter crude oil, lower crude oil quality, increasing environmental restrictions, and future projections of increasing oil prices have driven the development of processes for upgrading heavy feedstocks, specifically heavy oil, and bitumen.

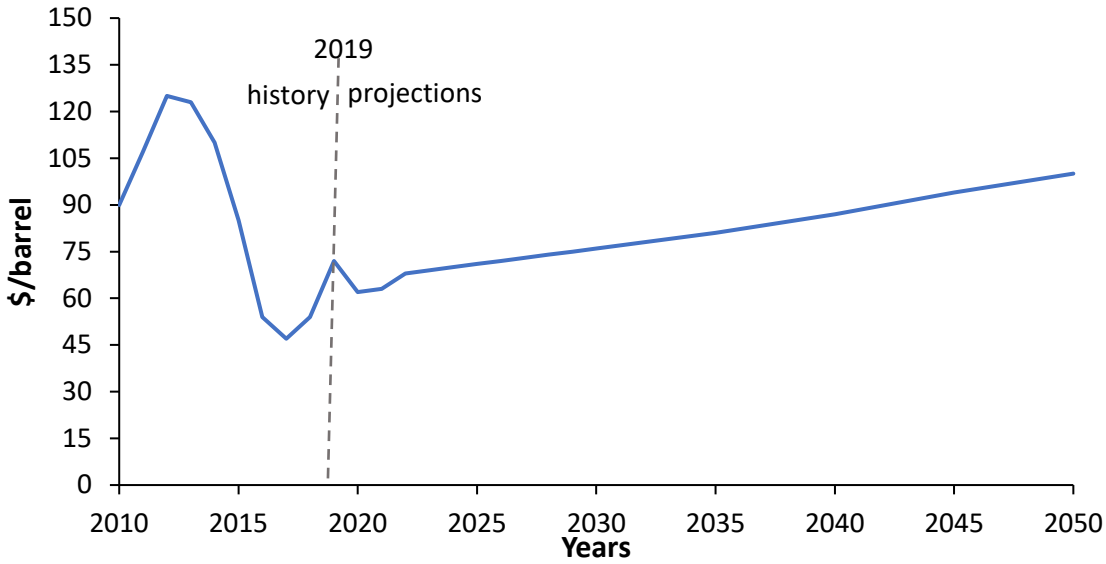

Figure 5. World average oil prices over the years [3]

1.2 Heavy feedstock upgrade processes

The most valuable products from a refinery tend to have high hydrogen/carbon (H/C) ratios, such as gasoline, jet fuel, and diesel. The main goal of petroleum refining processes is to provide products while maximizing profits by yielding an optimal distribution of products with high H/C ratios [7]. To achieve this, two different types of upgrading processes for heavy feedstocks are used. These consist of carbon rejection processes, lowering the C content of products, and hydrogen addition processes, which increase the H content. Carbon rejection processes include visbreaking, coking, solvent extraction, and residue catalytic cracking. The feeds are heated under an inert atmospheric environment to break them into smaller components. These processes transfer the hydrogen from larger to lighter molecules and reject carbon by forming coke. Carbon either in coke or the heavier products is considered as a rejected product because of their much lower value [10]. On the other hand, hydrogen addition processes, such as hydrocracking, fixed bed catalytic hydroconversion, hydrovisbreaking, and hydropyrolysis, consider the reaction of a heavy feedstock with an additional hydrogen supply in the presence of catalysts, which leads to a total increment in H/C ratio [7] [10]. Hydrogen addition processes are suitable for eliminating undesired components such as sulfur, nitrogen, oxygen, and metals which act as catalyst poisons, and fulfill the scarcity of hydrogen, hence produce high quality liquid oil products [11].

Numerous upgrading methods for converting petroleum into economically valuable and useful products are reported in the literature [12]. Amongst them, hydrocracking is recognized as one of the most effective upgrading processes for transforming heavy hydrocarbons into lighter ones [13]. The hydrocracking reactions occur under a high hydrogen partial pressure, elevated

temperature, and in the presence of a bifunctional catalyst. Hydrocracking is useful for upgrading the product streams of the aforementioned processes, including the heavy cycle oil from the catalytic cracker, heavy gas oils from the coker or visbreaker unit, residual fuel oils, and reduced crudes [14]. These feedstocks contain a high amount of sulfur, nitrogen, and metals such as nickel and vanadium. Since these compounds have a poisoning effect on hydrocracking catalysts, the feedstock typically requires hydrotreatment [14]. As a result, most of the hydrocracking processes comprise both hydrotreating and hydrocracking steps [15]. It is a well-established technology for producing enhanced quality middle distillates (MDs) by lowering their boiling points and removing impurities such as sulfur, nitrogen, and heavy metals. It increases refining margins by improving low-value products to high-demand products such as gasoline, diesel, and kerosene [16]. The main feedstock and products are summarized in Table 1 [14].

Table 1. Main Hydrocracking feedstocks and products [14]

FEEDSTOCK	PRODUCTS
Naphtha	LPG
Atmospheric gas oils	Naphtha
Atmospheric residue	Diesel
Vacuum gas oil	LPG
	Naphtha
	Ethylene feedstock
	Kerosene/jet fuel
	Diesel
	Lube oil base stock
Vacuum residues	LPG
	Naphtha
	Kerosene/jet fuel
	Gasoil
	Fuel oil
Tars and derived bitumen's (metal content<500 ppm)	Diesel

Hydrocracking technology plays a crucial role as one of the major conversion processes in refineries, as seen in Figure 6 [17]. The flexibility of the hydrocracking process provides several possible process configurations. These configurations can be divided into two major categories: single-stage and two-stage. The differences between both of these are a partial or complete conversion of feed to lighter products, the type of catalyst, and process selectivity [18]. The typical hydrocracking process utilizes reactors with fixed catalytic beds with a temperature between 300-500 °C, total pressure between 85-200 bar, hydrogen-to-oil-ratio between 500-1700 Nm^3m^{-3}, corresponding to molar hydrogen to oil ratio of about 8 to 30, and

hydrogen consumption between 200-600 Nm^3m^{-3}, corresponding to a molar hydrogen consumption of about 4 to 10 per mole of oil fed [14]. Due to the overall exothermic nature of the hydrocracking process, multiple beds are generally used and cooling is achieved by introducing hydrogen recycle gas between catalyst beds [15]. The catalytic environment has significant benefits, such as high conversion rate, less coke formation, stable products, and applicable adjustment of diverse feedstocks [12]. On the other hand, the required high pressure equipment, consumption of hydrogen, and catalysts result in huge capital and operating costs. Additionally, feedstocks with a high concentration of asphalt and resins can greatly impact catalyst activity due to coke formation. It is also challenging to achieve a high-quality MD fraction while preventing coke formation reactions [11]. Despite the high costs and challenges, hydrocracking is still considered an efficient technology because of its lighter, high-quality and valuable products, which are required to meet the environmental legislation covering transportation and heating fuels.

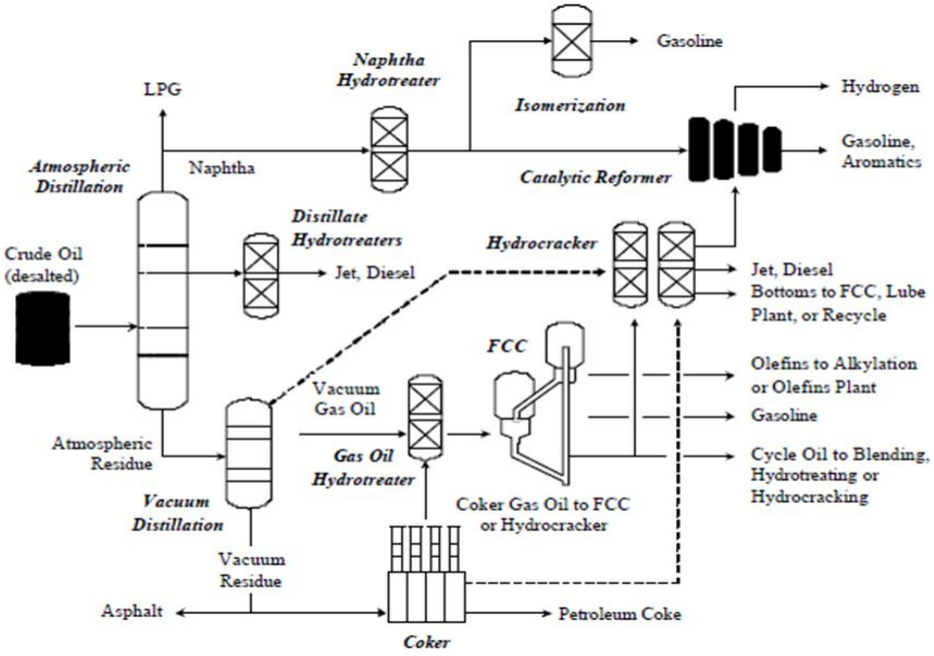

Figure 6. Flow diagram of a typical high-conversion oil refinery [17]

The chemistry of hydrotreating and hydrocracking is commonly referred to as hydroprocessing. There are two types of reactions occurring in hydroprocessing units: the elimination of impurities and hydrocarbon cracking. Hydrotreating is performed to remove heteroatom impurities present in the feedstocks. For instance, transforming sulfur (S) atoms into hydrogen sulfide (H_2S), nitrogen (N) atoms into ammonia (NH_3), and oxygen (O) atoms into water (H_2O) [19]. Hydrocracking transforms long-chain components in the feed to products with a lower molecular weight by splitting the side chains and saturating the aromatics and olefins. Table 2 lists the chemical reactions that typically occur in hydroprocessing units [15]. These reactions are very hydrogen-consuming and strongly exothermic, so controlling heat

release is one of the most important considerations in the design and operation of hydrotreaters and hydrocrackers [14]. The conversions in hydroprocessing can be categorized as favorable or unfavorable reactions. Desulfurization, denitrogenation, saturation, and cracking are favorable reactions. Catalyst poisoning and coking (metals deactivating the catalyst) are unfavorable reactions typically occurring in hydroprocessing units [15]. One of the distinctive features of the hydrocracking process is the ability to isomerize alkanes to a large extent before cracking reactions become significant [20].

Table 2. List of the hydroprocessing reactions [15]

REACTION TYPE	REACTIONS
Minimal C–C bond breaking	
Hydrodesulfurization (HDS)	$\mathbf{R-S-R^{*} + 2H_2 \rightarrow RH + R^{*}H + H_2S}$
Hydrodenitrogenation (HDN)	$\mathbf{R=N-R^{*} + 3H_2 \rightarrow RH + R^{*}H + NH_3}$
Hydrodeoxygenation (HDO)	$\mathbf{R-O-R^{*} + 2H_2 \rightarrow RH + R^{*}H + H_2O}$
Hydrodemetallation (HDM)	$\mathbf{R-M + ½\,H_2 + A \rightarrow RH + MA}$
Saturation of aromatics	$\mathbf{C_{10}H_8 + 2H_2 \rightarrow C_{10}H_{12}}$
Saturation of olefins	$\mathbf{R=R^{*} + H_2 \rightarrow HR-R^{*}H}$
Isomerization	$\mathbf{n-RH \rightarrow i-RH}$
Significant C–C bond breaking	
Dealkylation of aromatic rings	$\mathbf{\theta-CH_2R + H_2 \rightarrow \theta-CH_3 + HR}$
Opening of naphthene rings	$\mathbf{Cyclo-C_6H_{12} \rightarrow C_6H_{14}}$
Hydrocracking of paraffins	$\mathbf{R-R^{*} + H_2 \rightarrow RH + R^{*}H}$
Other reactions	
Coke formation	$\mathbf{2\,\theta-H \rightarrow \theta-\theta + 2H_2}$
Mercaptan formation	$\mathbf{R=R^{*} + H_2S \rightarrow HSR-R^{*}H}$

Environmental regulations limit the concentration of aromatics, olefins, and oxygen-containing compounds in gasoline, as a result, the octane number decreases [21]. This decrease can be compensated by blending gasoline with isomers of n-pentane (n-C_5) and n-C_6 alkanes, which have a higher octane number than their n-alkane forms [22]. The isomerization of n-C_5 and n-C_6 alkanes is typically carried out over bifunctional catalysts containing Pt or palladium (Pd) supported on an acid material [21]. Therefore, it would be beneficial to investigate and improve the conversion of n-alkanes into their branched isomers over a bifunctional catalyst.

1.3 Bifunctional catalysts

Bifunctional catalysts containing acid and metal sites are utilized in hydrotreating and hydrocracking processes [23] [24]. The acid sites provide the cracking reaction, and metal sites provide hydrogenation–dehydrogenation (HD/DHD) reactions [16] [25]. These catalysts

were first created for the catalytic reforming of naphtha and have been used industrially since the 1950s [26]. Today, metal and acid bifunctional catalysts have become a basic part of many industrially relevant chemical processes for energy, environmental, and consumer-based applications [27]. Some of these processes include selective ring-opening (an increase of cetane number), hydroisomerization (an increase of octane number), hydrocracking of heavy oils, reforming, and dewaxing [28] [29] [30]. Hydroconversion processes aiming for the hydroisomerization and hydrocracking of alkanes can also be conducted by the monofunctional acid catalysts. However, bifunctional catalysts are more advantageous, since they provide the opportunity to perform hydroconversion processes under milder conditions, e.g. at lower temperatures [31]. The conversion of saturated hydrocarbons into unsaturated ones over the metal sites are much more reactive than on the monofunctional acid catalyst [26]. With a bifunctional catalyst, broader product varieties can be achieved and the product distribution can be more easily adjusted via the operating conditions [32]. Their selectivity to the target products is generally much higher than the selectivity of monofunctional acid catalysts [33]. Also, the production of petroleum products or fine chemicals, which entails several sequential reaction steps catalyzed by acid and metal sites, can be produced in one apparent step [34]. As a result, bifunctional catalysts provide a significant reduction in energy consumption and waste generation [35].

Even though the chosen composition of the catalyst is dependent on the desired product and the feedstock to be processed, common properties can be observed for all bifunctional catalysts [26]. The bifunctional catalysts are made up of Bronsted acid sites (BAS) for the skeletal isomerization and metal sites for the HD/DHD reactions [9]. Finely dispersed noble metals, such as Pt and Pd provide the most active metal functions in their reduced state [36]. Amongst noble metals, Pt-based catalysts have been confirmed to outperform Pd-based catalysts, due to a higher hydrogenation capacity and metal dispersion values of the Pt phase [37]. Usual acidic supports for bifunctional catalysts are zeolites (typically USY, Beta, Mordenite, ZSM-5, ZSM-22), silicoaluminophosphates (usually SAPO-11, SAPO-31, SAPO-41), mesoporous materials (typically MCM-41, Al/MCM-41), and amorphous oxides or mixtures of oxides (usually HF-treated γ-Al_2O_3, SiO_2-Al_2O_3, ZrO_2/SO_4^{2-}) [38] [39]. Zeolites are one of the most promising support types due to higher acid strength, low coke-forming tendency, high resistance to contaminants such as aromatic, organic nitrogen, and sulfur, easy regeneration, and molecular shape selectivity [40]. When combined with alumina, they are frequently chosen to provide the acid function in the hydroconversion process because of their large variety of topologies, chemical compositions, and acido-basic properties. Therefore, zeolites are able to provide many different possibilities in the design of catalysts with desired activity and selectivity behaviors [41].

The general mechanism of alkane hydroisomerization over bifunctional catalysts with Pt metal and zeolite acid sites is displayed in Figure 7. The commonly admitted hydrocracking reaction scheme contains seven reaction steps: (1) diffusion of a hydrocarbon molecule to metal site, (2) dehydrogenation of a hydrocarbon molecule on a metal site, (3) diffusion of the resultant olefin to an acid site, (4) isomerization and/or cracking of this olefin on acid sites, (5) diffusion of the products to a metal site, (6) hydrogenation of the reaction products, and (7) diffusion of the reaction product to the gas phase [33].

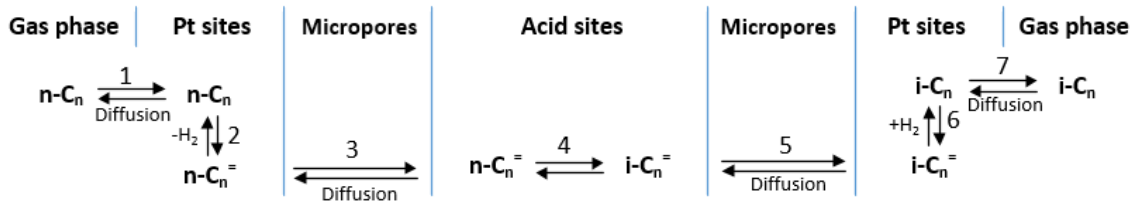

Figure 7. Scheme of alkane hydroisomerization over bifunctional catalysts [33]

The behavior of bifunctional catalysts depends on both the process conditions and the catalytic properties. The chain length of the reacting alkane and the operating conditions can affect the catalyst's selectivity, activity, and stability [20] [42]. The main catalytic property that determines performance is the balance between the metal and acid functions, together with the distance between them [43] [44]. In general, maximum isomerization activity, selectivity, and stability can only be obtained if the acid function is "well-balanced" by the metal function [32]. This implies that the metal function is sufficiently active when compared with the acid function and an appropriate distance between metal and acid sites is attained [26]. The balance between the metal and acid functions is one of the core parameters in the development of a hydrocracking catalyst. By carefully balancing the metal and acid functions, the catalyst selectivity and activity can be adapted to a specific desired product, which is generally chosen to be either gasoline or an MD fraction [45]. An ideal bifunctional catalyst designed on a strong metal function provides flexibility in hydrocarbon conversion [27]. The catalysts with weaker cracking capacity and stronger HD/DHD functions tend to generate higher boiling products, such as middle distillates [46]. The incorporation of metal sites may reduce cracking reactions [47]. On the other hand, in the case of a highly acidic catalyst, a distribution of products with lower boiling products is often attained due to the tendency for excessive cracking, which decreases the overall quality of the fuel [27] [48]. There are multiple routes to make the metal/acid balance more beneficial, such as tuning the ratio between the total amount of exposed metal sites and the total amount of acid sites (nMe/nA), adjusting the distance between both types of active sites, weakening the acid through the use of heteroatom implemented acid supports or reducing the acid density by adding non-acid species and improving the metal function through the formation of bimetallic sites [9] [49] [50].

2 The effects of metal/acid balance on catalytic performances for n-alkane hydroisomerization over bifunctional catalysts

The balance between metal and acid functions determines the hydroisomerization performance for bifunctional catalysts as mentioned in the introduction section. A bifunctional catalyst with a strong metal function and a weak acid function is utilized to maximize the hydroisomerization against hydrocracking of n-alkane [39]. It is stated that if the acid function is stronger than the metal function, the intermediate species on acid sites will undergo a cracking reaction before the HD/DHD reaction on metal sites. In the opposite cases, the conversion of the intermediates towards cracking will be confined due to the limited number of acid functions [9]. Additionally, the proximity between metal and acid sites affects the isomerization yields for bifunctional catalysts [27]. As a result, it is necessary to adjust ratios and distances between both active sites for the improvement of hydroisomerization. In the present study, several articles from literature studies will be discussed to show the effect of the balance between metal and acid sites and the degree of proximity between metal and acid functions.

2.1 The effects of the metal/acid balance on the mechanism and performance of bifunctional catalysts

The effects of metal/acid balance can be experimentally investigated by simultaneously modifying the ratio between metal and acid sites, nMe/nA. This modification can be achieved by changing the density of acid or metal loading. The activity, stability, and selectivity of the catalysts are governed by the nMe/nA ratio. After a certain nMe/nA ratio, where the activity of the metal function is high enough in comparison to the activity of the acid function, both the activity and selectivity of the catalyst depend solely on the acid function [9]. It has been shown that the rate limiting reaction changes from HD/DHD over Pt sites to skeletal rearrangement or cracking of olefinic intermediates over acid sites [44]. The HD/DHD reactions are at quasi-equilibrium and the limiting step occurs on the acid function for an ideal bifunctional catalyst [51]. The fundamental requirement for ideal catalytic performance is that the nMe/nA ratio should be sufficiently high to set the acid-catalyzed skeletal isomerization of alkene intermediates as a rate-limiting step. Thus, the turnover frequency (TOF) of these catalysts becomes high and sequential cracking reactions and coke formation become limited, which leads to improved selectivity, stability, and activity towards MD [52]. However, it has been found that nMe/nA values should be kept within an optimal range for optimal catalytic

performance, which indicates that an excessively high nMe/nA ratio might not be reasonable due to the risk of blocking micropores with metal site particles [9] [53].

Numerous studies have specifically investigated the effect of different nMe/nA values. Wang et al. [9] tested the n-hexadecane (n-C_{16}) hydroisomerization over Pd/SAPO-41 catalysts with different nMe/nA ratios. They found that Pd/SAPO-41 catalysts with nMe/nA values between 0.18 and 0.78 show sufficiently adequate catalytic performances such as higher activity and selectivity towards iso-alkanes products. On the other hand, for catalysts with nMe/nA smaller than 0.18, the cracking of isomer products was increased by the favored acid function. Furthermore, for catalysts with nMe/nA larger than 0.78, the excess amount of Pd particles blocked the micropores of SAPO-41, seriously restraining the diffusion of hydrocarbon chains inside the catalyst [9]. In conclusion, preserving the nMe/nA ratio within an appropriate range is essential for attaining the desired catalytic behavior [53].

Zhang et al. [54] also investigated the effect of the bimetallic sites on the metal/acid balance by preparing the Pd–Ni_2P/SAPO-31 catalyst with 0.05 wt.% Pd and 4 wt.% Ni_2P additions. The highest isomerization yield achieved by the addition of bimetallic sites was 72 %, yet the isomerization yield obtained by only Pd or Ni_2P loadings were 1.74 and 1.10 times lower, respectively. This significant improvement in performance induced by the bimetallic sites is mainly caused by the enhanced metal/acid balance. Figure 8 shows two possible reaction mechanisms for n-C_{16} hydroisomerization and hydrocracking over both Pd/SAPO-31 and Pd–Ni_2P/SAPO-31 bifunctional catalysts, which mainly differ on the nMe/nA value. For Figure 8a, the nMe/nA value is 0.019 and the average number of acid sites in contact with one n-C_{16} molecule during hydroisomerization (n_{as}) is 2.24 for the Pd/SAPO-31 catalyst. For the catalysts with relatively lower nMe/nA values, the parallel hydroisomerization mechanism shown in Figure 8a occurs, indicating that all branched and cracking products are the primary products from the direct conversion of the n-C_{16}. Since there are insufficient metal sites on the catalyst, the number of acid sites that alkene intermediates can encounter during diffusion from the Pt sites is quite high, resulting in a high possibility of consecutive conversion of alkene intermediates. Since the n_{as} value is 2.24, the dehydrogenated alkene intermediates encounter approximately 2 or 3 acid sites during the diffusion step. Therefore, this “unbalanced” parallel hydroisomerization mechanism considers the consecutive isomerization and cracking of isomer products. In Figure 8b, the nMe/nA value increases from 0.019 to 0.115 and the n_{as} decreases from 2.24 to 1.77 for the Pd–Ni_2P/SAPO-31 catalyst. For comparatively higher ratios of nMe/nA, the hydroisomerization and hydrocracking reactions of n-C_{16} over the Pd–Ni_2P/SAPO-31 bifunctional catalyst take place in a serial reaction mechanism as shown in Figure 8b. Since the n_{as} value is 1.94, alkene intermediates encounter around 1 or 2 acid sites during their journey toward to metal site. In this case, instead of further conversion on

the acid sites, the alkene intermediates are able to undergo hydrogenation on the metal sites, providing lower cracking/isomer and multi-branched/mono-branched product ratios [54]. Therefore, the serial reaction mechanism can be considered as ideal for higher isomer production, in which only one transformation of the alkene intermediate on the acid sites can occur during their diffusion from the Pt sites [16]. As a result, the Pd–Ni_2P/SAPO-31 catalyst is considered as the most suitable catalyst compared to the Pd/SAPO-31 and Ni_2P/SAPO-31 catalysts due to its more suitable nMe/nA value [9].

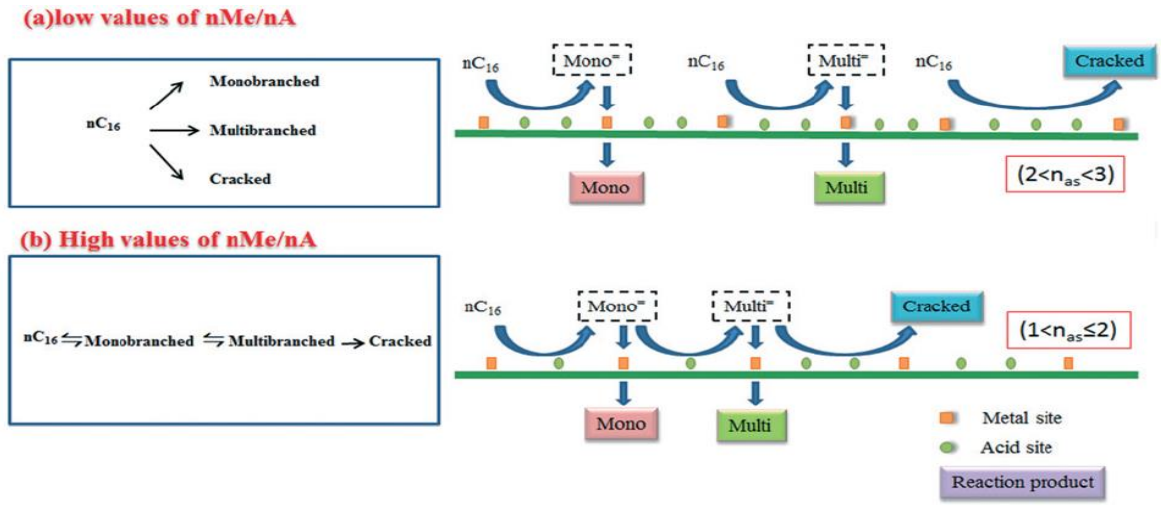

Figure 8. The scheme of n-C_{16} hydroisomerization mechanisms over a bifunctional catalyst with (a) low values of nMe/nA (b) high values of nMe/nA [9]

Alvarez et al. [55] also investigated the effect of different nMe/nA values, increasing from 0.002 to 0.48, for the hydroisomerization of n-decane (n-C_{10}) over a series of Pt/HY bifunctional catalysts. They aimed to understand the effect of the nMe/nA ratio on the hydroisomerization mechanism, catalytic activity, and stability. In Figure 9a, 9b, and 9c, a representative scheme for the n-C_{10} conversion at low, intermediate, and high values of nMe/nA are shown [56]. For catalysts with nMe/nA less than 0.03, the initial activity and stability were low and increased with higher nMe/nA. This result suggests that the HD/DHD reactions are the rate-limiting steps of the catalytic process for the low nMe/nA values. The average distance between two Pt sites is too high, so the number of encountered acid sites by the intermediate alkenes becomes accordingly excessive. Therefore, there is a major probability of several successive transformations of the alkenes before HD/DHD reactions on the metal sites. This implies that all i-decanes (i-C_{10}) and cracking products were directly derived from n-C_{10} molecules, instead of being obtained from the sequential reaction mechanism as shown in Figure 9c. For catalysts with nMe/nA between 0.03 and 0.17, activity remained constant and the acid function became the rate-limiting step since there was an adequate number of Pt sites for all acid sites. However, there was still a great distance between two Pt sites for some of the n-alkene

molecules, resulting in several consecutive conversions of n-C_{10} into the mono-branched or multi-branched i-C_{10} as shown in Figure 9b. For catalysts with a nMe/nA ratio higher than 0.17, no deactivation due to coking was detected and n-C_{10} molecules were converted sequentially into mono-branched i-C_{10}, then multi-branched i-C_{10} and finally into cracking products as shown in Figure 9c. For these catalysts, n-C_{10} undergoes only one transformation prior to hydrogenation due to the lower number of encountered acid sites. They found that the maximum yield for i-C_{10} products is achieved by a catalyst with a nMe/nA ratio higher than 0.17 [55].

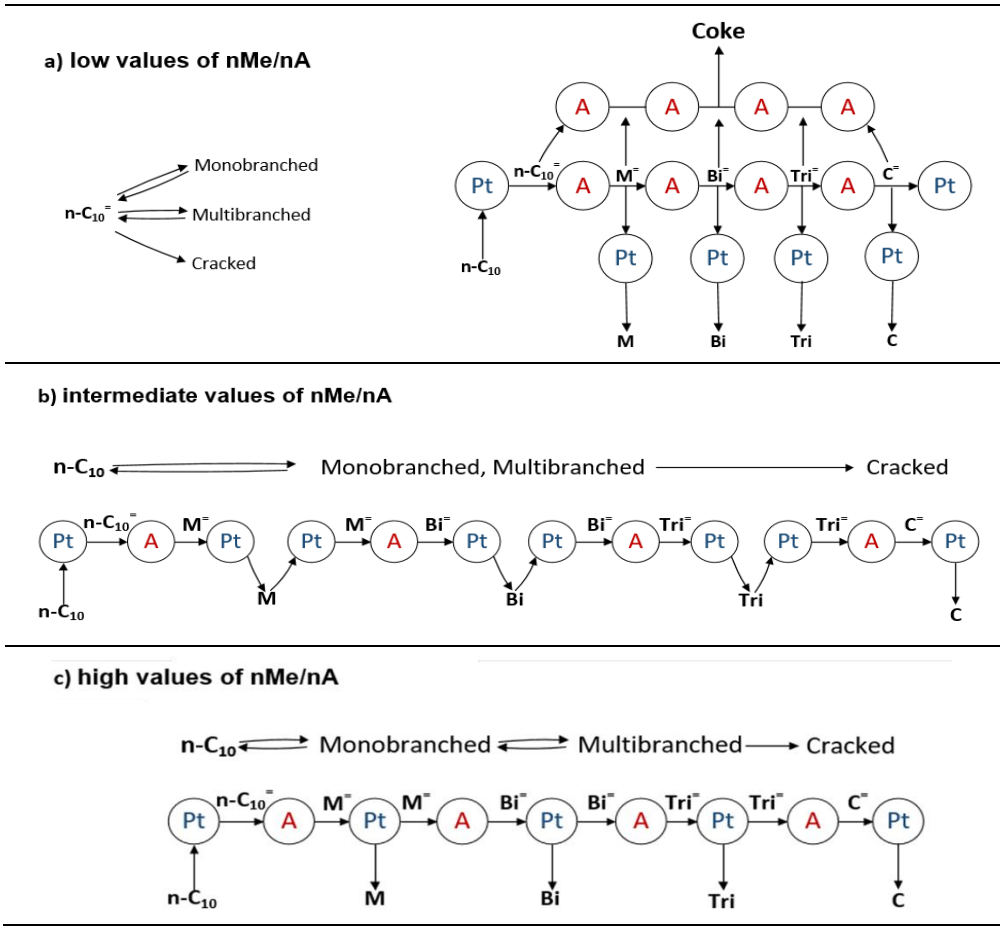

Figure 9. n-C10 transformations over bifunctional catalysts at: (a) low values of nMe/nA, (b) intermediate values of nMe/nA, and (c) high values of nMe/nA [56]

Batalha et al. [44] conducted a study over bifunctional catalysts with Pt and HBEA as metal and acid functions to investigate the influences of the metal/acid balance on n-C_{16} hydroisomerization. Three series of catalysts shown in Figure 10 were prepared. In the first series (S1), metal functions were located on the outer surface of the HBEA zeolite crystals of 12.5 µm with Pt contents from 0.2 to 1.5 wt.% (Pt/HBEA). The second (S2) and third (S3) series were obtained from an intimate mixture of Pt-Al_2O_3 and HBEA particles of 70 µm and from a physical mixture of Pt-Al_2O_3 and HBEA particles of 300 µm, respectively. The S2 and

S3 bifunctional catalysts were labeled as PtA-HBEA (a–b), where a and b were the wt.% of Pt-Al_2O_3 and HBEA, respectively. A fixed bed stainless steel reactor was used for n-C_{16} conversion. The temperature, total pressure, H_2/n-C_{16} molar ratio, and weight hourly space velocity were set to 220 °C, 30 bar, 20, and 2-100 h^{-1}, respectively.

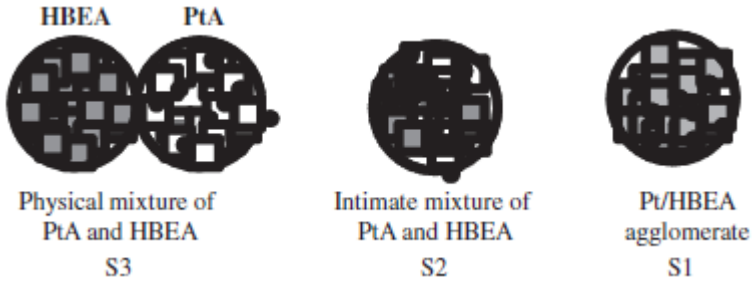

Figure 10. Schematic presentation of the series of bifunctional Pt-HBEA catalysts [44]

The ratio between the concentrations of accessible Pt atoms and acid sites, nMe/nA, was chosen to quantitatively describe the metal and acid balance. In Figure 11, the TOF values versus nMe/nA for all three catalyst series are shown. For all catalyst series, TOF increases with the nMe/nA until it approaches a nearly constant behavior, as seen in Figure 11. For low nMe/nA values, the HD/DHD reactions over the metal sites constitute the rate-limiting reaction for n-C_{16} hydroisomerization. For high nMe/nA values, the rearrangement of olefinic intermediates over the acid sites becomes the rate-limiting step. Thus, increasing the nMe/nA ratio above a certain value does not have an effect on the TOF. Also, it is noteworthy that for the same nMe/nA values, the S1 series of catalysts exhibit the highest TOF, followed by S2 and S3, suggesting higher activity with an increased degree of proximity between metal and acid functions.

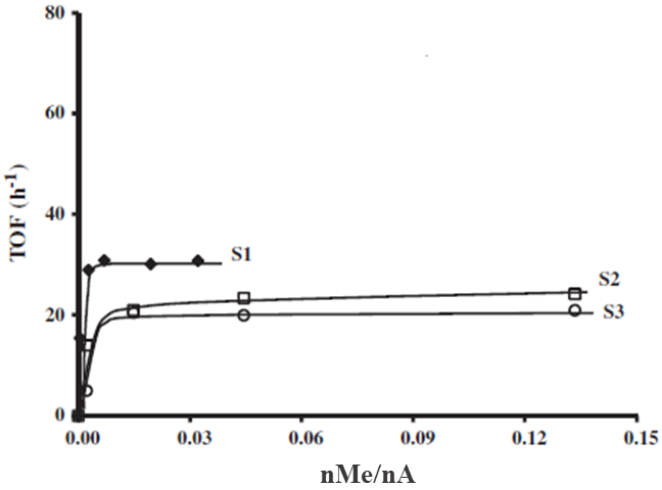

Figure 11. Acid site TOF of the catalysts series as a function of the nMe/nA ratio [44]

In Figure 12a and 12b, the cracking/isomers yield weight ratio (C/I) and multi-branched/mono-branched isomers yield weight ratio (Bi/M) versus nMe/nA values are plotted for the S1, S2,

and S3 catalysts. With the increasing nMe/nA value, the bifunctional catalyst becomes more selective toward to mono-branched isomer products. Also, the graphs show that the bifunctional reaction process is affected not only the nMe/nA but also the distance between the metal and acid sites since the C/I and Bi/M ratios change with different catalyst active site proximity. For the same nMe/nA values, the C/I ratio diminishes with the increased proximity between metal and acid sites. The similar results found for the Bi/M ratio except for the values up to 0.04 nMe/nA.

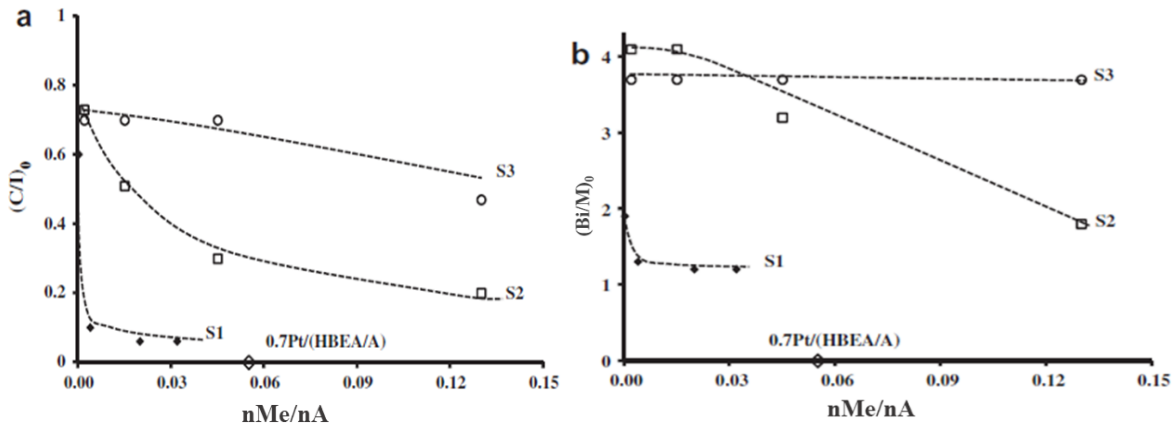

Figure 12. Initial values of the wt.% ratio of (a) $(C/I)_0$ and of (b) $(Bi/M)_0$ versus nMe/nA [44]

Since there is not a direct and accurate technique to properly evaluate the proximity between both sites, the degree of proximity was quantified by the abovementioned number of acid sites encountered by intermediates throughout their diffusion between two Pt sites, n_{as} [57]. As mentioned before, the nMe/nA values should be high enough so that the acid-catalyzed reactions can be the rate-limiting step and the n_{as} value should be close to 1 to catalyze only one skeletal rearrangement or cracking reaction of the olefinic intermediates through their journey between two Pt sites. It can be seen in Figure 13a that, for all S3 catalysts, the n_{as} values are close to 3; whereas for the S1 and S2 catalysts, the n_{as} value diminishes with the increasing number of nMe/nA values. For the same nMe/nA values, the S1 catalysts have the lowest n_{as} values and their decreasing trend is significantly stronger than the profiles for both S2 and S3 catalysts. In Figure 13b, when the distance between two active sites increases from 0.01 μm to 300 μm, all the n_{as} values change from 1 to 3.05 and moreover, the yield of i-C_{16} decreases from 80 % to 20 %. Therefore, if there is a shorter distance between both types of sites, a lower n_{as} value will be reached. As a result of this study, it was found that the balance between the metal and acid functions and their proximity are the main parameters that determine the rate and selectivity of n-C_{16} hydroisomerization. Moreover, the distance between acid and metal sites shows a strong influence on catalytic performance compared to the nMe/nA ratio [44].

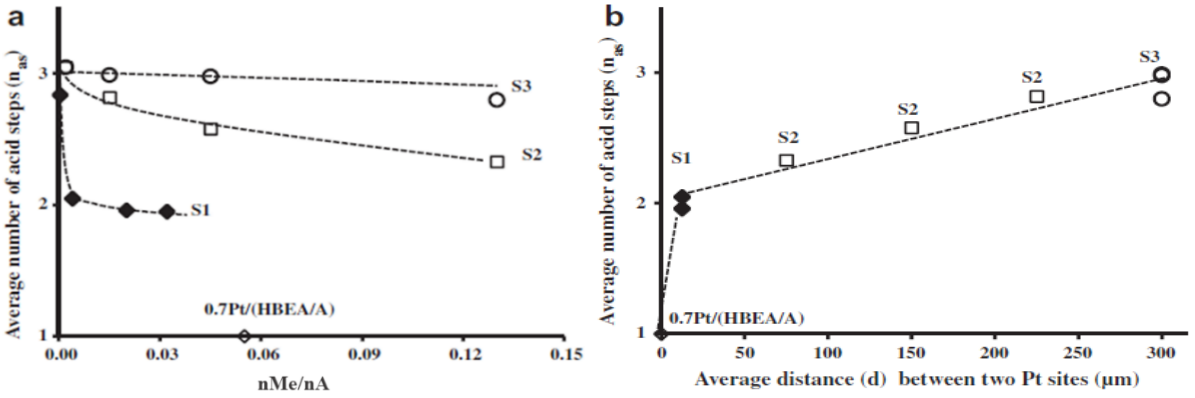

Figure 13. The average number of acid steps (n_{as}) involved in the transformation of one n-C_{16} versus (a) the nMe/nA ratio and (b) the distance (d, µm) between two Pt sites [44]

As a general conclusion of the aforementioned studies, the average number of acid sites in contact with an n-alkane molecule during hydroisomerization should be close to 1 in order to obtain a single reaction on the acid sites during their diffusion from the Pt sites. For this condition to occur, nMe/nA values would need to be high enough. However, an excessive amount of metal sites would also limit the pores and consequently n-alkane conversion and increase the cost of preparation. Thus, the possibility of an optimal range of nMe/nA values for achieving catalytic performances over bifunctional catalysts should be investigated. Lastly, the nMe/nA value is not the only parameter affecting the catalytic properties, but also the proximity between metal and acid sites has a strong effect on the catalytic performance of the bifunctional catalyst.

2.2 The effects of distance between metal and acid sites on the bifunctional catalyst performance

As mentioned previously, the distance between the metal and acid sites has also been presented as a strong influence in the catalytic performance of bifunctional catalysts. A well-balanced catalyst is described as an ideal bifunctional catalyst if it satisfies the proximity criteria [58]. Numerous publications have explored the intimacy criterion throughout the years. It is stated that the metal and acid sites should be sufficiently close to guarantee that the diffusion of olefinic intermediates does not hinder kinetics [59]. Some of the studies especially have indicated that the greatest proximity between metal and acid sites improves the selectivity to the desired product [60]. However, recent studies have revived the discussion on the optimal distance between the two functions for improved efficiency [61]. The distance between metal and acid sites is mainly dependent on the noble metal site deposition location and the zeolite crystal particle size. In the following sections, the effects of the different

deposition and zeolite crystal particle size on the diffusion distance and bifunctional catalyst performance have been discussed.

2.2.1 The effects of different metal site depositions on the diffusion distance and bifunctional catalyst performance

The different depositions of noble metal sites strongly influence the catalytic performance of bifunctional catalysts. If the bifunctional catalysts have identical nMe/nA values but the different deposition of the noble metals as shown in Figure 14, on acid supports or alumina binder, the performance of the catalysts could be considerably different [59] [61].

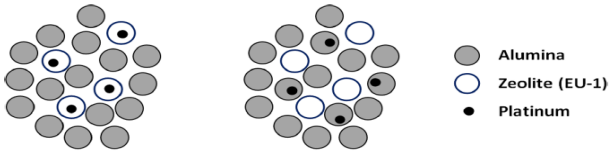

Figure 14. Scheme of two catalyst groups with different degree of intimacy between metal and acid sites [59]

A criterion for optimal site proximity was initially proposed by Weisz et al. [60], who stated that the closest distance between the metal and acid sites is necessary for optimal activity and selectivity. Pt/C or Pt/SiO_2 metal site particles and silica-alumina acid site particles with the same size were prepared separately to investigate the effect of the intersite distance. Due to the limitation of techniques at that time, the distance between metal and acid sites was tuned by varying the size of the mentioned particles for n-heptane ($n\text{-}C_7$) hydroisomerization. It was found that the yields of i-heptane ($i\text{-}C_7$) over catalysts with smaller component particle size, such as 5 or 70 μm, were higher than those of catalysts with 1000 μm particle size. The reason can be explained by the diffusivity of n-alkane reaction intermediates which have to diffuse from the metal site to the acid site and at the same time, the i-alkene reaction intermediate must diffuse in the other direction. If there is a large distance between sites, reactions become controlled by the slower diffusion processes, resulting in a diminishment of catalytic activity. As a result, the i-alkenes are more likely to undergo secondary reactions, leading to a rise in the production of both gas and coke. It was found that the component particle size of catalysts should be below 100 μm to obtain a diffusion-uninhibited catalytic performance. The size was optimized in a range between 20 and 40 μm to prepare an efficient catalyst for high isomer yields. Weisz stated that the catalytic performance is not hampered by the diffusion of olefinic intermediates below such a distance [60].

Since the abovementioned research examined the effects of metal sites acid sites distance on the millimeter and micrometer scales, further research of the effects of nanometer and

atomic scales distance between two active sites needed to be conducted. In recent years, several researchers have investigated this effect by employing enhanced deposition methods.

Samad et al. [27] found a successful method for preparing Pt/silica-aluminum bifunctional catalysts by using anionic and cationic Pt precursors at a specific pH value. The authors studied the proximity criterion using a bifunctional catalyst containing Pt distributed over an acidic silica-aluminum support for n-C_7 isomerization with different degrees of proximity between metal and acid sites. The Pt sites were electrostatically deposited onto silica by utilizing cationic tetraamine ($Pt(NH_3)_4^{2+}$) precursors (PTA) at high pH values. On the contrary, the Pt sites were located onto alumina by employing anionic hexachloride ($PtCl_6^{2-}$) Pt precursors (CPA) at low pH values. With the help of these two type precursors, two different degrees of proximity between metal and acid sites were achieved. The metal and acid sites were located in the atomic distance, which was the closest proximity, for the catalysts obtained by electrostatic adsorption of PTA at a pH of 11 (PTA-11). Additionally, another catalyst prepared by dry impregnation (DI) of PTA over Al-Si supports (PTA-DI), showed the same level of proximity as PTA-11. The nanometer scale proximity between the metal and acid sites was achieved by the deposition of CPA onto alumina at 4 pH (CPA-4). The micrometer scale proximity between metal and acid sites was obtained by physical mixtures (PM) of metal and acid functions. Lastly, the L-# labeled catalysts shown in Figure 15 refer to the addition of inert layers made of quartz wool to further separate the metal and acid functions. The four series of catalysts with atomic, nanometer, micrometer, and millimeter scales of intimacy between metal and acid sites are summarized in Figure 15 [27].

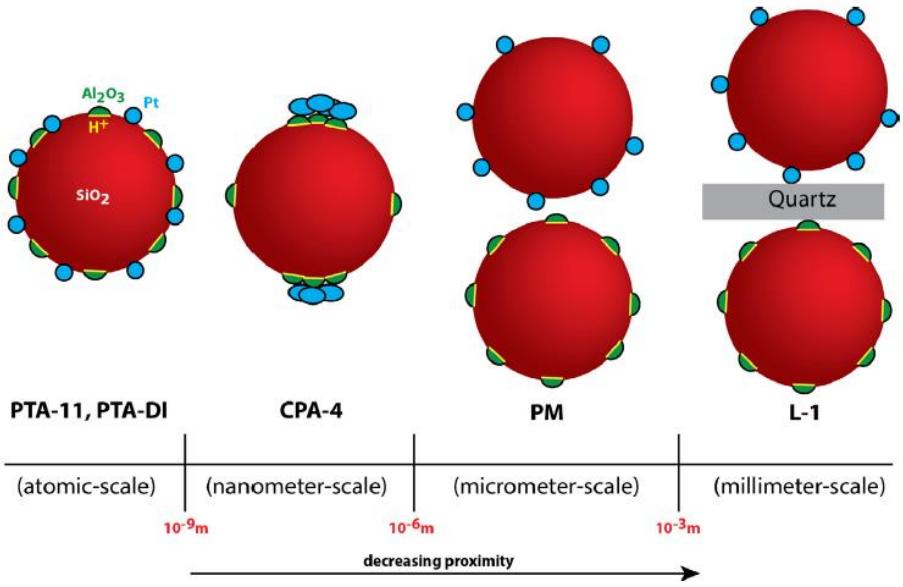

Figure 15. Schematics of catalyst configurations with varying degrees of intimacy between active sites [27]

The isomerization reaction of n-C_7 was executed in a U-shaped flow-type, fixed bed, quartz tube reactor, which was operated at the temperature of 350 °C and pressure of 1 atm. In Figure 16 shows the performance of the PM and L-# catalysts and a schematic representation of the reactor packing. The yellow circles, red circles, and gray strips indicate acidic SIRAL 80, Pt/R_Si and a layer of quartz wool, respectively. Pt/R_Si and Al_Si are the metal-only and acid-only monofunctional configurations and were tested separately to serve as a reference for comparison. Total catalyst mass for the 1:1 PM and layered configurations was 0.4 g, with equal mass (~0.2 g) of acid and metal components. Results showed that if the distance between two active sites increases to the millimeter scale, catalysts will approximately behave as monofunctional catalysts and their performance will decline quickly due to the fact that alkene intermediates cannot diffuse very far between two active sites. Thus, a large distance between sites prevents the isomerization reaction from taking place. All of the layered catalysts, from L1 to L3, showed a degree of deactivation and selectivity similar to the monofunctional catalyst (Pt/R_Si) as displayed in Figure 16b. On the other hand, the catalytic performance improved significantly for the PM catalyst compared to the rest since its metal and acid sites were mixed and located more closely. It can be seen that for the PM catalyst the selectivity of the i-C_7 product is enhanced and that cracking and cyclic products are decreased remarkably. Also, the initial activity of the PM catalyst is notably higher, which is 70 % for PM and 58 % for the L2 catalysts.

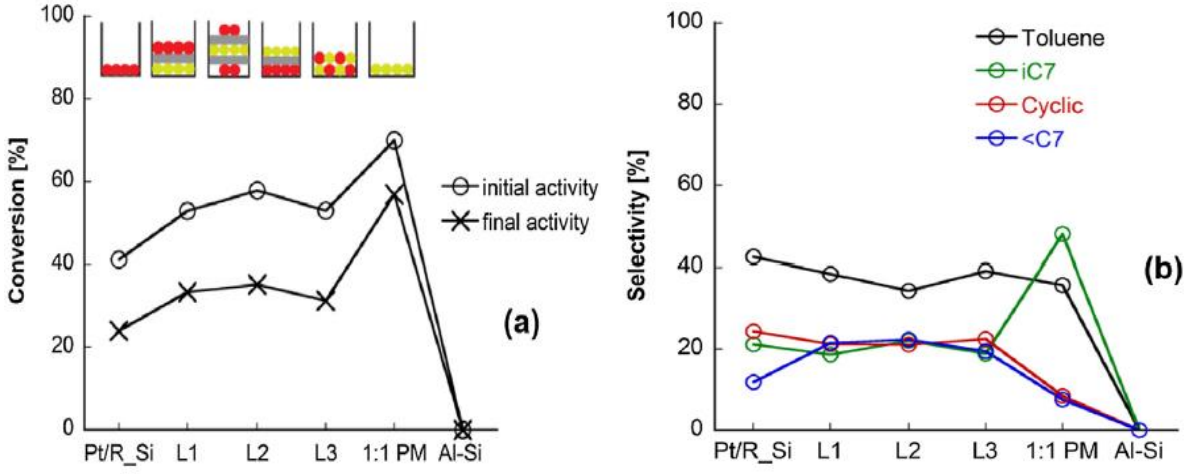

Figure 16. (a) n-C_7 conversion and (b) product distributions at approx. 22 % conversion for various configurations of Pt/R_Si and SIRAL 80 (Al-Si) based catalysts [27]

In Figure 17a, the product distribution at approx. 22 % conversion after time on stream (TOS) of 18 h for monofunctional and bifunctional catalysts are plotted. The metal-only catalyst Pt/R_Si prepared by non-acidic silica shows good selectivity toward i-C_7. Also, as shown in Figure 16, the initial and final conversions of n-C_7 over this metal-only catalyst were found to be 41 % and 24 %, respectively, thus indicating remarkable activity towards i-C_7. The other

metal-only catalyst Pt/R_Al prepared without using silica also shows notable selectivity toward i-C_7. On the other hand, the acid-only monofunctional Al-Si catalyst exhibits no activity under the tested conditions. In Figure 17b the bifunctional, weakly acidic Al-LSi 99 support was used, so PTA-11 and CPA-4 catalysts show quite similar performance to the Pt/R_Si metal-only monofunctional catalyst. Lastly, the PTA-DI catalyst shows no activity owing to its lower fractional metal dispersion (3 %) compared to the PTA-11 and CPA-4 catalysts and the low acidity of the Al-LSi 99 support. In Figure 17c and 17d, the bifunctional, strongly acidic, silica-rich Al-HSi 97 and SIRAL supported catalysts are shown. It can be seen that the catalyst prepared by CPA-4 (nanometer scale proximity) exhibits notably higher selectivity toward i-C_7 compared to the catalysts prepared by PTA-11 and PTA-DI (atomic scale proximity). As a result, the study found that the greatest bifunctionality is achieved by proximities between metal and acid in the nanometer and micrometer scales sites instead of an atomic scale separation [27].

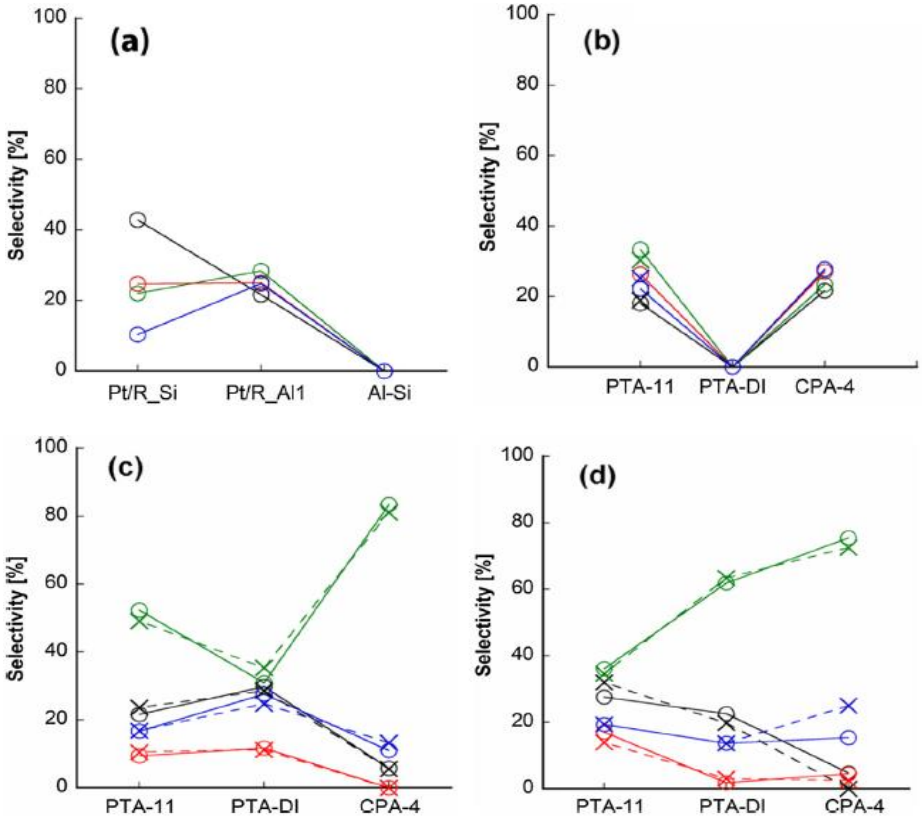

Figure 17. Product distribution at 22 % conversion of (a) monofunctional Pt/R_Si (metal), Pt/R_Al1 and Al-Si (acidic SIRAL 80) and bifunctional (b) Al-LSi 99, (c) Al-HSi 97 and (d) SIRAL 80 supported catalysts. (i-C_7: green, toluene: black, cyclic: red, <C_7: blue, o-solid lines: 0.7 wt.% catalyst, and x-dashed lines: 0.4 wt.% catalyst) [27]

In the study conducted by Gutierrez-Acebo et al. [59], two series of bifunctional catalysts with different nMe/nA ratios and different metal to acid site proximities were developed to test the

hydroconversion of the ethylcyclohexane (ECH) over Pt/EU-1 zeolite catalysts. The EU-1 zeolite and Pt particles were selected as acid and metal functions, respectively. The metal and acid balance was tuned by only changing the amount of metal sites. The distance between the metal and acid site was adjusted by depositing Pt particles either on the zeolite (Pt/HEU-1) or the alumina support (Pt/Al_2O_3). Then a mixture of 80 % of Al_2O_3 and 20 % of Pt/HEU-1 was mechanically mixed, in which nanometer scale proximity of the metal and acid sites proximity was attained (Pt-HEU-1/Al_2O_3). In comparison, a mixture of 80 % of Pt/Al_2O_3 and 20 % of HEU-1 was mechanically mixed, resulting in a microscale proximity of metal and acid sites (Pt-Al_2O_3/HEU-1). The hydroconversion of ECH was executed in a steel fixed bed reactor between 230 and 330 °C, a pressure of 10 bar, H_2/ECH ratio of 40, and weight hourly space velocity (WHSV) of 4 grams of ECH per gram of catalyst per hour.

In Figure 18 and Figure 19, the isomerization and cracking selectivity versus ECH conversion are shown for Pt-HEU-1/Al_2O_3 and Pt-Al_2O_3/HEU-1 catalysts with different wt.% Pt loadings. Since the acidity is the same for all catalysts, a higher Pt content increases the nMe/nA ratio. It can be seen that the Pt-Al_2O_3/HEU-1 and Pt-HEU-1/Al_2O_3 catalysts with 1% and 2.3% Pt loadings yield more isomerized and less cracked products compared to the other catalyst due to their relatively higher nMe/nA ratio.

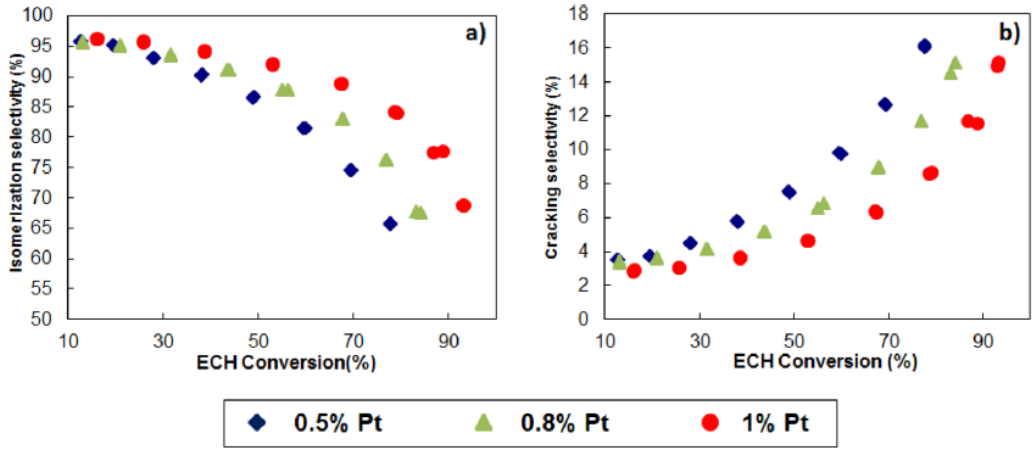

Figure 18. Evolution of the selectivity versus ECH conversion for the Pt-HEU-1/Al_2O_3 catalysts: (a) isomerization and (b) cracking [59]

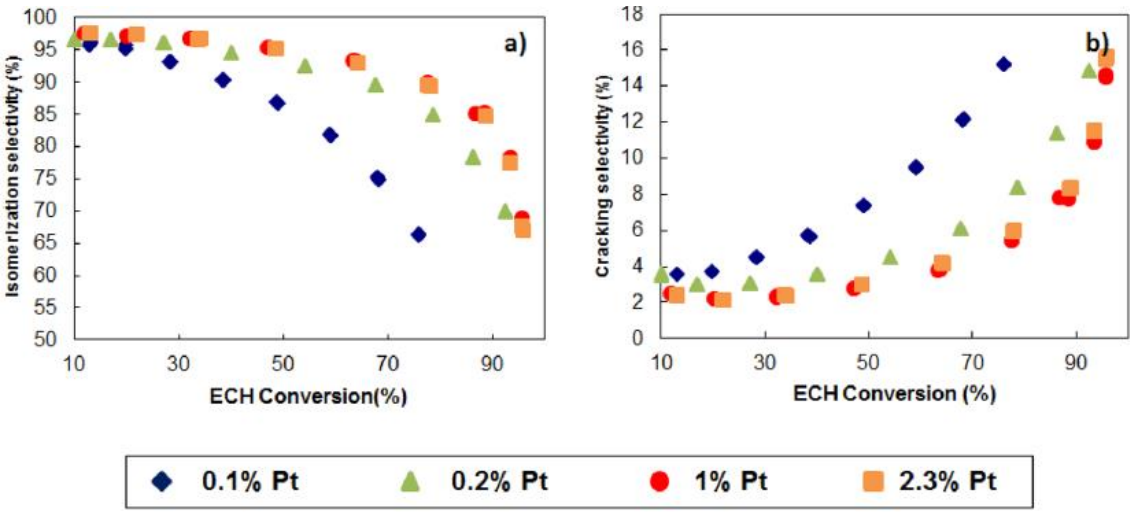

Figure 19. Evolution of the selectivity versus ECH conversion for the Pt-Al_2O_3/HEU-1 catalyst group: (a) isomerization and (b) cracking [59]

In Figure 20, the TOF versus and maximum i-cyclo C_8 isomerization yields for both catalyst series versus their nMe/nA ratios are shown for Pt-Al_2O_3/HEU-1 and Pt-HEU-1/Al_2O_3 catalysts. The results show that similar activity and selectivities are achieved for Pt-Al_2O_3/HEU-1 and Pt-HEU-1/Al_2O_3 catalysts at the same nMe/nA values, suggesting that nanoscale and microscale distances have a similar effect on catalyst performance. Consequently, it appeared that diffusion limitations did not occur at the tested operating conditions. As a result of this study, it can be concluded that the catalytic activity and selectivity was highly affected by the nMe/nA ratio but barely influenced by the distance between metal and acid functions [59].

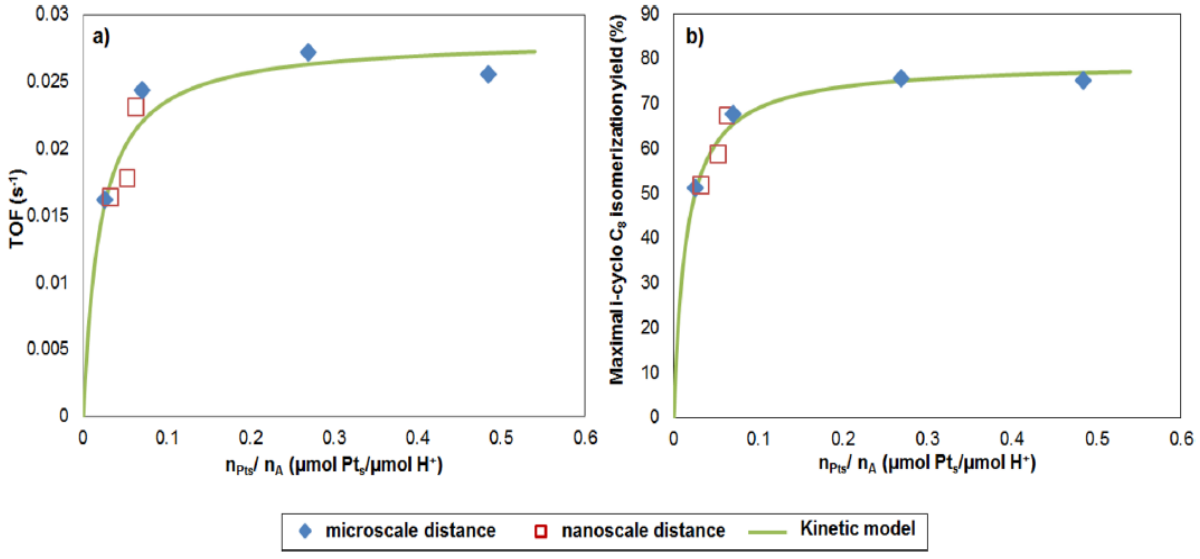

Figure 20. Evolution of the (a) TOF (s^{-1}) and (b) maximum i-cyclo C_8 isomerization yield (%) versus the metal/acid balance for both series of catalysts [59]

Zecevic et al. [61] also performed a systematic study to control the proximity between the active sites of bifunctional Pt/Y binder shaped catalysts, which are the most employed catalysts at the industrial level [9]. Firstly, 50 wt.% mesoporous zeolite Y (Y) and 50 wt.% Al-binder (A) were mixed via extrusion to produce the acid support Y/A. The Pt metal anions from the H_2PtCl_6 solution at pH 3 were deposited on the Al-binder by an electrostatic adsorption method (Pt-A/Y). Contrarily, the Pt metal cations from $Pt(NH_3)_4(NO_3)_2$ solution at pH 5 were located in the zeolite by an ion-exchange method (Pt-Y/A). The almost equivalent Pt loadings of both bifunctional catalysts, which were 0.6 wt.% for Pt-Y/A and 0.7 wt.% for Pt-A/Y, meet the requirement for the metal/acid balance for ideal hydrocracking. Moreover, it was verified that Pt particles were successfully placed inside the zeolite crystals and alumina phase by the help of High-Angle Annular Dark-Field Scanning Transmission Electron Microscopy imaging (HAADF-STEM) and Energy Dispersive X-ray (EDX) elemental mapping of 70-nm-thick ultramicrotomed sections of Pt-Y/A catalyst. Also, it was confirmed by the electron tomography that there was no Pt on the zeolite phase for Pt-A/Y and the alumina phase for Pt-Y/A catalysts. After the deposition process, two bifunctional catalysts were obtained with different arrangements of Pt particles. The HAADS-STEM images of a 70-nm-thick section of both catalysts with Pt particles of ~2.5 nm for Pt-Y/A, of ~3.5 nm for Pt-A/Y and an EDX map indicating Pt (yellow), Si (green) and Al (red) signals are shown in Figure 21. In Figure 21a and 21b, Pt is located inside the zeolite pores with the closest proximity to the acid site. In Figure 21c and 21d, Pt is deposited on the binder within a nanometer scale distance from the acid site. Additionally, since it is necessary to interpret only the effect of the distance between metal and site on the catalyst performance, all other morphologic parameters needed to be identically set. Because of this reason, the acidity of both catalysts was measured by temperature-programmed desorption of ammonia and results showed similar acidity.

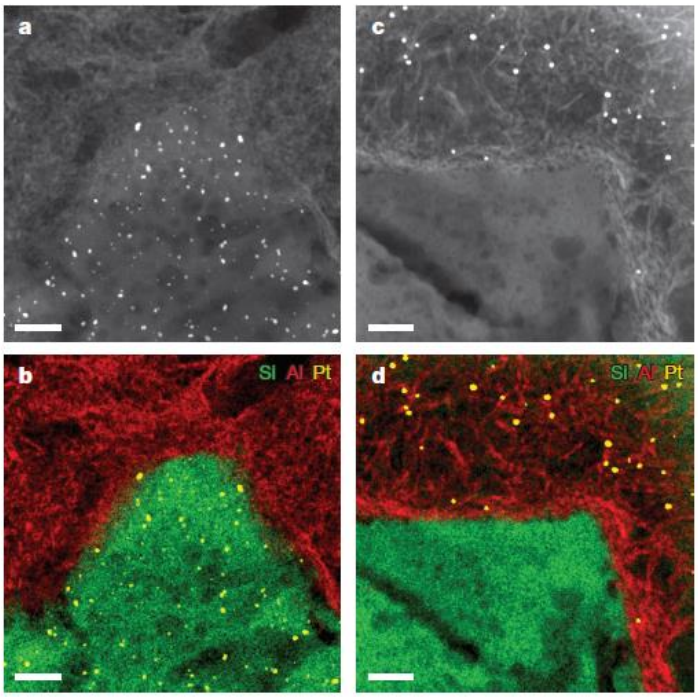

Figure 21. (a) The HAADF-STEM image of Pt-Y/A sample with Pt particles residing within the zeolite crystals, (b) EDX map of Pt-Y/A, (c) HAADF-STEM image of Pt-A/Y with Pt particles residing on the alumina binder and (d) EDX map of Pt-A/Y [61]

Experiments were performed at a pressure of 0.45 MPa and an H_2/n-C_{10} molar ratio of 214 or pressure of 0.65 MPa and an H_2/n-nonadecane (n-C_{19}) or an H_2/pristane (i-C_{19}) molar ratio of 14.6. According to the isomerization results shown in Figure 22a, 22b, and 22c, the conversion activity of n-C_{10} and n-C_{19} feedstocks over both catalysts are almost identical. However, the conversion activity of multi-branched i-C_{19} feedstock over Pt-Y/A catalyst is higher than the Pt-A/Y catalyst. Since the i-C_{19} molecule is a bulky molecule, it has a lower diffusivity than the other alkenes used as other feedstock, which is approximately 1.0 $\times 10^{-9}$ m^2s^{-1} for normal alkanes and 1.0 $\times 10^{-11}$ m^2s^{-1} for i-C_{19} molecules. Therefore, their transport is limited by diffusion and a closer distance between metal and acid sites is beneficial.

Furthermore, both catalysts show different selectivities for all three feedstocks, as shown in Figure 22d, 22e, and 22f. The Pt-A/Y catalyst, where the metal function located on the alumina, yields more isomer products than the Pt-Y/A catalyst, where the metal function located on the zeolite site. The results emphasize the necessity of a nanometer scale distance between the metal and acid functions for ideal performance. For the Pt-Y/A catalyst, where the Pt metal particles are present inside the zeolite crystal and in the closest proximity with acid sites, the alkane feedstock diffuses through the micropores of the zeolite to undergo an HD/DHD reaction at the metal site. It is suggested that the intermediate molecules generated on the metal sites are retained in the zeolite micropores network due to the strong adsorption

on acid sites. Consequently, it results in an increment in their residence time in the acidic environment, which leads to an increase in their cracking possibility and a decreased selectivity towards the desired products. On the other hand, for the Pt-A/Y catalyst, where the metal function is located on the alumina binder and a nanometer scale proximity between metal and acid site is attained, the acid sites are more reachable for the alkene intermediates formed on the metal sites. The alkene intermediates generated on the metal site diffuse from the wider pores of the alumina binder to the Y-zeolite, where they undergo isomerization on the outside and then diffuse immediately back to a metal site on the alumina binder. Consequently, the cracking of alkene intermediates is reduced, and the isomer product yield is increased. In this study, it was found that closer distances between both functions are detrimental for the isomerization selectivity [61].

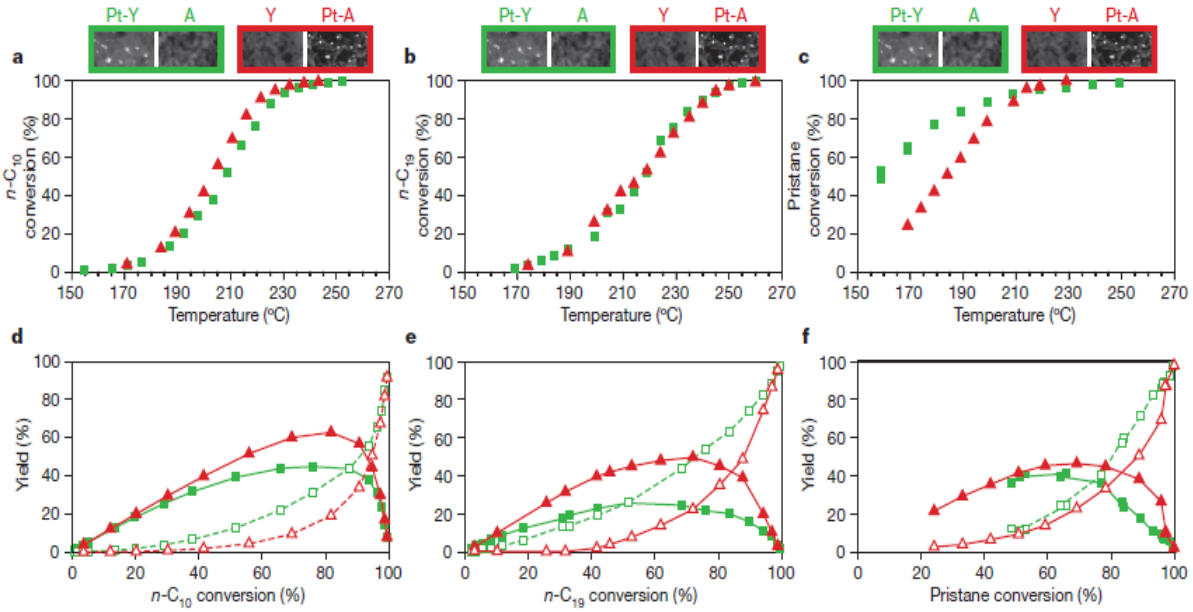

Figure 22. The conversion of the (a) n-$C_{10,}$ (b) n-$C_{19,}$ and (c) i-C_{19} versus the reaction temperature for Pt-Y/A (green squares) or Pt-A/Y (red triangles) catalysts. Product yields from (d) n-C_{10}, (e) n-C_{19}, and (f) i-C_{19} feedstock. (Solid lines and filled symbols: isomerized products; dashed lines and open symbols: cracked products) [61]

One of the most extensively used methods for the preparation of bifunctional catalysts for hydrocracking is the incipient wetness impregnation (IWI) method, which provides various diameters and locations of Pt metal particles [62]. If there is a non-uniform distribution of Pt particles, it can be hard to isolate the impact of the distance between the metal and acid sites on catalyst performance [63]. The colloidal impregnation (CI) method represents a more novel method with elevated nanometer scale distribution control technologies [64]. A colloidal solution including Pt particles with homogenous diameter is prepared, then the solution is

impregnated into supports [65]. If the Pt particle diameters are larger than the size of the pore mouth of the support, the Pt particles are located on the external surface [63].

In the study conducted by Lv et al. [63], a series of Pt/SAPO-11 catalysts were prepared by using IWI, CI, and a combination of CI and IWI (CI-IWI) methods with different wt.% Pt loading. The weight percentage (x) of Pt in the catalyst prepared by the IWI, CI, and CI-IWI methods are shown as IWIx, CIx, and CIx-IWIx respectively. For the CIx-IWIx catalyst, an additional amount of Pt (x wt.%) was filled on the CIx catalyst by applying the IWI method. The structure, acidity, and texture properties of the support and catalyst were tested by X-Ray Diffraction (XRD) patterns and NH_3-TPD profiles, with no noticeable alterations detected. The distribution of the Pt sites on Pt/SAPO-11 catalyst was determined through H_2 chemisorption, shown in Table 3. The characterization results indicate that Pt sites on CI-prepared catalysts were primarily located on the larger external surface through electrostatic interactions since the colloidal Pt particles (2.9 nm) have a uniform and larger diameter than the smaller micropores of SAPO-11 (0.63 nm). Whereas the Pt sites on IWI-prepared catalysts were mostly distributed in a non-uniform manner. Smaller particles (1.0 nm) are mainly located near the micropore mouth of SAPO-11 and the larger particles (8.0 nm) are deposited on the external surface as displayed in Table 3.

Table 3. Pt site distribution on Pt/SAPO-11 catalysts [63]

Catalysts	C_{Pt}^{total} (mmol/g)	C_{Pt}^{surf} (mmol/g)	C_{Pt}^{mouth} (mmol/g)
CI0.25	2.6	2.6	-
CI0.75	8.3	8.3	-
IWI0.25	6.9	0.8	6.1
CI0.5-IWI0.25	9.0	5.1	3.9

Their catalytic performance, including conversion and selectivity, were assessed by using n-C_{19} as a model feedstock in a stainless steel fixed-bed reactor with 10 mm inner diameter, at 290–370 °C temperature, 8.0 MPa pressure, 15-25 H_2/n-C_{19} molar ratio and a 2-4 h^{-1} liquid hourly space velocity (LHSV). The conversion was calculated according to the peak area normalization of the product chromatogram as follows:

$$T_{Con} = \frac{A_{Total} - A_{Residue}}{A_{Total}} * 100\% \quad (1)$$

where $A_{Residue}$ is the peak area of n-C_{19} in the liquid products, A_{Total} is the peak area sum of n-C_{19}, isomers and cracking products in the liquid products.

Then, the product selectivity was calculated as follows:

$$S_X = \frac{A_X}{A_{Total} - A_{Residue}} * 100\ \% \tag{2}$$

where S_{Iso}, S_{Mono}, S_{Multi}, S_{Crack} indicate the selectivity of isomers, mono-branched isomers, multi-branched isomers, and cracking products. Also, A_{Mono}, A_{Multi}, A_{Crack} are the peak area of isomers, mono-branched isomers, multi-branched isomers, and cracking products, respectively.

Lastly, the TOF of n-C_{19} at a conversion lower than 10% was calculated as follows:

$$TOF = \frac{(N_{Flow} * T_{Con})}{(W_{Cat} * N_{Acid})} \tag{3}$$

where N_{Flow} is the molar flow rate, T_{Con} is the conversion, W_{Cat} is the weight of the catalyst and N_{Acid} is the mole number of medium-strength acid sites per gram of catalyst.

The conversion of n-C_{19} over the Pt/SAPO-11 catalysts as a function of temperature is shown in Figure 23a. Firstly, the conversion of n-C_{19} for all catalysts increases with rising temperatures. The conversion and isomerization selectivity of the prepared Pt/SAPO-11 samples increase in the following order: CI0.1 < CI0.25 < CI0.5 ≈ CI0.75 ≈ CI1.0 < CI0.5-IWI0.25 < IWI0.25. The catalysts prepared by the CI method appear to be less active than the IWI0.25 and the CI0.5-IWI0.25 catalysts since they require higher reaction temperatures to reach the same conversion level. Moreover, as shown in Figure 23b, the IWI0.25 and CI0.5-IWI0.25 catalysts show higher isomerization selectivity than the catalysts prepared by the CI method. It was proposed that the isomerization selectivity can be enhanced by raising the concentration of the Pt sites close to the micropore mouth.

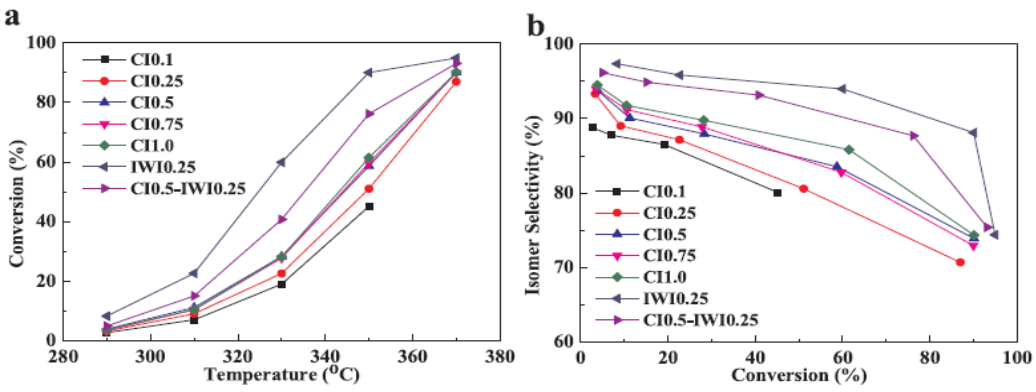

Figure 23. (a) Conversion of n-C_{19} as a function of reaction temperature and (b) isomerization selectivity as a function of conversion of n-C_{19} for Pt/SAPO-11 catalyst [63]

Since all of the prepared catalysts have the same acidity, differences in the nMe/nA ratio correspond to different concentrations of Pt particles. The TOF value as a function of the nMe/nA ratio is presented in Figure 24, where the TOF value represents the activity. For the CI catalysts, the TOF increases considerably until a nMe/nA value of around 0.0115, i.e. up to the catalyst with 0.5 % Pt loading, then their activity and selectivity remain largely the same. This means that the rate limiting step changes from the metal function to acid function and the sufficient number of Pt particles have been reached. Moreover, it can be seen that the CI0.5-IWI0.25 and IWI0.25 catalyst exhibits a higher TOF than the CI0.75 catalyst, even though both of them have a similar nMe/nA ratio. These results suggest that a higher concentration of Pt sites on the external surface has an insignificant effect on catalyst activity for high nMe/nA values. On the other hand, the effect on catalyst activity of increasing the amount of Pt sites close to the micropore mouth is quite significant. Therefore, it would be more advantageous to increase the amount of Pt particles close to the micropore mount to improve the activity of the Pt/SAPO-11.

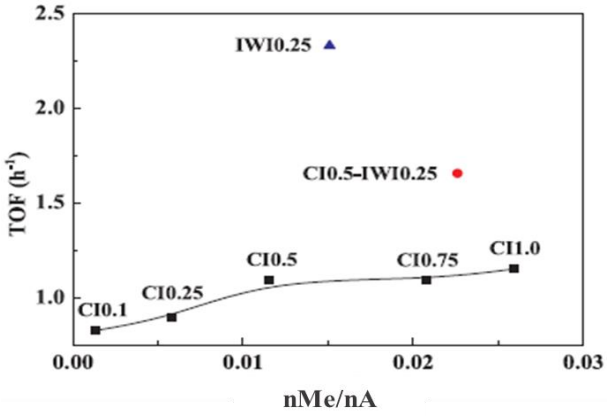

Figure 24. TOF versus nMe/nA value [63]

Additionally, product distributions for IWI0.25, CI0.75, and CI0.5-IWI0.25 were investigated to analyze the effect of the distribution of the Pt sites on the product selectivity. The product distributions for the IWI0.25, CI0.75, and CI0.5-IWI0.25 catalysts are presented in Figure 25. It can be seen that the isomerization selectivity towards mono-branched isomers can also be enhanced by raising the concentration of the Pt sites close to the micropore mouth.

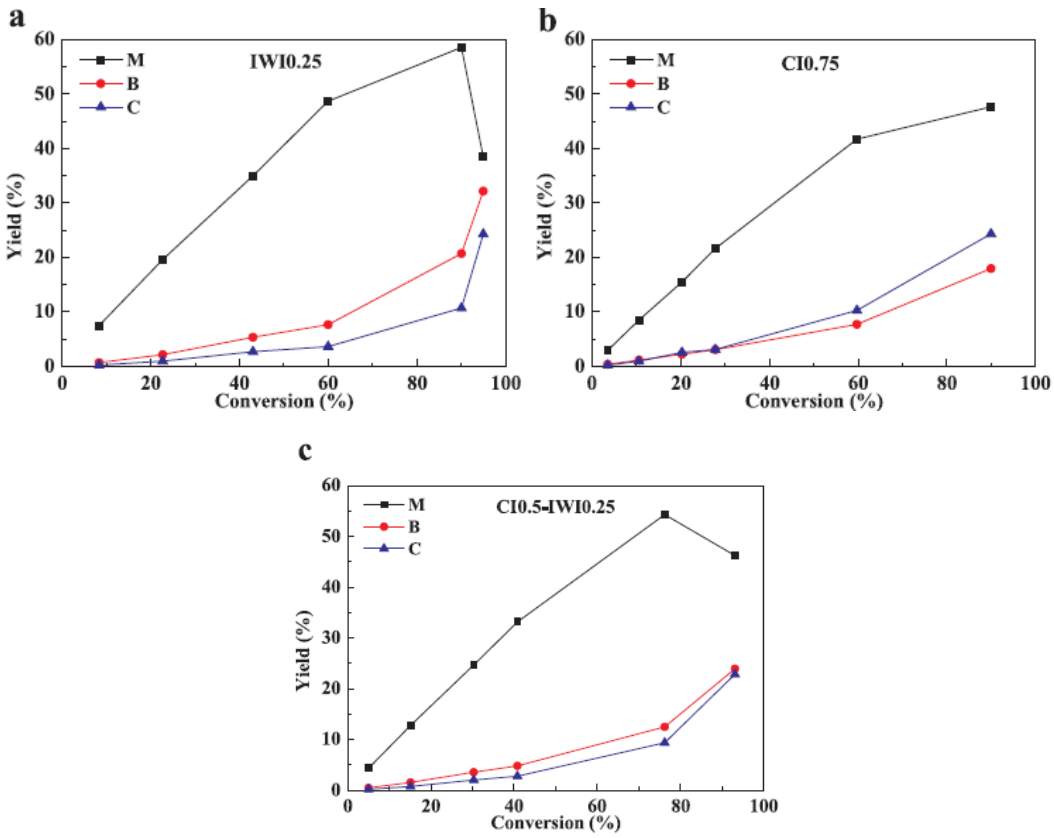

Figure 25. Product distributions over Pt/SAPO-11 catalysts. (a) IWI0.25, (b) CI0.75, (c) CI0.5-IWI0.25 (M: mono-branched, B: multi-branched isomers, C: cracking products) [63]

The results obtained from the abovementioned studies are explained as follows. Firstly, the n-alkene intermediates produced on the metal site diffuse to the acid site during the n-alkane hydroisomerization process. Then, they undergo a skeletal rearrangement reaction on the acid site to yield the corresponding i-alkenes. If the distance between metal and acid sites is too large, the possibility of encountering the acid site decreases due to the long diffusional path of the n-alkene intermediates. The transformation of n-alkene is hindered, thus diminishing the conversion towards isomer. Increasing the number of metal sites near the micropore mouth provides shorter metal and acid distances than those given by metal sites on the external surface. Therefore, n-alkenes diffuse more easily to the acid sites for their subsequent transformation into i-alkene intermediates, achieving higher isomerization selectivity. Once the isomerization occurs on the acid site, the i-alkane intermediates can diffuse back to the metal site to be hydrogenated into i-alkanes or encounter more acid sites throughout the diffusion path where rearrangement or cracking reactions occur [66]. The alkene intermediates can diffuse toward Pt sites rapidly if the Pt sites are located close to the micropore mouth, resulting in a higher isomer yield. Contrarily, if the Pt sites are located on the external surface and there is a long distance between metal and acid sites, multi-branched isomers and cracking product yields increase. In conclusion, the placement of the Pt sites, and their separation with acid

sites, can have a significant impact on product selectivity. It would be preferable to deposit the Pt sites close to the micropore mouth [63].

2.2.2 The effects of zeolite crystal particle size and thickness on the diffusion distance and bifunctional catalyst performance

In addition to the Pt loading method, zeolite crystal particle size and thickness also affects the distance between metal and acid functions within the microporous or mesoporous structure on the catalyst. In the literature, multiple studies that have specifically investigated the effect of the zeolite particle size on the distance and the performance of the bifunctional catalysts.

Li et al. [67] studied the hydroisomerization of n-C_{10} over two different bifunctional catalysts with an original zeolite (Pt/AY-ori) and an alkali-treated zeolite (Pt/AY-alk). The alkali-treatments to the original Y zeolite prior to Pt deposition led to different crystal particle sizes of the zeolite components. The average zeolite crystals size for Y-ori and Y-alk were found by XRD analysis to be 687 nm and 501 nm, respectively. The Pt particles were placed on the Y-alumina material by the electrostatic adsorption method. The hydroisomerization reaction of n-C_{10} was conducted in a stainless-steel batch type reactor at a temperature of 280 °C and pressure of 2.0 MPa. The conversion of the n-C_{10} was calculated as follows:

$$Conv.of\ n-C_{10}\ (\%) = \frac{1 - amount\ of\ n-C_{10}\ in\ product}{amount\ of\ n-C_{10}\ in\ feedstock} * 100 \quad (4)$$

The product yield, including isomerized i-C_{10} and cracked products, was calculated as follows:

$$Product\ yield\ (\%) = \frac{amount\ of\ i-C_{10}\ or\ cracked\ in\ product}{amount\ of\ n-C_{10}\ in\ feedstock} * 100 \quad (5)$$

The calculation of the ratio of multi-branched to mono-branched isomers (MuB/MB) was calculated as follows:

$$MuB/MB = \frac{amount\ of\ multibranched\ i-C_{10}\ in\ isomerized\ product}{amount\ of\ monobranched\ i-C_{10}\ in\ isomerized\ product} \quad (6)$$

The SEM images of Pt/AY-ori and Pt/AY-alk catalysts are illustrated in Figure 26. The Y-ori particles have a cleaner and smoother outer surface, whereas the Y-alk particles have irregular shapes, rough boundaries, and large openings on the zeolite outer layers. The imperfect areas located on the outer surface of zeolite crystals are mainly caused by the dissolution of the zeolite crystal framework in alkali conditions [68]. Moreover, the textural properties, including S_{BET}, V_{tot} and V_{mic}, and metal and acid characteristics of catalysts are quite similar.

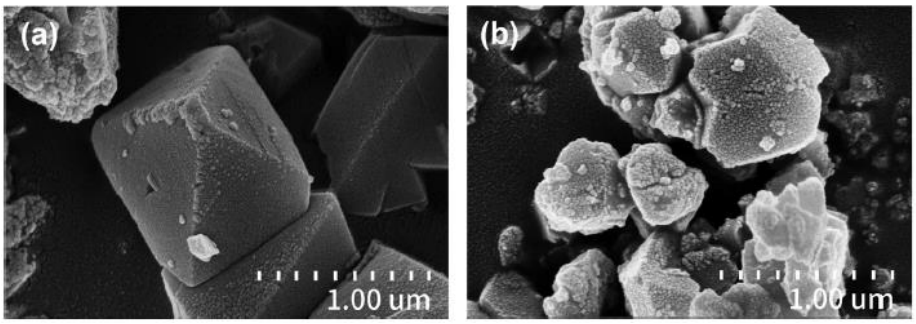

Figure 26. SEM images of zeolite samples: (a) Y-ori and (b) Y-alk [67]

In Figure 27, the graph of the n-C_{10} conversion versus reaction time for Pt/AY-ori and Pt/AY-alk catalysts is shown, indicating that the Pt/AY-alk catalyst displays slightly higher activity than the Pt/AY-ori catalysts. It is mainly caused by the improved dispersion of the protonic sites on the Pt/AY-alk catalyst compared to Pt/AY-ori. This improved dispersion is achieved by the reduced size of the zeolite crystals obtained with the alkali treatment [69]. With a good acid site dispersion, alkene intermediates are less likely to only diffuse through the non-acidic alumina route between two metal sites in Pt/AY-alk.

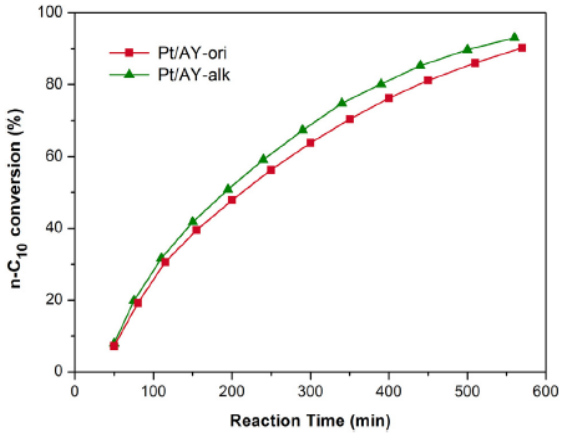

Figure 27. Time evolution of n-C_{10} conversion over Pt/AY-ori (green) and Pt/AY-alk (red) [67]

The isomerization and cracking products distribution versus n-C_{10} conversion over Pt/AY-ori and Pt/AY-alk catalysts are shown in Figure 28a. The solid lines with filled symbols show i-C_{10} products yield and solid lines with open symbols show cracked products (mostly n-C_4, n-C_5 and n-C_6) yield. The Pt/AY-alk catalyst provides more isomerized products than the Pt/AY-ori catalyst and has better resistance to unwanted secondary cracking reactions. Furthermore, in Figure 28b, the MuB/MB values of isomers are plotted against the n-C_{10} conversion, where the Pt/AY-alk catalyst exhibits lower MuB/MB ratios than those of the Pt/AY-ori catalyst. It is claimed that the shorter diffusion distance of an intermediate molecule within the micropores can be achieved with a smaller zeolite crystal size. As mentioned before, the ideal

hydroconversion is executed as a consecutive sequence where n-C_{10} molecules are converted sequentially into mono-branched i-C_{10}, then multi-branched i-C_{10} and finally into cracking products. Contrarily, for the non-ideal hydroconversion, the mono-branched isomers, multi-branched isomers, and cracking products are produced as simultaneous reactions of n-C_{10}. A smaller zeolite crystal size results in a lower number of acid sites that intermediate molecules can encounter during their movement inside the zeolite microporous structure and a decreased possibility of undesired secondary reactions [69]. Also, the multi-branched alkanes are more sensitive to skeletal conversion than mono-branched alkanes, resulting in poor resistance to cracking reactions [39]. As a result, the Pt/AY-alk catalyst outperforms than the Pt/AY-ori catalyst, leading to higher selectivity toward to isomerization and limited cracking product [67].

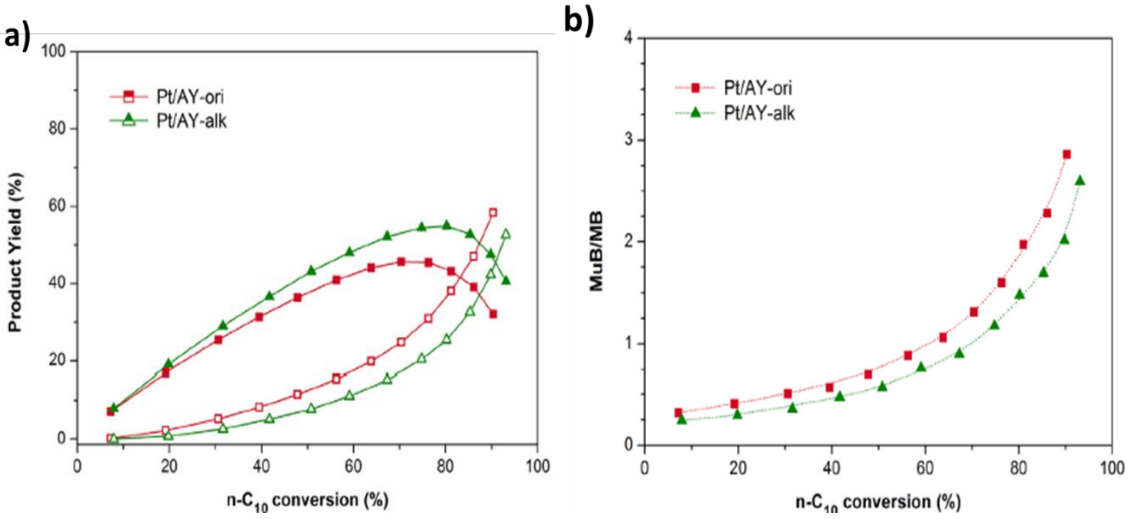

Figure 28. (a) Isomerized product (solid lines with filled symbols) and cracking products (solid line with open symbols) distribution versus n-C_{10} conversion (b) MuB/MB value of isomerized product against n-C_{10} conversion [67]

Zhang et al. [70] studied the performance of the micro/mesoporous Pt metal loaded Y/MCM-41 bi-porous composite bifunctional catalysts, Pt/MY-0, Pt/MY-2, and Pt/MY-5, for the hydroisomerization of the n-dodecane (n-C_{12}). The Y/MCM-41 materials include the original Y-zeolite and alkali-treated Y-zeolites for 2 and 5 hours, which are respectively represented as MY-0, MY-2, and MY-5. The prepared catalysts possess similar metal/acid balances (i.e. nMe/nA values) but different average Y zeolite crystal particle sizes. As shown in Figure 29, particle sizes of the Y zeolite crystals become diminished with the alkali-treatment and the reduction of the particle size is related to the treatment time. The mean particle size for MY-0, MY-2, and MY-5 were found to be 653 nm, 548 nm, and 421 nm, respectively. Then, the deposition procedure of the 0.7 wt.% Pt metal sites on Y/MCM-41 materials was executed using the IWI method with a H_2PtCl_6 aqueous solution as a precursor. Since the average

diameter of Pt crystal particles (4.0 nm) were larger than the zeolite micropores (1.0 nm), the Pt metal particles were deposited on the mesoporous MCM-41 materials and external surfaces of the Y-zeolite crystals. The n-C_{12} isomerization took place in a batch-type reactor at a temperature of 270 °C and a pressure of 2.0 MPa.

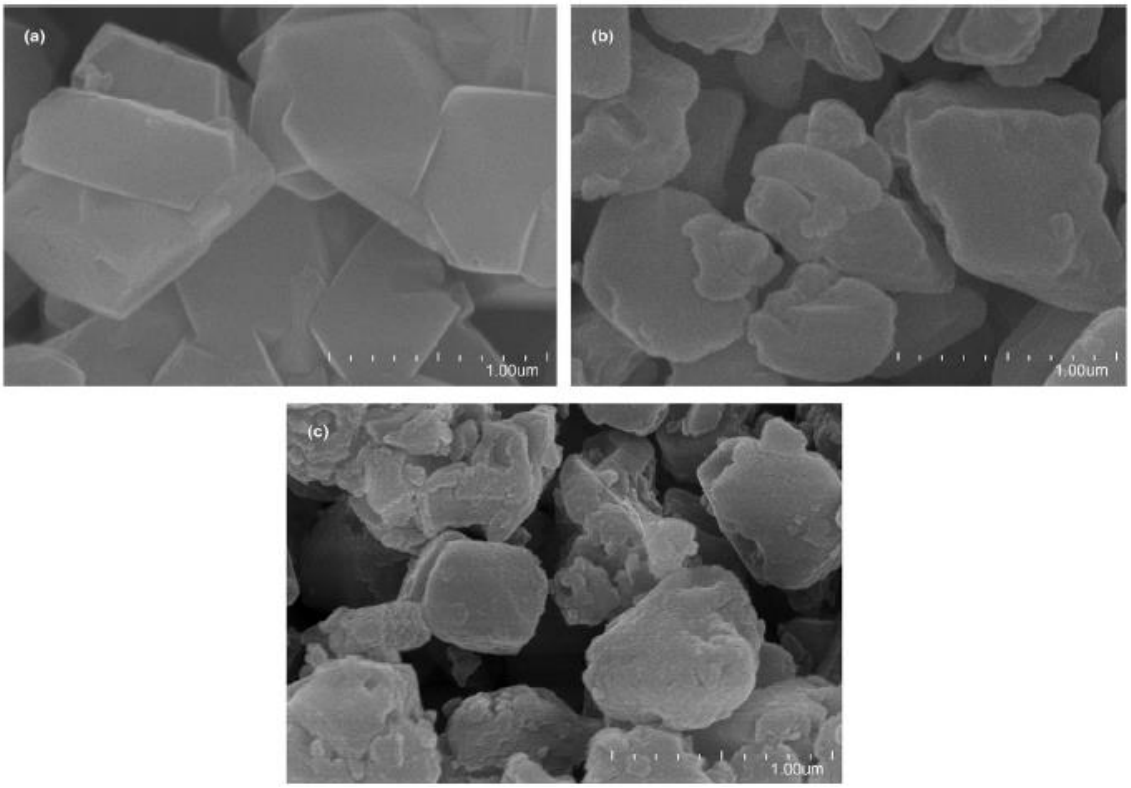

Figure 29. SEM images of Y zeolite crystals: (a) Y-0, (b) Y-2, and (c) Y-5 [70]

The isomerization selectivity of the long-chain alkanes on the microporous arrays is suppressed due to the strong adsorption of alkene intermediates on the acid sites and slow diffusion of heavy molecules [61]. On the other hand, the mesoporous MCM-41 materials showed higher performance due to their high specific surface area, large pore volume, and wide pore diameter [71]. However, the weak acidity of the mesoporous MCM-41 material is one of the main drawbacks to achieve high efficiency in the production of isomerized materials [72]. Therefore, the Pt metal-loaded micro/mesoporous composite catalyst is developed by combining the most favorable features of both microporous crystalline zeolites and mesoporous materials [73]. The microporous zeolite provides high acidity, whereas the mesoscale pores ensure reduced diffusion limitations and lower molecular residence time [74] [75]. The composite catalyst is formed as a result of coating the external surface of Y-zeolite crystals with the mesoporous MCM-41 layer. Additionally, there is another independent MCM-41 mesoporous phase around the composite particles. Both MCM-41 phases, the layer covering the external surface and the independent layer, work harmoniously to prohibit the closer proximity of the Y-zeolite crystals, providing better dispersion of the Y crystals in the

bi-porous catalytic system. With better dispersion, the possibility of the extended diffusion distance due to the close contacts of the contiguous zeolite crystals is minimized [70].

In Figure 30a, the conversion of n-C_{12} over the Pt/MY-0, Pt/MY-2, and Pt/MY-5 catalysts are plotted versus the reaction time. The Pt/MY-5 and Pt/MY-2 alkali-treated catalysts have superior conversion than the Pt/MY-0 catalyst. The results are related to the smaller particle size of zeolite crystals and better dispersion of the acid sites in the Pt/MY-2 and Pt/MY-5 catalytic systems.

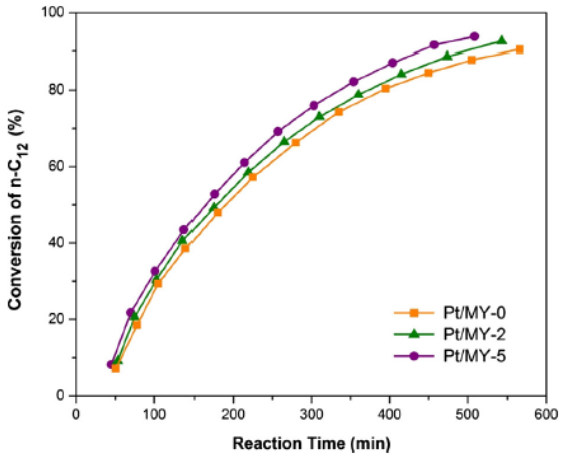

Figure 30. Overall n-C_{12} conversion versus reaction time [54]

Figure 31a shows the isomerized and cracked product yields for n-C_{12} hydroisomerization for all three catalysts are plotted against the n-C_{12} conversion, where the filled and hollow symbols represent the isomerized and cracked product yields, respectively. It can be seen that the alkali-treated catalysts, with a smaller particle size of the zeolite component, provide more isomerized products and less cracked products than the Pt/MY-0 catalyst. Furthermore, in Figure 31b, the MuB/MB of i-dodecane (i-C_{12}) values versus the corresponding conversion of n-C_{12} are plotted. The MuB/MB value is higher for the Pt/MY-0 catalyst than the Pt/MY-2 and Pt/MY-5 catalysts. This is indicative that the Pt/MY-0 catalyst generates the multi-branched isomerized and cracked product easier and quicker than the Pt/MY-2 and Pt/MY-5 catalysts owing to its poor cracking resistance. It was suggested that the diffusion distance of the alkene intermediates from the zeolite crystal pore mount to the microporous structure in Pt/MY-0 catalyst is longer than in the alkali-treated Pt/MY-2 and Pt/MY-5 catalysts due to smaller particle size, and as a consequence, minimized diffusion distance. There is a higher possibility for alkene intermediates to encounter more acid sites during transport within the zeolite crystal of the Pt/MY-0 catalyst, which leads to the higher skeletal transformation of alkene intermediates and the possibility of unwanted secondary reactions such as multiple branching and cracking reactions. Lastly, despite the almost identical metal and acid properties of the Pt/MY-2 and Pt/MY-5 catalysts, the Pt/MY-5 catalyst possesses higher isomerization

selectivity than the Pt/MY-2 catalyst due to the even smaller particle size of the Pt/MY-5 catalyst. It leads to shorter diffusion distances and less probability for shortened alkene intermediates to encounter the protonic acid sites between HD/HDH reactions. As a result, there is a remarkable effect on the bifunctional catalyst performance within limiting secondary reactions [70].

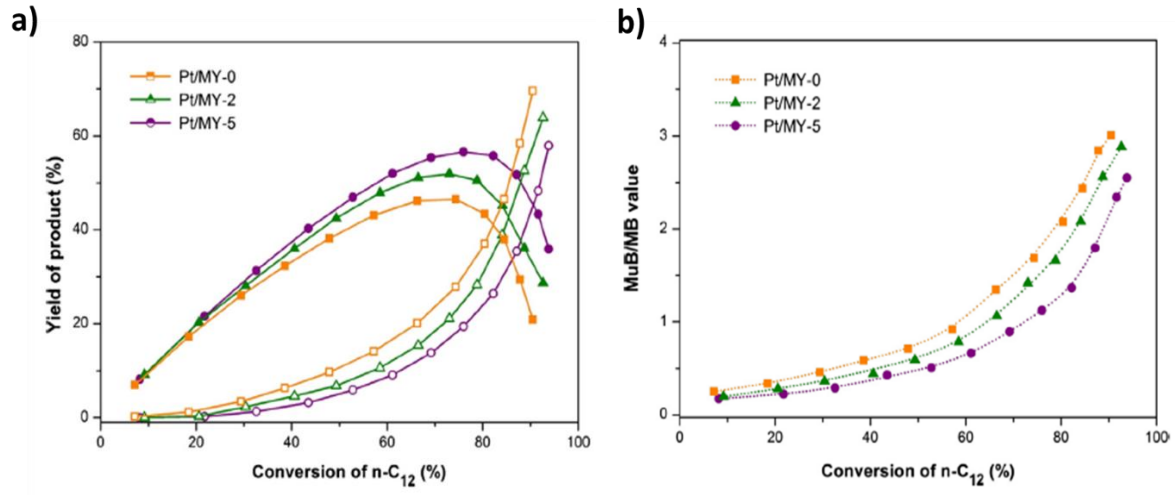

Figure 31. (a) Product yield versus conversion of n-C_{12} (b) MuB/MB value of isomerized products versus conversion of n-C_{12} [70]

Kim et al. [36] prepared a bifunctional catalyst with Pt nanoparticles (NPs) loaded on MFI-type (ZSM-5) zeolites and different crystal thicknesses ranging from 2 to 300 nm to explore the effect of zeolite crystal thickness and Pt location on the hydroisomerization of n-C_7. In this study, 2 nm thick MFI zeolite nanosheets, a nanocrystalline MFI zeolite of 10 nm thick, bulk zeolite with approx. 300 nm crystal thickness and a commercial MFI zeolite of 40 nm crystal thickness were produced and identified as NS-2, NC-10, B-300, and C-40, respectively. Reducing the diffusion lengths by creating nanocrystalline zeolites or mesopores within the zeolite crystal provides enhanced diffusion in the zeolite. The mesoporous zeolite and nanocrystalline zeolite catalysts show a significant improvement in the isomer selectivity of n-alkane hydroisomerization compared to the bulk zeolite [76]. The Pt NPs were loaded inside the zeolite pores by ion-exchange (IE) technique and on the external surface of the crystal by the CI method. The Pt content of catalysts prepared by the IE and CI methods are within the range of 0.81-0.99 wt.%, which is sufficient to supply the HD/DHD functions and keep Pt evenly dispersed in the catalytic system. The Pt locations and particle size of the conventional ZSM-5 and 2 nm thick MFI nanosheets prepared by IE and CI are displayed in Figure 32 [36]. For the catalysts prepared by the IE method, the Pt NPs are located near to acid sites, whereas for the catalysts prepared by the CI method, the Pt NPs are deposited only on the external surfaces. Moreover, it can be seen that for the 2 nm nanosheets the distance between metal and acid sites is almost the same, independent of the preparation method. Contrarily, for larger

nanosheets, there is a big difference in the distance between metal and acid sites for both methods. The hydroisomerization of n-C_7 was executed in a continuous-flow Pyrex reactor with an inner diameter of 13 mm under H_2 at atmospheric pressure using 0.1 g of powdered catalyst. The H_2/n-C_7 ratio, the temperature of the reactor, WHSV of n-C_7 were set to 10, 473-573 K, and 6.8 h^{-1}, respectively.

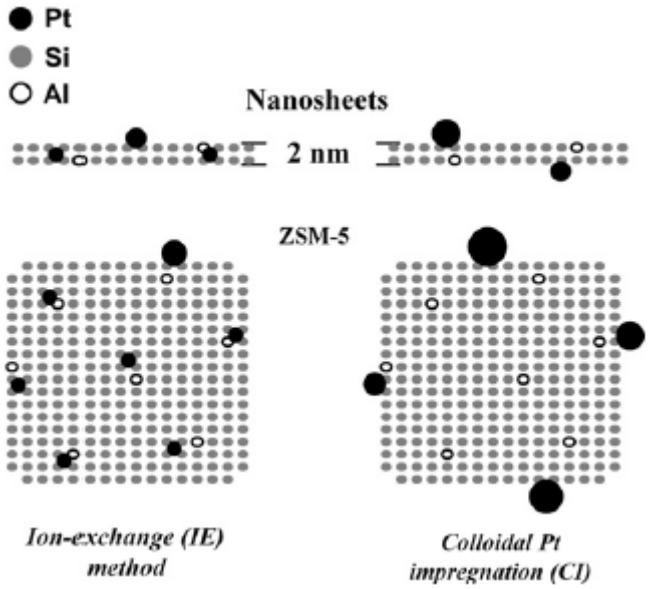

Figure 32. Schematic representation of Pt locations in conventional ZSM-5 and 2-nm thick MFI nanosheets prepared by the IE and CI methods [36]

Figure 33 illustrates the n-C_7 conversion of Pt(IE)/MFI and Pt(CI)/MFI catalysts versus the different reaction temperatures. Since all results show a similar S-curves for different catalysts in both preparation methods, the catalysts have enough number of HD/DHD Pt sites to balance the acidic function under the given reaction conditions. In the case of the insufficient Pt sites, the conversion of alkanes is controlled by Pt loading and dispersion.

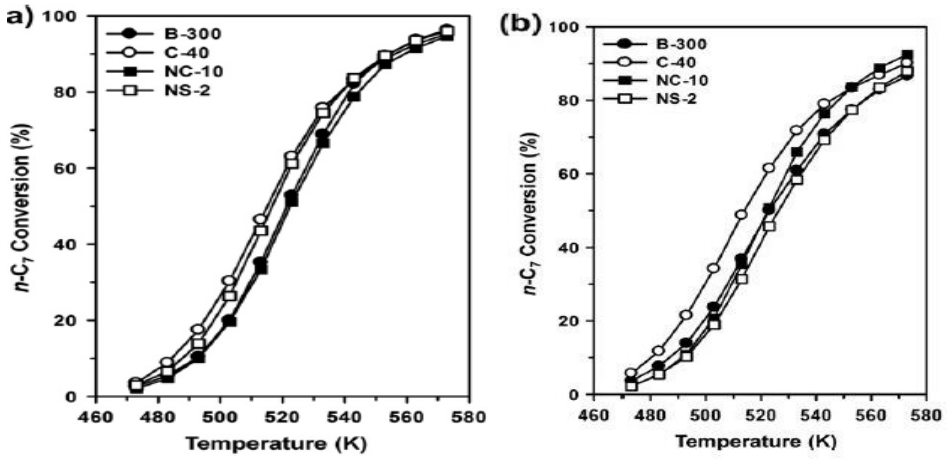

Figure 33. n-C_7 conversion by (a) Pt(IE)/MFI and (b) Pt(CI)/MFI catalysts plotted as a function of reaction temperature [36]

In Figure 34, selectivity toward i-C_7 versus total n-C_7 conversion is plotted with increasing reaction temperatures and the arrows show the maximum obtained i-C_7 mole percent. For the same n-C_7 conversion level, the i-C_7 yield increases with decreasing crystal thickness for both catalyst preparation methods. The maximum i-C_7 mole percent for Pt(IE)/B-300, Pt(IE)/C-40, Pt(IE)/NC-10, and Pt(IE)/NS-2 were found as 22 mol%, 29 mol%, 42 mol%, and 48 mol%, respectively. The maximum i-C_7 mole percent for Pt(CI)/B-300, Pt(CI)/C-40, Pt(CI)/NC-10 and Pt(CI)/NS-2 were found as 14 mol%, 27 mol%, 42 mol%, and 49 mol%, respectively. When comparing both methods, all catalysts show a very similar maximum i-C_7 mole percent except for the Pt(IE)/B-300 and Pt(CI)/B-300 catalysts. However, the effect of the zeolite crystal thickness is more impactful than the location of the Pt NPs. For instance, the difference between the Pt(IE)/NS-2 and Pt(IE)/B-300 catalyst is much larger than the difference between the Pt(IE)/B-300 and Pt(CI)/B-300 catalysts.

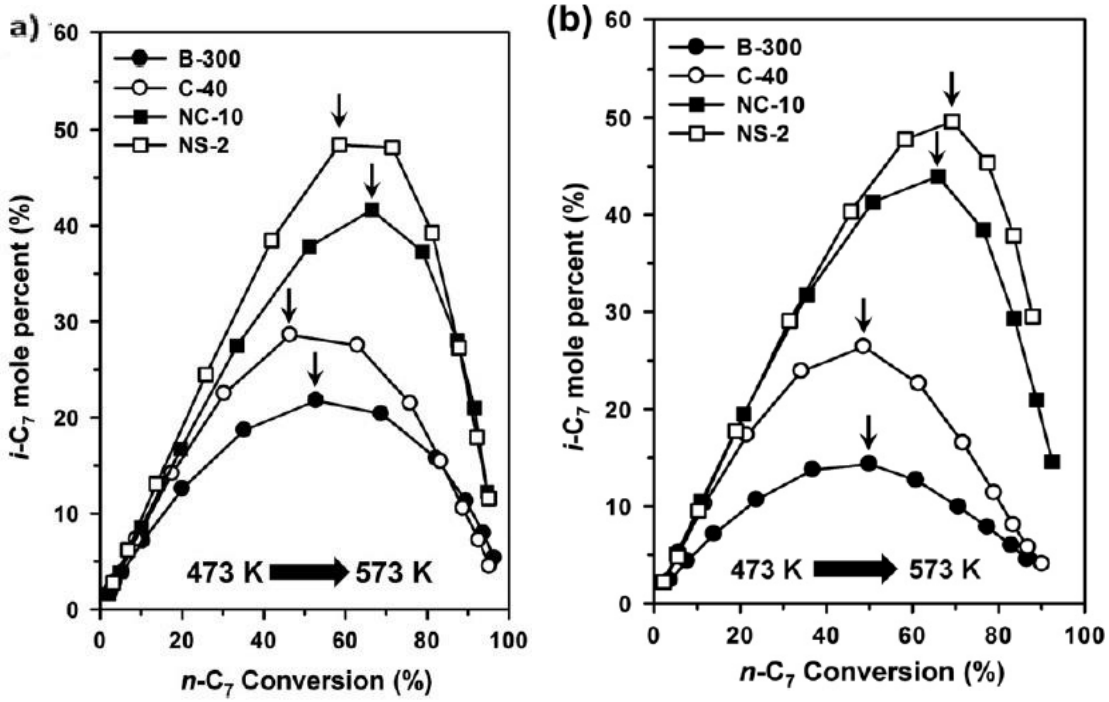

Figure 34. i-C_7 isomer yield (mol%) versus total n-C_7 conversion by (a) Pt(IE)/MFI and (b) Pt(CI)/MFI catalysts, plotted while increasing reaction temperatures [36]

The increased isomer selectivity of the thin zeolite crystals can be linked to easier diffusion of branched isomers inside the zeolite and therefore a lower probability of cracking reaction. The micropore opening of MFI zeolite is approx. 0.55 nm, which allows the entry of n-C_7 molecules with an approx. 0.43 nm molecular size. After the isomerization on the acid site, the molecular size of the branched i-C_7 molecules increases to 0.55 nm causing their diffusion to become hindered. For the larger zeolite crystals, the branched isomers are most likely transformed into the multi-branched isomers and cracked products due to their long residence time inside the

zeolite micropores. This results in a decreased yield of the i-C_7 products. For the 2 nm thin nanosheet (NS-2), the primary isomers can easily diffuse out from the inside of the zeolite crystal before the cracking reaction occurs, allowing an increased mono-branched isomer yield [36].

2.3 Kinetic studies

There has been an extensive amount of research on the reaction mechanism and kinetics of the skeletal rearrangement of light alkanes over a bifunctional catalyst. Kinetic parameters obtained through kinetic modeling can be important in the understanding and scaling of the hydrocracking process, including the design and optimization of catalytic reactors. Various kinetic models for the isomerization of n-C_6 have been suggested in the literature [77] [78] [79].

Holló et al. [80] investigated the kinetics of the skeletal rearrangement of n-C_5, n-C_6, n-C_7, and cyclohexane (c-C_6). Power law equations were obtained for the hydroisomerization of the aforementioned alkanes over mordenite-supported Pt catalysts at a temperature range of 180–220 °C, an H_2 partial pressure of 5–40 atm, and various with H_2/hydrocarbon ratio from 1 to 20. In Figure 35, the effects of the partial pressure of alkanes on alkane conversion are shown to be linear in a logarithmic scale at H_2 pressure of 4 bar, the temperature of 200 °C for n-C_5, n-C_6, and n-C_5, and temperature of 210 °C for c-C_6. In Figure 36, the effects of the partial pressure of hydrogen on alkane conversion are displayed to be linear in a logarithmic scale at alkane pressure of 4 bar and temperature of 210 °C. The slopes of each line provide the reaction orders for both alkanes and hydrogen.

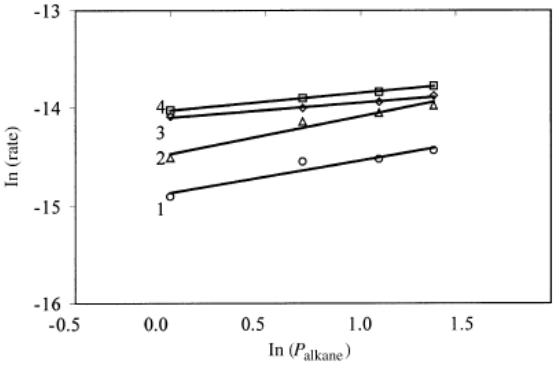

Figure 35. Reaction rates of alkanes as a function of alkane pressure (1) n-C_5, (2) n-C_6, (3) n-C_7, and (4) c-C_6 [80]

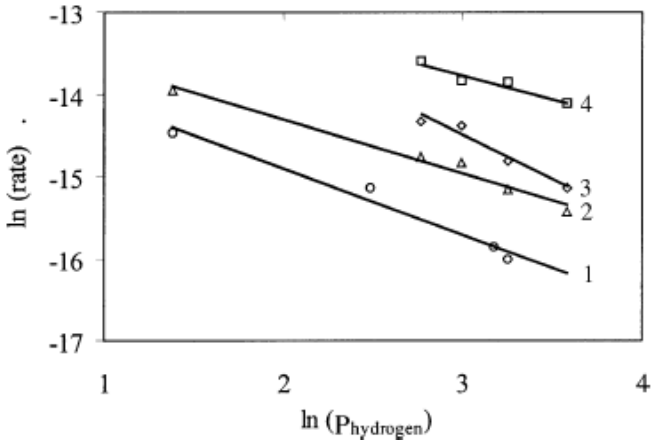

Figure 36. Reaction rates of alkanes as a function of hydrogen pressure (1) n-C_5, (2) n-C_6, (3) n-C_7, and (4) c-C_6 [80]

For modeling purposes, a simplified scheme of bifunctional catalytic hydroisomerization for n-C_6 is shown in Figure 37 [80]. The first step considers the adsorption of the n-C_6 molecule (1), then the adsorbed n-hexane diffuses toward platinum sites (2) where dehydrogenation occurs (3). After that, the n-hexene intermediate diffuses towards the acid sites through the zeolite micropores (4) where isomerization reaction takes place (5). Then, the isocarbenium ion diffuses back to the Pt sites (6) where it undergoes hydrogenation to produce isohexene (7). Lastly, isohexene is transported to the zeolite micropore sites (8) and is desorbed to the gas phase (9) [81].

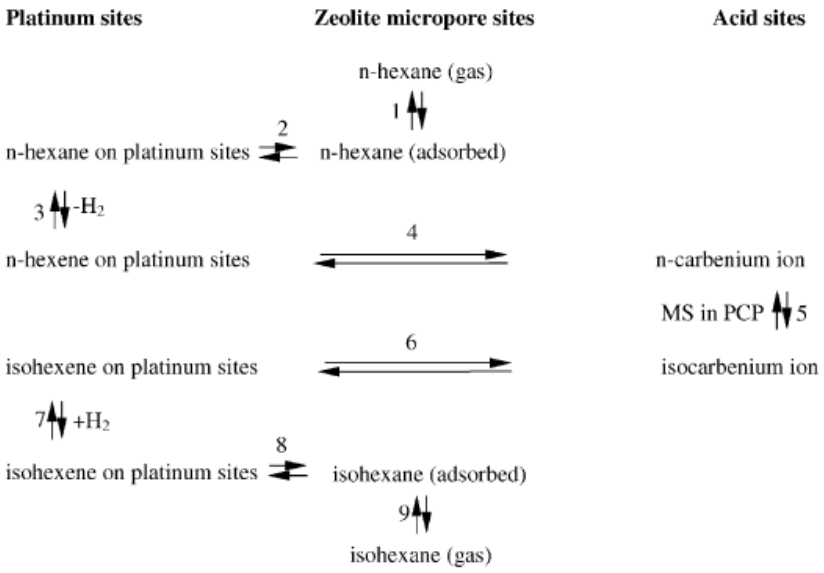

Figure 37. Reaction scheme of n-C_6 hydroisomerization [81]

The rate expression for all steps in Figure 37 is derived with rate constants, partial pressures, and surface coverages as follows:

$$r_1 = k_1 * P_{n-P} * \theta_{0,a} - k_{-1} * \theta_{n-P,a} \quad (7)$$

$$r_2 = k_2 * \theta_{n-P,a} * \theta_{0,Pt} - k_{-2} * \theta_{n-P,Pt} * \theta_{0,a} \quad (8)$$

$$r_3 = k_3 * \theta_{n-P,Pt} - k_{-3} * \theta_{n-O,Pt} * P_{H_2} \quad (9)$$

$$r_4 = k_4 * \theta_{n-O,Pt} * \theta_{0,H+} - k_{-4} * \theta_{n-carb,H+} * \theta_{0,Pt} \quad (10)$$

$$r_5 = k_5 * \theta_{n-carb,H+} * \theta_{0,Pt} - k_{-5} * \theta_{i-carb,H+} \quad (11)$$

$$r_6 = k_6 * \theta_{i-carb,H+} * \theta_{0,Pt} - k_{-6} * \theta_{i-O,Pt} * \theta_{0,H+} \quad (12)$$

$$r_7 = k_7 * \theta_{i-O,Pt} * P_{H_2} - k_{-7} * \theta_{i-P,Pt} \quad (13)$$

$$r_8 = k_8 * \theta_{i-P,Pt} * \theta_{0,a} - k_{-8} * \theta_{i-P,a} * \theta_{0,Pt} \quad (14)$$

$$r_9 = k_9 * \theta_{i-P,a} - k_{-9} * P_{i-P} * \theta_{0,a} \quad (15)$$

The balances for active site coverage are shown below:

$$\theta_{0,a} + \theta_{n-P,a} + \theta_{i-P,a} = 1 \quad (16)$$

$$\theta_{0,Pt} + \theta_{n-P,Pt} + \theta_{i-P,Pt} + \theta_{n-O,Pt} + \theta_{i-O,Pt} = 1 \quad (17)$$

$$\theta_{0,H+} + \theta_{n-carb,H+} + \theta_{i-carb,H+} = 1 \quad (18)$$

Apart from the rate determining step, all other steps are deemed to be in equilibrium. The equilibrium constant for the i-th step is given by Equation 19.

$$K_i = \frac{k_i}{k_{-i}} \quad (19)$$

The HD/DHD reactions are fast compared to isomerization on acid sites due to the highly sufficient Pt content of the catalyst [82]. The rate limiting step is assumed to be the skeletal rearrangement of the carbenium ions. The reverse reaction is neglected since kinetic parameters are determined at low conversions. The rate equation is derived as follow:

$$r = k_5 \frac{(K_{14} * P_{n-P})}{P_{H_2} + K_{14} * P_{n-P}} \quad (20)$$

By plotting the inverse of the reaction rate as a function of the partial pressure of H_2 at a constant partial pressure of alkenes, k_5 and K_{14} can be calculated from the ordinate intersection and slope of lines shown in Figure 38.

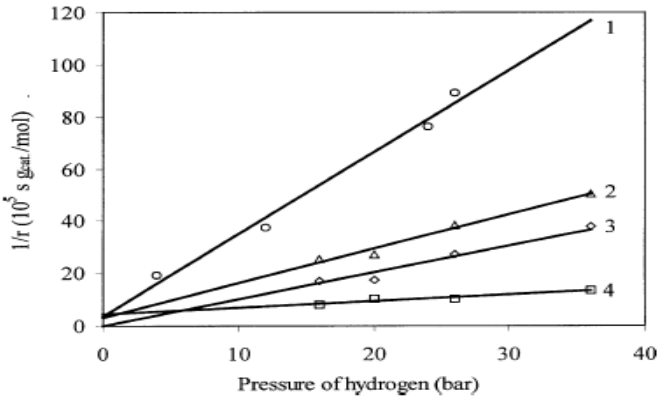

Figure 38. Linear regression of alkane hydroisomerization involving the skeletal isomerization of the carbenium ion as the rate determining step: (1) n-C_5, (2) n-C_6, (3) n-C_7, and (4) c-C_6 at T = 210 °C, $P_{alkanes}$ = 4 bar [80]

Cam et al. [21] also studied the kinetics of n-C_6 isomerization over nickel (Ni) or cobalt (Co) promoted Pd/H-ZSM-5 catalysts, which are Pd-Ni/HZSM-5 and Pd-Co/HZSM-5. This study claims that the previously suggested mechanism contradicts several experimental observations, including the positive reaction order with respect to hydrogen, and the reaction provides no olefins if it takes place over a sole metal catalyst without acidic support. For proceeding with the stable isomerization of n-alkanes and enhancing the branched isomer selectivity, it is necessary for hydrogen to be present in the reaction system [83]. Since the Arrhenius plot of the n-C_6 isomerization rate was not linear, the authors concluded that the rate equation could not be fitted with the power-law.

In the study, the authors found that the n-hexane isomerization rate presented a concave profile with respect to n-hexane conversion, suggesting that the reaction rate is slowed by products. This finding was experimentally confirmed by inserting 2-methylpentane into the reaction mixture. In consequence, the proposed kinetic model considered the partial pressure of 2-methylpenthane in the denominator of the rate equation. Moreover, Figure 39 indicates the dependences of the n-C_6 isomerization rate on the partial pressures of n-C_6 in Figure 39a and hydrogen Figure 39b. The behavior of these curves is indicative that n-C_6 and hydrogen appear in both the numerator and the denominator of the rate equation.

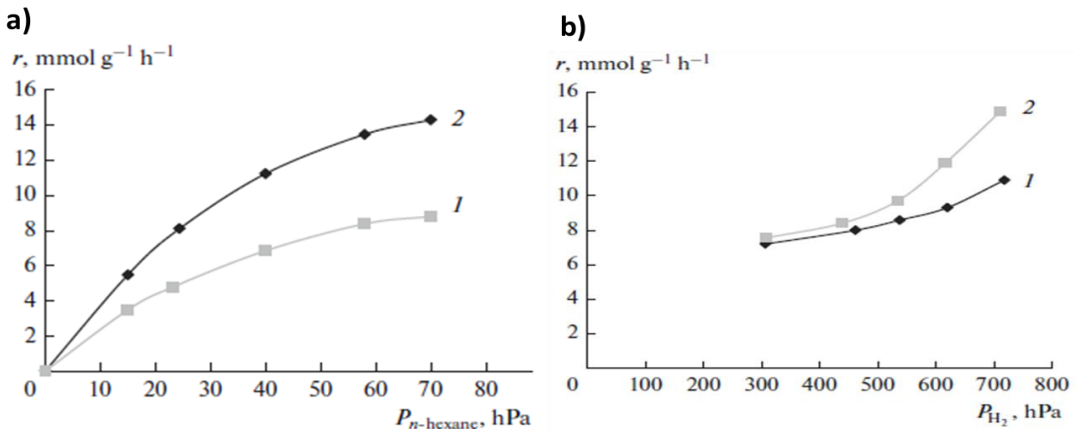

Figure 39. n-C_6 isomerization rate at 250 °C as a function of (a) n-C_6 partial pressure (P_{H2}=500 hPa, $P_{isohexane}$=20 hPa) and (b) hydrogen partial pressure ($P_{n\text{-}hexane}$=50 hPa, $P_{isohexane}$=20 hPa) for the (1) Pd–Ni/HZSM-5 and (2) Pd–Co/HZSM-5 catalysts [21]

The n-C_6 isomerization rate is given by the following equation:

$$r = \frac{k * P_{n-hexane}^{n_1} * P_{H_2}^{m_1} \gamma}{\left(1 + k_1 * P_{n-hexane}^{n_2} + k_2 * P_{H_2}^{m_2} + k_3 * P_{isohexanes}^{m_3}\right)^{2\alpha}} \quad (21)$$

The best fit between the experimental and calculated data was observed at $n_1 = n_2 = m_3 = 1$ and $m_1 = m_2 = \alpha = 0.5$. Thus, the reaction rate results in:

$$r = \frac{k * P_{n-hexane} * P_{H_2}^{0.5} \gamma}{\left(1 + k_1 * P_{n-hexane} + k_2 * P_{H_2}^{0.5} + k_3 * P_{isohexanes}\right)} \quad (22)$$

The rate constants shown in equation 22 were found from the experimental data and are presented in Table 4.

Table 4. Kinetic parameters for n-C_6 isomerization over Pd-Ni/HZSM-5 and Pd-Co/HZSM-5 [21]

Parameters	Preexponential factors	Activation energies (kj/mol)
	Pd-Ni/HZSM-5	
$\boldsymbol{k}$ $(\boldsymbol{mmol g^{-1} h^{-1} hPa^{-1.5}})$	5.96 x10^2	7420
$\boldsymbol{k_1}$ $(\boldsymbol{hPa^{-1}})$	8.93 x10^{-4}	-6700
$\boldsymbol{k_2}$ $(\boldsymbol{hPa^{-0.5}})$	2.83 x10^{-4}	-649
$\boldsymbol{k_3}$ $(\boldsymbol{hPa^{-1}})$	0.65	-450
	Pd-Co/HZSM-5	
$\boldsymbol{k}$ $(\boldsymbol{mmol g^{-1} h^{-1} hPa^{-1.5}})$	6.6 x10^4	11500
$\boldsymbol{k_1}$ $(\boldsymbol{hPa^{-1}})$	1.671 x10^{-3}	-6090
$\boldsymbol{k_2}$ $(\boldsymbol{hPa^{-0.5}})$	1.249 x10^{-6}	-10500
$\boldsymbol{k_3}$ $(\boldsymbol{hPa^{-1}})$	0.141	-2010

Even though the n-hexane isomerization over Pd-Ni/HZSM-5 and Pd-Co/HZSM-5 is in the same form, their rate constants are quite different. For Pd-Co/HZSM-5, the rate constant is larger, i.e. more active, than the rate constant for Pd-Ni/HZSM-5 at the same temperatures. Also, hydrogen seems to have a notable influence on the isomerization rate of the n-hexane but it is not absorbed as strong as the n-hexane or isohexane on the surface of the catalyst according to its adsorption coefficient.

3 Conclusions and Recommendations

It was claimed by Wang et al. [9], Zhang et al. [54], and Alvarez et al. [55] that the performance of bifunctional catalysts for hydroisomerization and hydrocracking is strongly influenced by the balance between metal and acid sites. Firstly, the effects of metal and acid functions on the activity, stability, and selectivity of bifunctional catalysts were investigated by changing the ratio between metal and acid sites, nMe/nA. For comparatively higher ratios of nMe/nA, the metal function activity is high enough compared to the acid function activity so the rate limiting step changes from HD/DHD over Pt sites to skeletal rearrangement or cracking over acid sites. The TOF of the catalyst becomes high and sequential cracking and coke formation reactions are minimized, leading to improved selectivity with a high isomer/cracking and mono-branched/multi-branched product ratios. According to the studies of Zhang et al. [54] and Alvarez et al. [55], a sequential reaction mechanism can be considered as ideal toward isomer production, in which only one transformation of the alkene intermediate on the acid sites can occur during their diffusion between two Pt sites. Moreover, Wang et al. [9] claimed that an excessive amount of metal sites would also limit access to the zeolite's micropores and consequently reduce n-alkane conversion, while also increasing the cost of preparation. Thus, it has been found that nMe/nA values should be kept within an optimal range for optimal catalytic performances.

Also, it has been found by Batalha et al. [44] that the nMe/nA value is not the only parameter affecting the catalytic properties, but also the proximity between metal and acid sites has a strong effect on the catalytic performance of the bifunctional catalyst. Weisz et al. [60] suggested that the closest proximity between metal and acid sites is necessary for optimal activity and selectivity. According to Weisz et al. [60] and Samad et al. [27], if the distance between two active sites increases to the millimeter scale, these catalysts act in a monofunctional manner due to the inability of the alkene intermediates to diffuse very far between sites. Thus, a large distance between sites prevents the ideal isomerization reaction from taking place. The i-alkenes are more likely to undergo secondary reactions, leading to a rise in the production of both cracked products and coke. However, Weisz's research only examined the effects of metal sites acid sites distances on the micrometer and millimeter scales. Therefore, further consideration of the nanometer and atomic scales distances between two active sites was investigated to explore the possibility of an optimal distance. It was shown by Samad et al. [27] and Gutierrez-Acebo et al. [59] that catalytic performance improved significantly for the catalyst with bifunctionality within the micrometer and nanometer scales compared to the catalyst in the millimeter scale since its metal and acid sites were mixed and located more closely. Similarly, Zecevic et al. [61] found that the catalyst prepared

by nanometer scale proximity exhibits notably higher selectivity toward isomer product compared to the catalyst prepared by atomic scale proximity. For the atomic scale proximity, the alkane feedstock diffuses through the micropores of the zeolite to undergo an HD/DHD reaction at the metal sites. It is suggested by Zecevic et al. [61] that the intermediate molecules generated on the metal sites are retained in the zeolite micropores network due to the strong adsorption on acid sites. Consequently, it results in an increment in their residence time in the acidic environment, which leads to an increase in their cracking possibility and a decreased selectivity towards the desired products. On the other hand, for the nanometer scale proximity between metal and acid side, the acid sites are more reachable for the alkene intermediates formed on the metal sites. The alkene intermediates generated on the metal site diffuse from the wider pores of the alumina binder to the Y-zeolite, where undergo isomerization on the outside and then diffuse immediately back to a metal site on the alumina binder. Consequently, the cracking of alkene intermediates is reduced and the isomer product yield is increased. In this study, it was found that closer distances between both functions are detrimental for the isomerization selectivity. The different nanometer scale distances either on the external surface or close to the micropore mouth were explored. It was found by Lv et al. [63] that increasing the number of metal sites near the micropore mouth provides shorter distances between metal and acid sites and higher isomerization yield rather than increasing the number of metal sites on the external surface. In conclusion, it would be preferable to deposit the Pt sites close to the micropore mouth. Additionally, it was claimed by Li et al. [67], Zhang et al. [70] and Kim et al. [36] that the diffusion distance between metal and acid functions on the catalyst is affected by the zeolite crystal particle size and thickness. The distance traveled by the alkene intermediates from the zeolite crystal pore mount to inside the microporous structure in a catalyst with larger zeolite crystals is longer than in the catalyst with smaller zeolite crystals. Therefore, smaller zeolite crystals ensure a lower possibility for alkene intermediates to encounter the acid sites while traversing the pores of the zeolite crystal, limiting the possibility of unwanted secondary reactions such as multiple branching and cracking.

As a result of this literature review, it was also found that a relatively high nMe/nA value is required for an ideal catalytic performance over the bifunctional catalyst. Moreover, it is suggested that if Pt metal particles are placed close to the micropore mouth of the zeolite aiming to nanometer scale proximity with acid sites and if the zeolite crystals have a comparably smaller size, greater bifunctionality and optimal high-quality diesel production can be achieved. It is claimed that alkene intermediates created at metal sites do not suffer slower and longer diffusion through zeolite micropores. This could potentially decrease the likelihood

of secondary unfavorable reactions such as multi-branching and cracking and increases the fuel quality by enhancing the selectivity toward the isomerized products.

In the work of Hollo et al. [80] and Cam et al. [21], the rate equations of n-C_6 hydroisomerization reactions have been examined from different points of view. The main goal of this study was to include the distance between the metal and acid sites to the microkinetic model by using experimental results. However, experimental studies could not be performed due to unexpected COVID-19 pandemic. As a future study, after an experimental examination of different spatial distribution for metal and acid sites, a kinetic model can be developed with the objective of directly considering the influence of the distance between metal and acid sites. A rate equation that takes the degree of intimacy as an additional parameter could be employed as a reference for improving or optimizing the design of bifunctional catalysts, since there is no literature study found that includes the distance between two active functions into the kinetic model. This study is recommended for future research as it will enable the optimization process to be performed more effectively.

4 References

[1] B. D. Vandegehuchte, I. R. Choudhury, J. W. Thybaut, J. A. Martens and G. B. Marin, "Integrated Stefan–Maxwell, Mean Field, and Single-Event Microkinetic Methodology for Simultaneous Diffusion and Reaction inside Microporous Materials.," *The Journal of Physical Chemistry C,* vol. 118, no. 38, pp. 22053-22068, 2014.

[2] B. D. Vandegehuchte, J. W. Thybaut and G. B. Marin, "Unraveling diffusion and other shape selectivity effects in ZSM5 using n-hexane hydroconversion single-event microkinetics.," *Industrial & Engineering Chemistry Research,* pp. 15333-15347, 2014.

[3] "International Energy Outlook," U.S. Energy Information Administration, Washington, DC, 2019.

[4] R. W. Bentley, "Global oil & gas depletion: an overview," *Energy policy,* vol. 30, no. 3, pp. 189-205, 2002.

[5] J. G. Speight, "Chapter 10 - Refinery of the Future," in *The refinery of the future*, Oxford, Gulf Professional Publishing, 2011, pp. 315-340.

[6] S. Dehkissia, F. Larachi and E. Chornet, "Catalytic (Mo) upgrading of Athabasca bitumen vacuum bottoms via two-step hydrocracking and enhancement of Mo–heavy oil interaction," *Fuel,* vol. 83, no. 10, pp. 1323-1331, 2004.

[7] L. C. Castañeda, J. A. D. Muñoz and J. Ancheyta, "Combined process schemes for upgrading of heavy petroleum," *Fuel,* vol. 100, pp. 110-127, 2012.

[8] J. G. Speight, "Chapter 21: Hydrocracking," in *The Chemistry and Technology of Petroleum*, Boca Raton, CRC Press, 2011, pp. 634-672.

[9] W. Wang, C. J. Liu and W. Wu, "Bifunctional catalysts for the hydroisomerization of n-alkanes: the effects of metal-acid balance and textural structure," *Catalysis Science & Technology,* 2019.

[10] J. G. Speight, "New approaches to hydroprocessing," *Catalysis Today,* vol. 98, no. 1-2, pp. 55-60, 2004.

[11] R. Tang, M. Yuan, K. Liu, H. Li, J. Zhang and Y. Tian, "Utilization of bifunctional catalyst for upgrading petroleum residue via cracking and gasification: Effect of catalysts," *Journal of the Energy Institute,* 2018.

[12] S. Akmaz and P. A. Caglayan, "Effect of catalyst, temperature, and hydrogen pressure on slurry hydrocracking reactions of naphthalene," *Chemical Engineering & Technology,* vol. 35, no. 5, pp. 917-930, 2015.

[13] S. C. Korre, M. T. Klein and R. J. Quann, "Hydrocracking of polynuclear aromatic hydrocarbons. Development of rate laws through inhibition studies," *Industrial & engineering chemistry research,* vol. 36, no. 6, pp. 2041-2050, 1997.

[14] J. Scherzer and A. J. Gruia, Hydrocracking science and technology, New york: Crc Press, 1996.

[15] M. Bricker, V. Thakkar and J. Petri, "Hydrocracking in Petroleum Processing," in *Handbook of Petroleum Processing*, Dordrecht, Springer, 2015, pp. 317-359.

[16] F. Regali, M. Boutonnet and S. Järås, "Hydrocracking of n-hexadecane on noble metal/silica–alumina catalysts," *Catalysis today,* vol. 214, pp. 12-18, 2013.

[17] P. R. Robinson and G. E. Dolbear, "Hydrotreating and Hydrocracking: Fundamentals," in *Practical Advances in Petroleum Processing*, New York, Springer, 2006, pp. 177-218.

[18] S. Parkash, "Hydrocracking Processes," in *Refining processes handbook*, Elsevier, 2003.

[19] M. A. Fahim, T. A. Al-Sahhaf and A. Elkilani, "Chapter 7: Hydroconversion," in *Fundamentals of petroleum refining*, Elsevier, 2009.

[20] J. W. Thybaut, C. S. Laxmi Narasimhan, J. F. Denayer, G. V. Baron, P. A. Jacobs, J. A. Martens and G. B. Marin, "Acid− metal balance of a hydrocracking catalyst: Ideal versus nonideal behavior," *Industrial & engineering chemistry research,* vol. 44, no. 14, pp. 5159-5169, 2005.

[21] L. L. Cam, T. Nguyen, T. D. T. Kim, N. A. Gaidai, Y. A. Agafonov, A. H. Cam, H. T. Cuong and A. L. Lapidus, "Kinetics of n-hexane isomerization over supported palladium catalysts," *Kinetics and Catalysis,* vol. 58, no. 3, pp. 311-320, 2017.

[22] N. V. Chekantsev, M. S. Gyngazova and E. D. Ivanchina, "Mathematical modeling of light naphtha (C5, C6) isomerization process," *Chemical Engineering Journal,* vol. 238, pp. 120-128, 2014.

[23] C. Marcilly, Acid-basic catalysis: Application to refining and petrochemistry, Paris: IFP publications, 2006.

[24] M. Guisnet and J. P. Gilson, Zeolites for cleaner technologies, London: Imperial College Press, 2002.

[25] P. S. Mendes, J. M. Silva, M. F. Ribeiro, A. Daudin and C. Bouchy, "From powder to extrudate zeolite-based bifunctional hydroisomerization catalysts: on preserving zeolite integrity and optimizing Pt location," *Journal of industrial and engineering chemistry,* vol. 62, pp. 72-83, 2018.

[26] P. S. Mendes, J. M. Silva, M. F. Ribeiro, A. Daudin and C. Bouchy, "Synergies, cooperation and other effects: a review for hydroconversion catalysts," *Catalysis Today,* 2019.

[27] J. E. Samad, J. Blanchard, C. Sayag, C. Louis and J. R. Regalbuto, "The controlled synthesis of metal-acid bifunctional catalysts: The effect of metal: acid ratio and metal-acid proximity in Pt silica-alumina catalysts for n-heptane isomerization," *Journal of catalysis,* vol. 342, pp. 203-212, 2016.

[28] G. B. McVicker, M. Daage, M. S. Touvelle, C. W. Hudson, D. P. Klein, W. C. Baird Jr, B. Cook, J. Chen, S. Hantzer, D. Vaughan, E. S. Ellis and O. Feelay, "Selective ring opening of naphthenic molecules," *Journal of Catalysis,* vol. 210, no. 1, pp. 137-148, 2002.

[29] C. A. Monteiro, D. Costa, J. L. Zotin and D. Cardoso, "Effect of metal–acid site balance on hydroconversion of decalin over Pt/Beta zeolite bifunctional catalysts," *Fuel,* vol. 160, pp. 71-79, 2015.

[30] F. Anaya, L. Zhang, Q. Tan and D. E. Resasco, "Tuning the acid–metal balance in Pd/and Pt/zeolite catalysts for the hydroalkylation of m-cresol," *Journal of Catalysis,* vol. 328, pp. 173-185, 2015.

[31] J. Weitkamp, "Catalytic hydrocracking—mechanisms and versatility of the process," *ChemCatChem,* vol. 4, no. 3, pp. 292-306, 2012.

[32] H. L. Coonradt and W. E. Garwood, "Mechanism of hydrocracking. Reactions of Paraffins and Olefins," *Industrial & Engineering Chemistry Process Design and Development,* vol. 3, no. 1, pp. 38-45, 1964.

[33] M. Guisnet, ""Ideal" bifunctional catalysis over Pt-acid zeolites," *Catalysis today,* vol. 218, pp. 123-134, 2013.

[34] M. Guisnet, "Catalysis on bifunctional Pt acid zeolites. A route to cleaner processes," *Polish Journal of Chemistry,* pp. 637-656, 2003.

[35] W. F. Hölderich, "New aspects in the performance of heterogeneous catalysts for intermediates and fine chemicals," *Heterogeneous Catalysis and Fine Chemicals,* p. 83, 1988.

[36] J. Kim, W. Kim, Y. Seo, J. C. Kim and R. Ryoo, "n-Heptane hydroisomerization over Pt/MFI zeolite nanosheets: Effects of zeolite crystal thickness and platinum location," *Journal of catalysis,* vol. 301, pp. 187-197, 2013.

[37] P. Sánchez, F. Dorado, M. J. Ramos, R. Romero, V. Jiménez and J. L. Valverde, "Hydroisomerization of C6–C8 n-alkanes, cyclohexane and benzene over palladium and platinum beta catalysts agglomerated with bentonite," *Applied Catalysis A: General,* vol. 314, no. 2, pp. 248-255, 2006.

[38] M. A. Ali, T. Tatsumi and T. Masuda, "Development of heavy oil hydrocracking catalysts using amorphous silica-alumina and zeolites as catalyst supports.," *Applied Catalysis A: General,* vol. 233, no. 1-2, pp. 77-90, 2002.

[39] H. Deldari, "Suitable catalysts for hydroisomerization of long-chain normal paraffins," *Applied Catalysis A: General,* vol. 293, pp. 1-10, 2005.

[40] A. Corma and A. Martínez, "Zeolites in refining and petrochemistry," *Stud. Surf. Sci. Catal,* vol. 157, pp. 337-366, 2005.

[41] V. M. Akhmedov and S. H. Al-Khowaiter, "Recent advances and future aspects in the selective isomerization of high n-Alkanes," *Catalysis Reviews,* vol. 49, no. 1, pp. 33-139, 2007.

[42] G. G. Martens, G. B. Marin, J. A. Martens, P. A. Jacobs and G. V. Baron, "A fundamental kinetic model for hydrocracking of C8 to C12 alkanes on Pt/US–Y zeolites.," *Journal of Catalysis,* vol. 195, no. 2, pp. 253-267, 2000.

[43] P. S. Mendes, J. M. Silva, M. F. Ribeiro, P. Duchêne, A. Daudin and C. Bouchy, "Quantification of metal-acid balance in hydroisomerization catalysts: A step further toward catalyst design," *AIChE Journal,* vol. 63, no. 7, pp. 2864-2875, 2017.

[44] N. Batalha, L. Pinard, C. Bouchy, E. Guillon and M. Guisnet, "n-Hexadecane hydroisomerization over Pt-HBEA catalysts. Quantification and effect of the intimacy between metal and protonic sites," *Journal of catalysis,* pp. 122-131, 2013.

[45] R. Henry, M. Tayakout-Fayolle, P. Afanasiev, C. Lorentz, G. Lapisardi and G. Pirngruber, "Vacuum gas oil hydrocracking performance of bifunctional Mo/Y zeolite catalysts in a semi-batch reactor," *Catalysis Today,* vol. 220, pp. 159-167, 2014.

[46] J. W. Ward, "Hydrocracking processes and catalysts. Fuel Processing Technology," *Fuel Processing Technology,* vol. 35, no. 1-2, pp. 55-85, 1993.

[47] N. Musselwhite, K. Na, K. Sabyrov, S. Alayoglu and G. A. Somorjai, "Mesoporous aluminosilicate catalysts for the selective isomerization of n-Hexane: the roles of surface acidity and platinum metal.," *Journal of the American Chemical Society,* vol. 137, no. 32, pp. 10231-10237, 2015.

[48] J. W. Scott and A. G. Bridge, "The continuing development of hydrocracking," *Advances in Chemistry,* vol. 103, pp. 113-129, 1971.

[49] O. Ben Moussa, L. Tinat, X. Jin, W. Baaziz, O. Durupthy, C. Sayag and J. Blanchard, "Heteroaggregation and Selective Deposition for the Fine Design of Nanoarchitectured Bifunctional Catalysts: Application to Hydroisomerization.," *ACS Catalysis,* vol. 8, no. 7, pp. 6071-6078, 2018.

[50] J. Zhang, H. Wu, A. Zhao, X. Bai, O. V. Kikhtyanin, W. Wu and R. Zhang, "Synthesis of MgAPO-31 nanocrystals via different heating methods and their catalytic performance in the hydroisomerization of n-decane," *Journal of Porous Materials,* vol. 24, no. 2, pp. 437-442, 2016.

[51] J. Weitkamp and S. Ernst., "Factors influencing the selectivity of hydrocracking in zeolites," in *Guidelines for mastering the properties of molecular sieve*, New York, Plenum Press, 1990, pp. 343-354.

[52] J. Francis, E. Guillon, N. Bats, C. Pichon, A. Corma and L. J. Simon, "Design of improved hydrocracking catalysts by increasing the proximity between acid and metallic sites," *Applied Catalysis A: General,* Vols. 409-410, pp. 140-147, 2011.

[53] X. Wei, O. V. Kikhtyanin, V. N. Parmon, W. Wu, X. Bai, J. Zhang, L. Xiao, X. Su and Y. Zhang, "Synergetic effect between the metal and acid sites of Pd/SAPO-41 bifunctional catalysts in n-hexadecane hydroisomerization," *Journal of Porous Materials,* vol. 25, no. 1, pp. 235-247, 2018.

[54] Y. Zhang, W. Wang, X. Jiang, X. Su, O. Kikhtyanin and W. Wu, "Hydroisomerization of n-hexadecane over a Pd–Ni2P/SAPO-31 bifunctional catalyst: synergistic effects of bimetallic active sites," *Catalysis Science & Technology,* pp. 1-10, 2017.

[55] F. Alvarez, F. R. Ribeiro, G. Perot, Y. C. Thomazeau and M. Guisnet, "Hydroisomerization and Hydrocracking of Alkanes: 7. Influence of the Balance between Acid and Hydrogenating Functions on the Transformation ofn-Decane on PtHY Catalysts," *Journal of Catalysis,* vol. 162, no. 2, pp. 179-189, 1996.

[56] A. de Lucas, P. Sánchez, F. Dorado, M. J. Ramos and J. L. Valverde, "Effect of the metal loading in the hydroisomerization of n-octane over beta agglomerated zeolite based catalysts.," *Applied Catalysis A: General,* vol. 294, no. 2, pp. 215-225, 2005.

[57] N. Batalha, L. Pinard, Y. Pouilloux and M. Guisnet, "Bifunctional hydrogenating/acid catalysis: quantification of the intimacy criterion," *Catalysis letters,* vol. 143, no. 6, pp. 587-591, 2013.

[58] G. Ertl, H. Knözinger and J. Weitkamp, Preparation of solid catalysts, Weinheim: Wiley-VCH, 1999.

[59] E. Gutierrez-Acebo, C. Leroux, C. Chizallet, Y. Schuurman and C. Bouchy, "Metal/acid bifunctional catalysis and intimacy criterion for ethylcyclohexane hydroconversion: when proximity does not matter," *ACS Catalysis,* vol. 8, no. 7, pp. 6035-6046, 2018.

[60] P. B. Weisz, "Polyfunctional heterogeneous catalysis," *Advances in Catalysis,* vol. 13, pp. 137-193, 1962.

[61] J. Zecevic, G. Vanbutsele, K. P. de Jong and J. A. Martens, "Nanoscale intimacy in bifunctional catalysts for selective conversion of hydrocarbons," *Nature,* vol. 528, no. 7581, p. 245, 2015.

[62] M. Rivallan, E. Seguin, S. Thomas, M. Lepage, N. Takagi, H. Hirata and F. Thibault-Starzyk, "Platinum Sintering on H-ZSM-5 Followed by Chemometrics of CO Adsorption and 2D Pressure-Jump IR Spectroscopy of Adsorbed Species," *Angewandte Chemie International Edition,* vol. 49, no. 4, pp. 785-789, 2010.

[63] G. Lv, C. Wang, K. Chi, H. Liu, P. Wang, H. Ma, Q. Wei and Z. Tian, "Effects of Pt site distributions on the catalytic performance of Pt/SAPO-11 for n-dodecane hydroisomerization," *Catalysis Today,* vol. 316, pp. 43-50, 2018.

[64] G. A. Somorjai and J. Y. Park, "Colloid science of metal nanoparticle catalysts in 2D and 3D structures. Challenges of nucleation, growth, composition, particle shape, size control and their influence on activity and selectivity," *Topics in Catalysis,* vol. 49, pp. 126-135, 2008.

[65] Y. Zhao, L. Jia, J. A. Medrano, J. R. Ross and L. Lefferts, "Supported Pd catalysts prepared via colloidal method: the effect of acids," *ACS catalysis,* vol. 3, no. 10, pp. 2341-2352, 2013.

[66] J. W. Thybaut and G. B. Marin, "Multiscale aspects in hydrocracking: from reaction mechanism over catalysts to kinetics and industrial application," *Advances in Catalysis,* vol. 59, pp. 109-238, 2016.

[67] M. Li, Y. Zhang, H. Wang, S. Yu, D. Liu and Y. Wang, "Influence of zeolite crystal size on selective conversion of n-alkane: Controlling intermediates' diffusion distances inside the micropores," *Fuel,* vol. 254, p. 115709, 2019.

[68] Y. Tao, H. Kanoh, L. Abrams and K. Kaneko, "Mesopore-modified zeolites: preparation, characterization, and applications," *Chemical reviews,* vol. 106, no. 3, pp. 896-910, 2006.

[69] P. M. Lima, T. Garetto, C. L. Cavalcante Jr and D. Cardoso, "Isomerization of n-hexane on Pt–Ni catalysts supported on nanocrystalline H-BEA zeolite," *Catalysis Today,* vol. 172, no. 1, pp. 195-202, 2011.

[70] Y. Zhang, D. Liu, Z. Men, K. Huang, Y. Lv, M. Li and B. Lou, "Hydroisomerization of n-dodecane over bi-porous Pt-containing bifunctional catalysts: Effects of alkene intermediates' journey distances within the zeolite micropores," *Fuel,* no. 236, pp. 428-436, 2019.

[71] C. T. Kresge, M. E. Leonowicz, W. J. Roth, J. C. Vartuli and J. S. Beck, "Ordered mesoporous molecular sieves synthesized by a liquid-crystal template mechanism," *nature,* vol. 359, no. 6397, pp. 710-712, 1992.

[72] K. C. Park and S. K. Ihm, "Comparison of Pt/zeolite catalysts for n-hexadecane hydroisomerization," *Applied Catalysis A: General,* vol. 203, no. 2, pp. 201-209, 2000.

[73] Y. Zhang, Y. Liu and Y. Li, "Synthesis and characteristics of Y-zeolite/MCM-48 biporous molecular sieve," *Applied Catalysis A: General,* vol. 345, no. 1, pp. 73-79, 2008.

[74] X. H. Vu, U. Armbruster and A. Martin, "Micro/mesoporous zeolitic composites: Recent developments in synthesis and catalytic applications," *Catalysts,* vol. 6, no. 12, p. 183, 2016.

[75] X. Liu, T. Yang, P. Bai and L. Han, "Y/MCM-41 composites assembled from nanocrystals," *Microporous and mesoporous materials,* vol. 181, pp. 116-122, 2013.

[76] C. H. Christensen, I. Schmidt and C. H. Christensen, "Improved performance of mesoporous zeolite single crystals in catalytic cracking and isomerization of n-hexadecane," *Catalysis Communications,* vol. 5, no. 9, pp. 543-546, 2004.

[77] M. Guisnet, V. Fouche, M. Belloum, J. P. Bournonville and C. Travers, "Isomerization of n-hexane on platinum dealuminated mordenite catalysts II. Kinetic study," *Applied catalysis,* vol. 71, no. 2, pp. 295-306, 1991.

[78] A. Van de Runstraat, J. A. Kamp, P. J. Stobbelaar, J. Van Grondelle, S. Krijnen and R. A. Van Santen, "Kinetics of hydro-isomerization of n-hexane over platinum containing zeolites," *Journal of Catalysis,* vol. 171, no. 1, pp. 77-84, 1997.

[79] E. Blomsma, J. A. Martens and P. A. Jacobs, "Mechanisms of heptane isomerization on bifunctional Pd/H-Beta zeolites," *Journal of catalysis,* vol. 159, no. 2, pp. 323-331, 1996.

[80] A. Holló, J. Hancsok and D. Kalló, "Kinetics of hydroisomerization of C5–C7 alkanes and their mixtures over platinum containing mordenite," *Applied Catalysis A: General,* vol. 229, no. 1-2, pp. 93-102, 2002.

[81] A. Van de Runstraat, J. Van Grondelle and R. A. Van Santen, "Microkinetics Modeling of the Hydroisomerization of n-Hexane," *Industrial & engineering chemistry research,* vol. 36, no. 8, pp. 3116-3125, 1997.

[82] M. Guisnet and V. Fouche, "Isomerization of n-hexane on platinum dealuminated mordenite catalysts III. Influence of hydrocarbon impurities," *Applied catalysis,* vol. 71, no. 2, pp. 307-317, 1991.

[83] Y. C. Yang and H. S. Weng, "The role of H2 in n-butane isomerization over Al-promoted sulfated zirconia catalyst," *Journal of Molecular Catalysis A: Chemical,* vol. 304, no. 1-2, pp. 65-70, 2009.

FACULTY OF ENGINEERING AND ARCHITECTURE

Impact of the spatial distribution of active material on the performance of n-hexane hydrocracking with a bifunctional catalyst

Seniz Rodoplu
Student number: 01801037

Supervisors: Prof. dr. Vladimir Galvita, Juan Mirena Seguias
Counsellor: Prof. dr. ir. Joris Thybaut

Master's dissertation submitted in order to obtain the academic degree of
Master of Science in Chemical Engineering

Academic year 2019-2020

GHENT UNIVERSITY